Journal of Nanomaterials

# Application of Nanomaterials in Bioengineering

Lead Guest Editor: Mauro Pollini
Guest Editors: Federica Paladini and Ian R. Cooper

# Application of Nanomaterials in Bioengineering

Journal of Nanomaterials

# Application of Nanomaterials in Bioengineering

Lead Guest Editor: Mauro Pollini
Guest Editors: Federica Paladini and Ian R. Cooper

# Editorial Board

# Contents

**Application of Nanomaterials in Bioengineering**
Mauro Pollini, Federica Paladini, and Ian R. Cooper
Editorial (2 pages), Article ID 1924385, Volume 2018 (2018)

**Tribomechanical Properties of a Carbon-Based Nanolayer Prepared by Nitrogen Ion Beam Assisted Deposition for Finger Joint Replacements**
Tomas Horazdovsky and Radka Vrbova
Research Article (9 pages), Article ID 3749309, Volume 2018 (2018)

**Preparation and Drug Release Study of Novel Nanopharmaceuticals with Polysorbate 80 Surface Adsorption**
Xiaojun Tao, Yu Li, Qian Hu, Li Zhu, Zixuan Huang, Jiajin Yi, Xiaoping Yang, Jianzhuo Hu, and Xing Feng
Research Article (11 pages), Article ID 4718045, Volume 2018 (2018)

**The Recent Advances of Magnetic Nanoparticles in Medicine**
Ting Guo, Mei Lin, Junxing Huang, Chenglin Zhou, Weizhong Tian, Hong Yu, Xingmao Jiang, Jun Ye, Yujuan Shi, Yanhong Xiao, Xuefeng Bian, and Xiaoqian Feng
Review Article (8 pages), Article ID 7805147, Volume 2018 (2018)

**Surface Disinfections: Present and Future**
Matteo Saccucci, Erika Bruni, Daniela Uccelletti, Agnese Bregnocchi, Maria Sabrina Sarto, Maurizio Bossù, Gabriele Di Carlo, and Antonella Polimeni
Review Article (9 pages), Article ID 8950143, Volume 2018 (2018)

**Carbon Nanomaterials for Breast Cancer Treatment**
M. L. Casais-Molina, C. Cab, G. Canto, J. Medina, and A. Tapia
Review Article (9 pages), Article ID 2058613, Volume 2018 (2018)

**Icariin-Loaded $TiO_2$ Nanotubes for Regulation of the Bioactivity of Bone Marrow Cells**
Yanli Zhang, Chundong Liu, Liangjiao Chen, Aijie Chen, Xiaoli Feng, and Longquan Shao
Research Article (12 pages), Article ID 1810846, Volume 2018 (2018)

Hindawi
Journal of Nanomaterials
Volume 2018, Article ID 1924385, 2 pages
https://doi.org/10.1155/2018/1924385

*Editorial*

# Application of Nanomaterials in Bioengineering

**Mauro Pollini**,[1] **Federica Paladini**,[1] **and Ian R. Cooper**[2]

[1]*University of Salento, Lecce, Italy*
[2]*University of Brighton, Brighton, UK*

Correspondence should be addressed to Mauro Pollini; mauro.pollini@unisalento.it

Received 29 May 2018; Accepted 30 May 2018; Published 28 June 2018



Serious concerns about multidrug-resistant microorganisms and increasing healthcare costs have encouraged research efforts in the definition of novel prevention and treatment of infectious diseases. Nanotechnologies provide interesting unconventional routes towards novel approaches in bioengineering by exploiting the unique properties of some materials at nanometric scale. The development of innovative biomaterials and biological systems can have a huge impact on medicine, in particular when conventional methods and therapies fail.

The purpose of this special issue is to provide the reader with the most recent scientific advances in bioengineering, by analysing the potential of different nanomaterials for a wide range of biomedical applications such as surface disinfection, drug delivery, cancer therapy, and tissue engineering. Such variety of applications indicates the great interest of the scientific community towards nanotechnologies as an effective platform to develop novel approaches for health and wellbeing. Among the contributions submitted to this special issue, relevant papers and review articles with different topics have been selected for publication.

In "The Recent Advances of Magnetic Nanoparticles in Medicine" by T. Guo et al., the potential of magnetic nanoparticles for application in medicine is discussed. Categories, properties, modification, and applications of magnetic nanoparticles in MRI, in tumour magnetic inductive hyperthermia, and as a vector are presented.

In "Surface Disinfections: Present and Future" by M. Saccucci et al., the discussion is focused on antibiotic resistance in hospital infections and surface disinfection, with a specific focus on disinfection procedures by using nanomaterials. Among them, the authors discuss the use of graphene-based nanomaterials as novel antimicrobial drugs.

In "Tribomechanical Properties of a Carbon-Based Nanolayer Prepared by Nitrogen Ion Beam Assisted Deposition for Finger Joint Replacements" by T. Horazdovsky and R. Vrbova, research on the mechanical properties of deposited nanolayers of carbon on titanium alloys using a nitrogen laser is discussed. The paper discusses the positive effect of surface bombardment by nitrogen lasers, in relation to decreased fault wear and potential increase in material usability.

In "Preparation and Drug Release Study of Novel Nanopharmaceuticals with Polysorbate 80 Surface Adsorption" by X. Tao et al., the authors describe the preparation of donepezil drug-loaded nanoparticles with cholesterol-modified pullulan as nanocarrier and surface modification for enhanced targeting and sustained release. The article aims to provide experimental basis for the research of pharmaceutical preparation in the treatment of nervous system diseases.

In "Carbon Nanomaterials for Breast Cancer Treatment" by M.L. Casais-Molina et al., the applications of carbon nanomaterials in the identification, diagnosis, and treatment of breast cancer are discussed. In particular, this review article describes the potential of carbon nanomaterials for drug delivery and/or release, for photodynamic therapy, for use as contrast agents in diagnosing and locating breast tumours, and for biosensors.

In "Icariin-Loaded $TiO_2$ Nanotubes for Regulation of the Bioactivity of Bone Marrow Cells" by Y. Zhang et al., the fabrication of $TiO_2$ nanotubes loaded with icariin is presented for application in dental implants. The research explores the effect of icariin-loaded $TiO_2$ nanotubes on bone marrow cells and the potential of icariin as an osteogenesis agent in bone tissue engineering.

*Mauro Pollini*
*Federica Paladini*
*Ian R. Cooper*

Hindawi
Journal of Nanomaterials
Volume 2018, Article ID 3749309, 9 pages
https://doi.org/10.1155/2018/3749309

*Research Article*

# Tribomechanical Properties of a Carbon-Based Nanolayer Prepared by Nitrogen Ion Beam Assisted Deposition for Finger Joint Replacements

**Tomas Horazdovsky**[1] **and Radka Vrbova**[2]

[1]*Faculty of Mechanical Engineering, Czech Technical University in Prague, Prague, Czech Republic*
[2]*Institute of Dental Medicine, General University Hospital in Prague and First Faculty of Medicine, Charles University, Prague, Czech Republic*

Correspondence should be addressed to Tomas Horazdovsky; tomas.horazdovsky@fs.cvut.cz

Received 25 December 2017; Revised 30 March 2018; Accepted 8 April 2018; Published 20 May 2018

Academic Editor: Ian R. Cooper



This paper presents the tribomechanical test results of Ti6Al4V alloy modified by carbon-based nanolayers with a thickness of 20 nm and 40 nm, prepared by nitrogen ion beam assisted deposition. The presence of carbon and nitrogen compounds was observed in the modified surface after ion bombardment. Nonstoichiometric $TiN_x$ was mainly detected near the interface nanolayer/titanium substrate and in the substrate itself. Ion bombardment led to an improved surface hardness of ~13 GPa in comparison to unmodified Ti6Al4V titanium alloy (~5.5 GPa) and alloy coated by carbon nanolayer without nitrogen ion assistance (~7 GPa). The decreasing of friction coefficient was achieved from 0.5–0.6 for untreated Ti6Al4V alloy to 0.1 for treated Ti6Al4V alloy. Wear testing using a joint wear simulator proved that the modified Ti6Al4V alloy has a higher resistance compared to the unmodified Ti6Al4V alloy. The primary local wear fault of the treated surface was observed after 240,000 cycles in comparison to enormous wear on the untreated surface after just 10,000 cycles. Treating the Ti6Al4V load-bearing components of implants with carbon-based nanolayers assisted by nitrogen ions is very promising in terms of extending the lifetime of implants and thereby reduces patient burden.

## 1. Introduction

Titanium (Ti) and its alloys are currently the most attractive materials for biomedical applications due to their beneficial biological compatibility and good mechanical properties. They are used mainly for joint replacements such as knee, hip, shoulder, elbow, wrist, and spine or as dental implant materials.

The Ti6Al4V alloy is the most commonly used material in current implantology. It is characterized by good biocompatibility, high tensile strength and corrosion resistance, and relatively low Young's modulus (~110 GPa) compared with currently used surgical metals [1]. Nevertheless, it has a high stiffness compared to human cortical bone (~20 GPa) [2, 3] which can cause stress shielding effect [4, 5]. Alloying elements, such as Al and V, are considered nonbeneficial to the human organism [6, 7]. For these reasons, more favourable titanium alloys (e.g., based on Nb, Ta, Zr, and Cr) with lower Young's modulus have been developed and optimized [8–10]. Another problem with commonly used Ti6Al4V alloy is its relatively high coefficient of friction [1, 11]. This relates to the lower wear resistance, which may result in debris release. The released ions can activate the immune system [12], induce a local inflammatory reaction, or damage the bone structure, which in turn leads to long-term health problems or aseptic implant loosening [13–15].

The longevity of the implant in the human body is influenced by the factors mentioned above. However, the tribological properties and surface hardness play the greatest role, especially in big load-bearing joint replacements. Surface treatment, such as nitriding, carburizing, and oxidation, can improve the wear resistance of Ti materials by forming a hard surface layer [16, 17]. Ti materials coated by a carbon-based nanolayer are very promising for joint's replacements.

Table 1: Chemical composition of Ti6Al4V alloy.

| Element | Content (wt%) |
|---|---|
| Al | 5.50–6.75 |
| V | 3.50–4.50 |
| Fe | 0.30 |
| C | 0.10 |
| O | 0.20 |
| N | 0.05 |
| H | 0.0125 |
| Ti | Balance |

These nanolayers are characterized as being biocompatible with excellent low friction properties, high hardness, and good wear resistance in comparison with Ti substrate. Many techniques are used for their deposition, such as chemical vapour deposition (CVD), plasma-enhanced chemical vapour deposition (PECVD), filtered cathode vacuum arc (FCVA), ion beam assisted deposition (IBAD) [18–23], and pulsed laser deposition (PLD) [24–26]. The adhesion of the carbon nanolayer onto the substrate, its microstructure, chemical composition, surface hardness, friction, and internal stress distribution can be improved by the optimization of the deposition conditions and ion bombardment during surface treatment [22, 27–31]. Nitrogen ion assistance leads to atomic mixing on the coating/substrate interface and to the formation of $TiN_x$ compounds in the modified zone. Newly formed compounds harden the substrate and significantly participate in the tribomechanical property enhancement of the coated material [32, 33].

In this respect, the development of surface modifications aimed at the carbon-based materials bombarded with nitrogen ions is very promising for load-bearing applications. The role of this modifications for real applications needs to be examined in more detail.

The purpose of this work is to characterize and test the Ti6Al4V alloy modified by ion beam assisted deposition of carbon-based nanolayer for finger joint replacements. This system is designed to improve the sliding properties of titanium alloy without risk of delamination known in thick diamond like carbon (DLC) coatings.

## 2. Materials and Methods

*2.1. Specimens Preparation.* The Ti6Al4V alloy containing $\alpha + \beta$ phase was used as a base material for the preparation of test specimens. The chemical composition of this alloy is shown in Table 1. Specimens in the form of a cylinder (20 mm in diameter and 8 mm in height) were cut from the titanium bar. The surface of each specimen was ground by a series of abrasive papers with grit of 150, 320, 500, 800, 1000, and 2000 and polished with diamond paste of 5 $\mu$m and 1 $\mu$m into the mirror like gloss ($R_a$ = 0.02 $\mu$m) using a Leco machine. The substrates were ultrasonically cleaned in isopropyl alcohol for 20 minutes before the deposition process.

*2.2. Deposition Process.* The deposition of carbon-based nanolayer was performed by ion beam assisted deposition (IBAD). The specimen was placed in a holder positioned on a cooled rotary manipulator in a vacuum chamber. The chamber was evacuated and the work pressure was maintained at about $5 \cdot 10^{-3}$ Pa during deposition. The carbon nanolayer was deposited by the electron beam evaporation of a carbon target of high purity (99.9%) with sequential nitrogen ion bombardment. The acceleration voltage was 90 kV and the fluence of the implanted nitrogen ions was $1 \cdot 10^{17}$ cm$^{-2}$. The deposition rate was about 0.10 nm·s$^{-1}$. Two groups of specimens with two different thicknesses were prepared. Approximate values of 20 nm (IBAD 20 nm) and 40 nm (IBAD 40 nm) have been determined. The control group contained specimens with carbon nanolayer without nitrogen ion bombardment (C 40 nm) and unmodified specimens (Ti6Al4V). A quartz thickness monitor located in the apparatus measured the thickness of the carbon-based nanolayer.

*2.3. Characterizations of Treated Surface.* The chemical composition of titanium surface modified with implanted nitrogen ions was measured by means of Auger electron spectroscopy (AES) in a PHI SAM 545 spectrometer. For excitation, an electron beam of 3 keV and 1 $\mu$A, with a diameter of 40 $\mu$m, was used. Two symmetrically inclined Ar ion beams of 1 keV sputtered the specimens. For carbon, the sputtering rate is estimated to be 0.7 nm/min.

The phase composition of titanium alloy modified by carbon nanolayer with nitrogen ion assistance was established by the X-ray diffraction (XRD) measurement using a PANalytical X'Pert PRO powder diffractometer. Cobalt radiation with a wavelength of 0.1789 nm and geometry with the parallel beam with an incident angle of 0.5° was used.

Qualitative changes of carbon bonding structure after ion implantation were analysed by Raman spectroscopy. The Raman spectra were found using a Renishaw RM1000 Raman microscope with an Ar laser and excitation at 514.5 nm.

The surface hardness of modified specimens (IBAD 20 nm, IBAD 40 nm, and C 40 nm) and unmodified specimens (Ti6Al4V) was measured by the nanoindentation method on a Hysitron TriboIndenter apparatus with a Berkovich diamond tip. Indents with 10 $\mu$m separation in the matrix 3 × 4 were applied on each specimen. The maximum indentation force was 5000 $\mu$N. The partial load-unload function was used to measure the depth profile of the surface hardness. NanoScratch test method was used for a detection of adhesion behaviour of deposited nanolayer. Scratch testing was performed with conospherical diamond tip (angle 60° tip radius 1 $\mu$m). The tip was cleaned with ethanol. The normal forces in scratch testing were continuously increasing from 2 to 3000 $\mu$N. The scratch length was 10 $\mu$m and the scratching speed was 1 $\mu$m/1.5 s.

The coefficient of friction was determined on a pin-on-disc tribometer equipped with a 100Cr6 steel ball of 6 mm diameter. Modified specimens (IBAD 20 nm and IBAD 40 nm) were compared with the Ti6Al4V reference specimens. The normal load during the test was 2 N with the velocity of 6 cm·s$^{-1}$ and a radius of rotation of 4 mm.

The distribution of contact pressure between the relatively rigid spherical part of the titanium joint and the much more flexible spherical cup made from polyetheretherketone

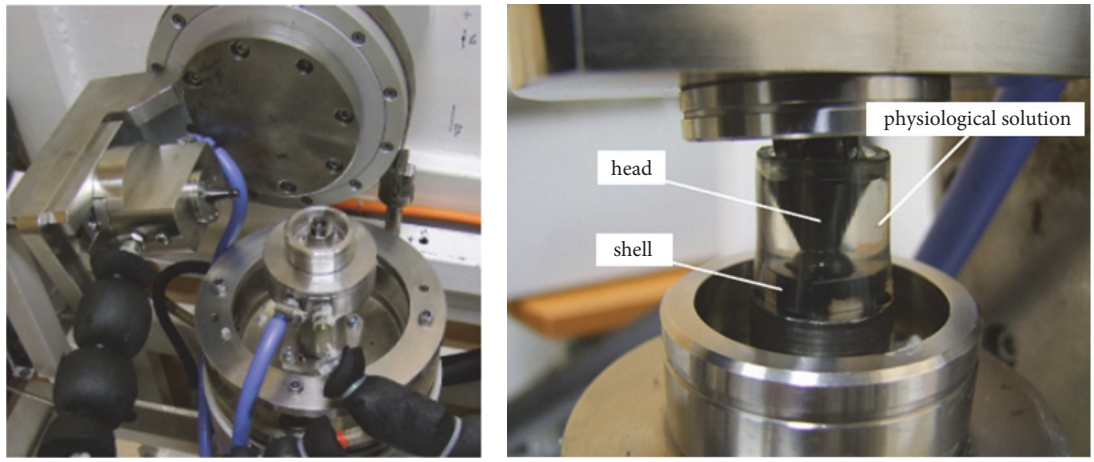


(a) (b)

Figure 1: Finger joint wear simulator: (a) wear testing component arrangement; (b) test detail.

(PEEK) was calculated by FEM (Finite Element Method, program Abaqus) analysis. Furthermore, the contact pressure was monitored as a function of the position in the cup, from centre to edge, for three values of the coefficient of friction (0.1–0.3).

Sliding behaviour was investigated on a finger joint wear simulator (Figure 1). For this purpose, the modified Ti6Al4V head (IBAD 40 nm) with a 10 mm diameter and a PEEK cup was used. The normal load of 100 N was applied during the test.

## 3. Results and Discussion

*3.1. Chemical Composition.* The results of the nitrogen depth distribution and elemental chemical composition of the surface area have been published in detail elsewhere [34]. The maximum concentration of nitrogen lies in the substrate matrix, overlaps partially with the mixing area nanolayer/substrate, and interferes with the carbon-based nanolayer. Minimal nitrogen enrichment of the carbon-based nanolayer was observed. High ion energy has caused nitrogen penetration through the nanolayer into the substrate. Nitrogen peak movement deeper into the specimen was observed with the increasing thickness of the nanolayer. Implanted nitrogen behind the carbon-based nanolayer penetrated the substrate in the modified projected range and modified longitudinal straggling, which causes an increase in the maximum nitrogen concentration from approx. 17.4 ± 1.6 at% for specimens with a nanolayer 20 nm in thickness to approx. 18.9 ± 1.9 at% for specimens with a nanolayer 40 nm in thickness. Oxygen contamination below 20 at% was detected in the narrow region on both the surface and nanolayer/substrate interface. The presence of oxygen on the nanolayer/substrate interface is likely caused by air exposure before the deposition process and by imperfect removal in the sputter cleaning.

*3.2. Phase Composition.* X-ray diffraction (XRD) method was used to determine the phase composition of the modified

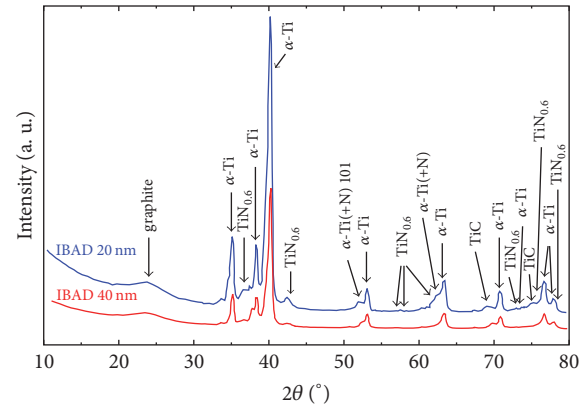


Figure 2: XRD spectra of modified specimens.

titanium alloy. Figure 2 shows XRD spectra of modified specimens IBAD 20 nm and IBAD 40 nm. Nonstoichiometric $TiN_x$ phases, TiC, and graphite were detected in the surface area. The structural $\alpha$-phase of the Ti6Al4V alloy was confirmed, but no $\beta$-phase was found in the diffraction pattern. The structural $\alpha$-phase with incorporated nitrogen $\alpha$-Ti(+N) was found. The $\alpha$-Ti(+N) structural phase marks the hexagonal structure derived from the $\alpha$-Ti phase, but with enlarged lattice parameters due to incorporation of nitrogen in interstitial sites of the Ti matrix [31]. The uneven dispersion of implanted nitrogen with a near-Gaussian distribution [35] induces a TiN and Ti(+N) mixture formation in the implanted region [31].

Nitrogen concentration profiles [34] indicate that the observed $TiN_x$ phase forms in the titanium matrix behind the carbon nanolayer. Results indicate the mixed area at the interface of carbon nanolayer and Ti6Al4V alloy due to ion bombardment. Formation of observed TiC compound is expected in this area. The new phases are located on the interface of titanium substrate/carbon-based nanolayer and the titanium sublayer. The results confirmed that the

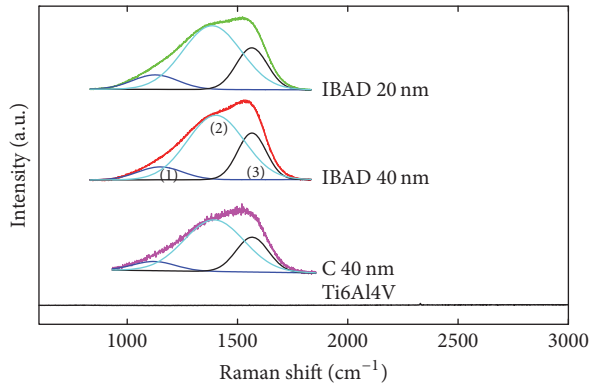


FIGURE 3: Raman spectra of carbon-based nanolayers prepared by nitrogen ion beam assisted deposition (IBAD 20 nm; IBAD 40 nm) and carbon-based nanolayer without nitrogen ion bombardment (C 40 nm).

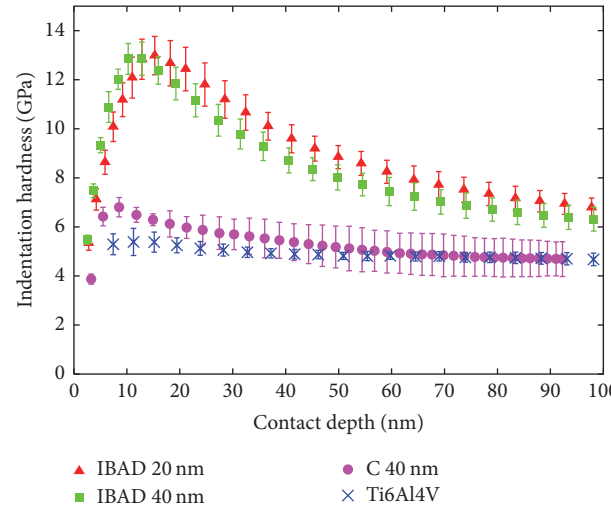


FIGURE 4: Depth profiles of the indentation hardness measurements.

implanted nitrogen stabilizes the $\alpha$-phase of the Ti6Al4V alloy [32, 33].

*3.3. Raman Spectroscopy.* Qualitative changes of carbon bonding structure after ion implantation were analysed by Raman spectroscopy. Figure 3 shows Raman spectra of the carbon-based nanolayers deposited with assistance of nitrogen ions (IBAD 20 nm, IBAD 40 nm) and the spectrum of carbon nanolayer deposited without nitrogen ion bombardment (C 40 nm). The peak parameters are stated in Table 2. Consistent fits are achieved using a combination of three peaks. Peak 1 (1123–1150 cm$^{-1}$) has responded to nanocrystalline or amorphous diamond fraction [36]. Peak 2 (1385–1402 cm$^{-1}$), known as a D peak, demonstrates the presence of disordered graphitic carbon, and peak 3 (1565–1567 cm$^{-1}$), the so-called G peak, belongs to crystalline graphitic carbon occurring in the nanostructure [30, 37]. The results show that ion bombardment during the deposition process increased peak intensity of Raman spectra for both thicknesses of carbon-based nanolayers. The ratio of the areas under the peaks increased due to nitrogen ion bombardment (Table 2). These results indicated that the high energy ion bombardment causes the graphitisation of carbon nanolayer for both applied thicknesses. According to Robertson's theory [38], ion bombardment helps to form the binding hybridization of amorphous carbon and related materials. The formation of $sp^2/sp^3$ binding hybridization is related to the local density produced by ion bombardment at various conditions. Many researchers have confirmed that ion bombardment at low energies (tens and hundreds of eV) induces the formation of $sp^3$ "diamond bonds" [39–41]. The high energy ion bombardment used here causes the accelerated nitrogen to penetrate into the titanium substrate. Part of this energy is dissipated in the atom displacements, and the rest of the energy is dissipated as phonons in due course [34]. Vlcak [29] demonstrated that 45 keV nitrogen ion bombardment modified the carbon bonds in defect $sp^2$ and defect $sp^3$ hybridization, resulting in graphitisation of the carbon. The conversion of $sp^3$ bonds to $sp^2$ bonds with increasing ion energy also confirmed Han et al. [42] and Wei et al. [43].

*3.4. Surface Hardness.* The resulting depth profiles of the indentation hardness are presented in Figure 4. The depth profile results of the control specimen (Ti6Al4V) show an almost constant trend in comparison with the coated specimens. The hardness increase ($H_{IT}$ 5.5 ± 0.6 GPa) in the near surface region of the control specimen is caused by strengthening after mechanical polishing. The specimens modified by carbon nanolayer without nitrogen ion assistance (C 40 nm) have maximum hardness values $H_{IT}$ 6.8 ± 0.4 GPa. The specimens with carbon-based nanolayers deposited with the assistance of nitrogen ions (IBAD 20 nm, IBAD 40 nm) have comparable values. The maximum hardness is close to $H_{IT}$ 12.9 ± 0.8 GPa and $H_{IT}$ 12.8 ± 0.7 GPa for specimens IBAD 20 nm and IBAD 40 nm, respectively. Depth profiles are characterized by maximum values with a sharply decreasing trend approaching the hardness values of the control specimen. The influence of titanium alloy substrate is assumed near the interface with nanolayer. The nitrogen enrichment of titanium substrate together with the atomic mixing on the nanolayer/substrate interface led to the formation of hard $TiN_x$ and TiC compounds. The presence of these phases detected by XRD causes specimen hardening with a graphitic nanolayer on top the surface [18, 22]. The results clearly show that specimen C 40 nm has lower hardness in comparison with specimens IBAD 20 nm and IBAD 40 nm. Relatively low hardness of amorphous carbon is well known [44]. The specimens coated with the carbon nanolayers deposited with nitrogen ion bombardment show a hardness increase due to substrate hardening (nitriding, formation of new hard TiN and TiC compounds). The Raman spectra show graphitisation of carbon nanolayers (degradation) after ion implantation (IBAD 20 nm and IBAD 40 nm) which is in accordance with the literature [29, 38]. However, formation of new compound in the titanium alloy surface causes hardening of the substrate at the same time.

Table 2: The results of Raman spectra.

| Layer type | Peak no. 1 Peak position ($cm^{-1}$) | 1 Intensity (a.u.) | 2 Peak position ($cm^{-1}$) | 2 Intensity (a.u.) | 3 Peak position ($cm^{-1}$) | 3 Intensity (a.u.) | Ratio $I(1+2)/I3$ |
|---|---|---|---|---|---|---|---|
| IBAD 20 nm | 1127 ± 15 | (0.818 ± 0.016)E6 | 1385 ± 16 | (4.653 ± 0.044)E6 | 1565 ± 13 | (1.629 ± 0.012)E6 | 3.36 |
| IBAD 40 nm | 1150 ± 16 | (0.721 ± 0.008)E6 | 1402 ± 19 | (4.577 ± 0.009)E6 | 1565 ± 12 | (1.672 ± 0.010)E6 | 3.17 |
| C 40 nm | 1123 ± 11 | (0.539 ± 0.006)E6 | 1394 ± 10 | (4.286 ± 0.011)E6 | 1567 ± 18 | (1.564 ± 0.009)E6 | 3.09 |

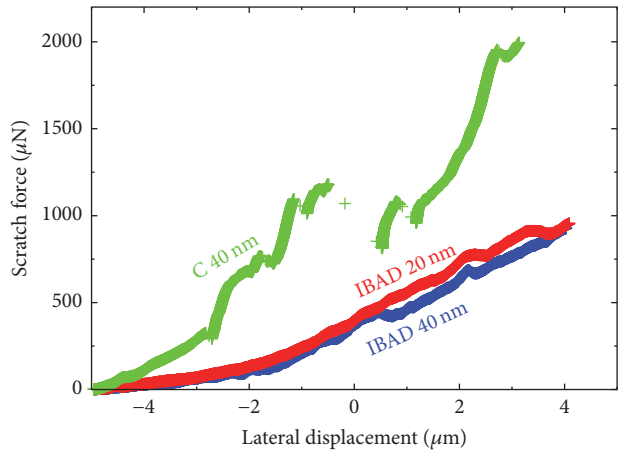


Figure 5: The trend of the scratch force according to the lateral displacement of the tip.

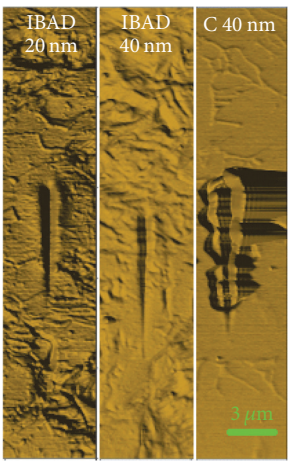


Figure 6: Images of specimen surface after nanoscratch test.

Thus specimens IBAD 20 nm and IBAD 40 nm show higher hardness in comparison with specimen C 40 nm which is consistent with other results. Presented results indicated that high energy ion bombardment causes graphitisation of carbon nanolayer (lubricating layer) and surface hardening of the substrate.

The comparable surface hardness of modified specimens IBAD 20 nm and IBAD 40 nm is given by applied fluence of implanted nitrogen. Applied fluence of implanted ions was $1 \cdot 10^{17}$ $cm^{-2}$ in both types of specimens (IBAD 20 nm and IBAD 40 nm). Many researchers reported that surface hardness of nitrogen implanted titanium materials increases with increasing fluence [16, 33]. Presented results confirm character of hardening which is the formation of new compounds in the substrate due to nitrogen incorporation. Specimen C 40 nm shows approximately comparable hardness with the substrate. Very low thickness of carbon-based nanolayer is on the detection limit of the nanoindentation method. Therefore, hardness profiles in Figure 4 mainly reflect the structural changes in the substrate.

*3.5. Adhesion.* The adhesion of carbon-based nanolayers to a substrate was investigated by nanoscratch testing. Figure 5 presents the typical trends of the scratch force according to the lateral displacement of the tip for the specimens coated by carbon-based nanolayers with ion bombardment (IBAD 20 nm and IBAD 40 nm) and for the specimen coated by a carbon nanolayer without ion bombardment (C 40 nm). The scratch force increases with increasing lateral displacement. A comparison of the curves in Figure 5 shows that the scratch force for the same lateral displacement value is greater for specimen C 40 nm. This indicates easier penetration of the tip into the material which is in agreement with the presented hardness results. The specimens coated by a carbon-based nanolayer with ion bombardment (IBAD 20 nm and IBAD 40 nm) show similar trends. A comparable behaviour is given by a character of substrate hardening. A smooth course of the scratch force along the lateral displacement is observed on specimens coated by carbon-based nanolayers with ion bombardment, while the course of the scratch force on the specimen coated by a carbon nanolayer without ion assistance shows step decrease in the scratch force. The visible jumps (curve discontinuities) indicate delamination of the carbon nanolayer. It is confirmed by the scans of scratches of the tested specimens (Figure 6). The carbon-based nanolayers deposited with ion bombardment show no signs of delamination. It can be assumed that the ion bombardment improved the adhesion of the nanolayers.

*3.6. Coefficient of Friction.* Figure 7 shows the dependence of the coefficient of friction on the number of cycles for the coated specimens (IBAD 20 nm, IBAD 40 nm) and for the control substrate (Ti6Al4V). The lubrication effect of carbon-based nanolayer on Ti6Al4V alloy is demonstrated. The two

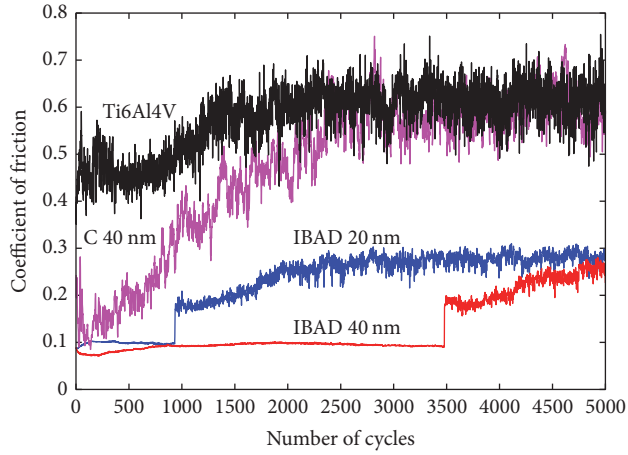


FIGURE 7: Coefficient of friction versus the number of cycles for modified specimens (IBAD 20 nm, IBAD 40 nm) in comparison with coated specimen without ion bombardment (C 40 nm) and unmodified control specimen (Ti6Al4V).

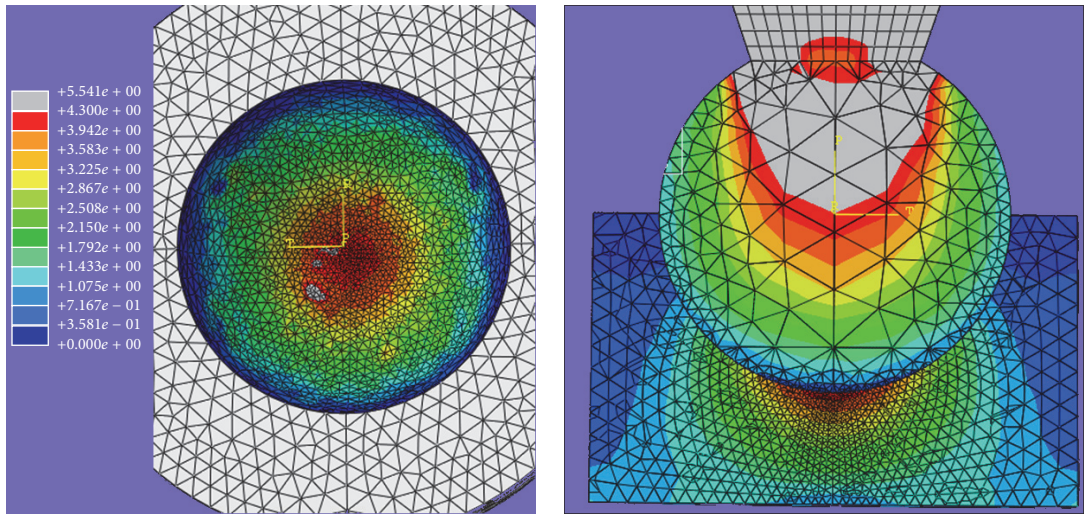


(a) (b)

FIGURE 8: Contact pressure distribution between the PEEK cup (a) and Ti6Al4V head (b) simulated by FEM analysis using the Abaqus program.

surface modifications IBAD 40 nm and IBAD 20 nm have comparable coefficient of friction values of 0.106 ± 0.003 and 0.104 ± 0.005, respectively. Carbon-based nanolayers of both thicknesses show much lower coefficient of friction versus the coefficient of friction of 0.635 ± 0.139 for control Ti6Al4V substrate. A thicker nanolayer (IBAD 40 nm) increased the duration of the lubrication effect by more than three times compared to a thinner nanolayer (IBAD 20 nm). The achieved results are consistent with the results of other research works [22, 45]. Step increasing in the coefficient of friction implies the failure of the thin carbon-based nanolayer on specimens IBAD 20 nm and IBAD 40 nm. However, the coefficient of friction does not reach the value of unmodified substrate as in the case of specimen C 40 nm. Hardened substrate by nitrogen implantation poses friction resistant surface with low friction coefficient, typical for nitrogen ion implanted titanium materials. Gordin et al. [46] observed on nitrogen implanted Ti-Nb-Ta titanium alloy comparable value of coefficient of friction of about 0.3.

*3.7. Contact Pressure Distribution and Joint Wear Simulation.* The distribution of contact pressure was calculated by FEM analysis using the Abaqus program. Figure 8 shows a 3D model of the finger joint with contact pressure distribution (the head (Ti6Al4V) and the cup (PEEK)). The simulation was performed with load force $F = 100$ N and coefficient of friction $\mu = 0.1$. The maximum contact pressure of about 4 MPa was found in the deepest point of the cup under the ideal geometrical shape of the head and cup. Values vary from 0 MPa (around the perimeter of the cup, contact angle of 90°) to $p_{max} \sim 4$ MPa (at the deepest point of the cup). Figure 9 presents the evolution of contact pressure in the cup in dependence on the contact angle for different values of the

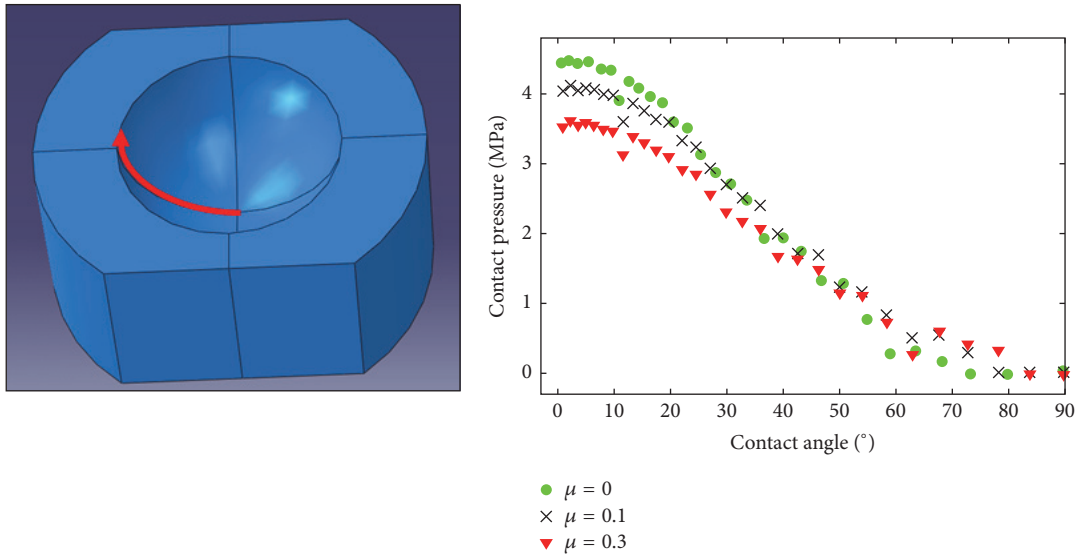


Figure 9: The calculated contact pressure distribution inside the cup of joint: (a) evaluated trajectory, red arrow; (b) the dependence of contact pressure on the contact angle for different value of coefficients of friction.

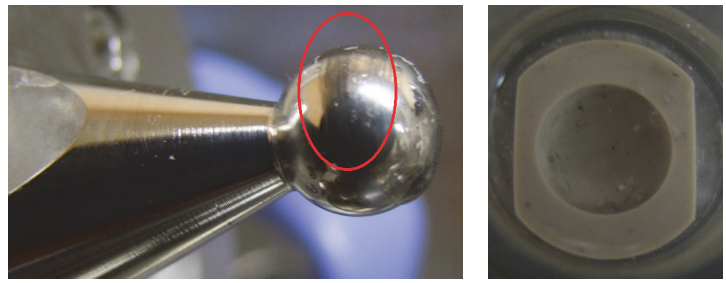

Figure 10: Unmodified Ti6Al4V head and the cup after 10,000 cycles.

coefficient of friction. It is evident that the friction coefficient values affect the course of the contact pressure. The contact pressure varies in dependence on coefficient of friction up to the contact angle of approx. 25° (i.e., in the centre of the cup). Maximum contact pressure decreases with increasing coefficient of friction. Lower values of contact pressure, however, do not mean lower contact stress or transmission of less force. For the higher coefficient of friction, the force transmission is realised mainly through shear stresses instead of normal stresses.

The joint wear simulator (Figure 1) was used for wear evaluation of the Ti6Al4V alloy head modified by carbon-based nanolayer (IBAD 40 nm). The experimental model of a finger joint replacement, the head from modified Ti6Al4V, and the cup from PEEK were used. The appearance of component surfaces tested by sliding test was evaluated qualitatively. The Ti6Al4V head without a modified surface was used as a control. Enormous wear of the head and cup after 10,000 cycles in comparison with the modified Ti6Al4V head is evident (Figure 10). The first wear signs of the IBAD 40 nm nanolayer were observed after 240,000 cycles and were detected only in a local area (Figure 11). More extensive wear occurred after 510,000 cycles.

## 4. Conclusion

The carbon-based nanolayer with nitrogen ion assistance was deposited by IBAD method on the Ti6Al4V substrate. The proposed surface treatment of the titanium alloy, in two thickness variants, leads to an improvement of tribomechanical properties. The formation of $TiN_x$ and TiC compounds in the modified surface area was found. Nitrogen ion bombardment had a more positive effect on higher values of indentation hardness than the layer deposited without ion bombardment. The larger thickness of carbon-based nanolayer improves friction test duration, but no influence on surface hardness was observed. The proposed surface modification (IBAD 40 nm) of the Ti6Al4V joint head provides functional surface protection with a resulting reduction in wear and significant increase in lifetime. This modification of the titanium surface is very promising for biomedical application, especially in an area of load-bearing joint replacements.

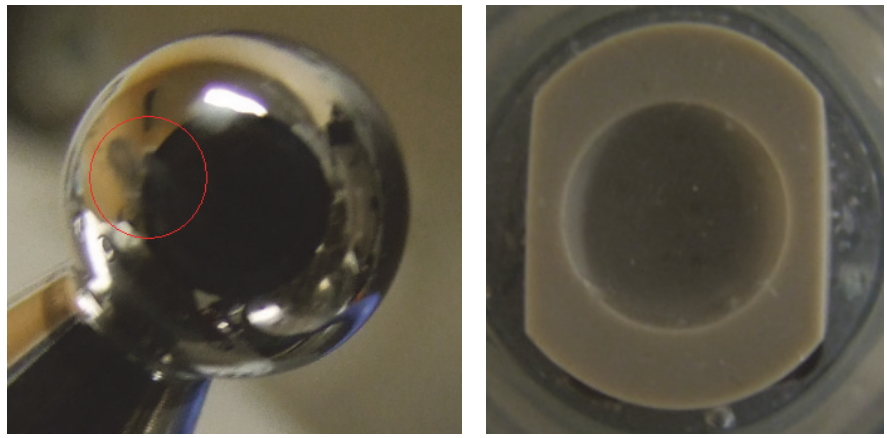

Figure 11: First local wear fault of the IBAD 40 nm modification after 240,000 cycles.

## Conflicts of Interest

The authors declare that there are no conflicts of interest regarding the publication of this paper.

## Acknowledgments

This research has been supported by the Ministry of Education, Youth and Sports of the Czech Republic Project SGS15/186/OHK2/3T/12, the Czech Technical University in Prague Project SGS18/173/OHK2/3T/12, and the Program PROGRES Q29 (Charles University, Czech Republic).

## References

[1] J. Black and G. Hastings, *Handbook of biomaterial properties*, Chapman & Hall, London, 1998.

[2] R. Godley, D. Starosvetsky, and I. Gotman, "Corrosion behavior of a low modulus $\beta$-Ti-45%Nb alloy for use in medical implants," *Journal of Materials Science: Materials in Medicine*, vol. 17, no. 1, pp. 63–67, 2006.

[3] M. Jelínek, P. Vaněk, Z. Tolde et al., "PLD prepared bioactive BaTiO3 films on TiNb implants," *Materials Science and Engineering C: Materials for Biological Applications*, vol. 70, pp. 334–339, 2017.

[4] R. Huiskes, H. Weinans, and B. Van Rietbergen, "The relationship between stress shielding and bone resorption around total hip stems and the effects of flexible materials," *Clinical Orthopaedics and Related Research*, vol. 274, pp. 124–134, 1992.

[5] B. Piotrowski, A. A. Baptista, E. Patoor, P. Bravetti, A. Eberhardt, and P. Laheurte, "Interaction of bone-dental implant with new ultra low modulus alloy using a numerical approach," *Materials Science and Engineering C: Materials for Biological Applications*, vol. 38, no. 1, pp. 151–160, 2014.

[6] C. C. Gomes, L. M. Moreira, V. J. S. V. Santos et al., "Assessment of the genetic risks of a metallic alloy used in medical implants," *Genetics and Molecular Biology*, vol. 34, no. 1, pp. 116–121, 2011.

[7] M. Geetha, A. K. Singh, R. Asokamani, and A. K. Gogia, "Ti based biomaterials, the ultimate choice for orthopaedic implants—a review," *Progress in Materials Science*, vol. 54, no. 3, pp. 397–425, 2009.

[8] M. Niinomi, Y. Liu, M. Nakai, H. Liu, and H. Li, "Biomedical titanium alloys with Young's moduli close to that of cortical bone," *Regenerative Biomaterials*, vol. 3, no. 3, pp. 173–185, 2016.

[9] I. V. Okulov, A. S. Volegov, H. Attar et al., "Composition optimization of low modulus and high-strength TiNb-based alloys for biomedical applications," *Journal of the Mechanical Behavior of Biomedical Materials*, vol. 65, pp. 866–871, 2017.

[10] M. Fischer, P. Laheurte, P. Acquier et al., "Synthesis and characterization of Ti-27.5Nb alloy made by CLAD® additive manufacturing process for biomedical applications," *Materials Science and Engineering C: Materials for Biological Applications*, vol. 75, pp. 341–348, 2017.

[11] A. Mishra, "Analysis of friction and wear of titanium alloys," in *Proceedings of the International Journal of Mechanical Engineering and Robotics Research*, vol. 3, pp. 570–573, 2014.

[12] S. Podzimek, M. Tomka, T. Nemeth, L. Himmlova, P. Matucha, and J. Prochazkova, "Influence of metals on cytokines production in connection with successful implantation therapy in dentistry," *Neuroendocrinology Letters*, vol. 31, no. 5, pp. 657–662, 2010.

[13] A. V. Lombardi Jr., T. H. Mallory, B. K. Vaughn, and P. Drouillard, "Aseptic loosening in total hip arthroplasty secondary to osteolysis induced by wear debris from titanium-alloy modular femoral heads," *Journal of Bone and Joint Surgery—American Volume*, vol. 71, no. 9, pp. 1337–1342, 1989.

[14] P. A. Lalor, P. A. Revell, A. B. Gray, S. Wright, G. T. Railton, and M. A. R. Freeman, "Sensitivity to titanium. A cause of implant failure?" *The Journal of Bone & Joint Surgery (British Volume)*, vol. 73, no. 1, pp. 25–28, 1991.

[15] K. Müller and E. Valentine-Thon, "Hypersensitivity to titanium: Clinical and laboratory evidence," *Neuroendocrinology Letters*, vol. 27, no. 1, pp. 31–35, 2006.

[16] A. Zhecheva, W. Sha, S. Malinov, and A. Long, "Enhancing the microstructure and properties of titanium alloys through nitriding and other surface engineering methods," *Surface and Coatings Technology*, vol. 200, no. 7, pp. 2192–2207, 2005.

[17] R. P. Van Hove, I. N. Sierevelt, B. J. Van Royen, and P. A. Nolte, "Titanium-Nitride Coating of Orthopaedic Implants: A Review of the Literature," *BioMed Research International*, vol. 2015, Article ID 485975, 2015.

[18] V. J. Trava-Airoldi, L. F. Bonetti, G. Capote, L. V. Santos, and E. J. Corat, "A comparison of DLC film properties obtained by r.f.

PACVD, IBAD, and enhanced pulsed-DC PACVD," *Surface and Coatings Technology*, vol. 202, no. 3, pp. 549–554, 2007.

[19] J. P. Davim and F. Mata, "Chemical vapour deposition (CVD) diamond coated tools performance in machining of PEEK composites," *Materials and Corrosion*, vol. 29, no. 8, pp. 1568–1574, 2008.

[20] G.-G. Wang, H.-Y. Zhang, W.-Y. Li et al., "The preparation and evaluation of graded multilayer ta-C films deposited by FCVA method," *Applied Surface Science*, vol. 257, no. 11, pp. 5064–5069, 2011.

[21] S. A. Ahmad Kamal, R. Ritikos, and S. Abdul Rahman, "Wetting behaviour of carbon nitride nanostructures grown by plasma enhanced chemical vapour deposition technique," *Applied Surface Science*, vol. 328, pp. 146–153, 2015.

[22] P. Vlcak and I. Jirka, "Protective sliding carbon-based nanolayers prepared by argon or nitrogen ion-beam assisted deposition on Ti6Al4V alloy," *Journal of Nanomaterials*, vol. 2016, Article ID 1697090, 9 pages, 2016.

[23] H. Huang, X. Wang, and J. He, "Synthesis and properties of graphite-like carbon by ion beam-assisted deposition," *Materials Letters*, vol. 57, no. 22-23, pp. 3431–3436, 2003.

[24] P. Ren, E. Pu, D. Liu, Y. Wang, B. Xiang, and X. Ren, "Fabrication of nitrogen-doped graphenes by pulsed laser deposition and improved chemical enhancement for Raman spectroscopy," *Materials Letters*, vol. 204, pp. 65–68, 2017.

[25] R. J. Narayan, "Pulsed laser deposition of functionally gradient diamondlike carbon-metal nanocomposites," *Diamond and Related Materials*, vol. 14, no. 8, pp. 1319–1330, 2005.

[26] I. N. Mihailescu, D. Bociaga, G. Socol et al., "Fabrication of antimicrobial silver-doped carbon structures by combinatorial pulsed laser deposition," *International Journal of Pharmaceutics*, vol. 515, no. 1-2, pp. 592–606, 2016.

[27] D. F. Wang, K. Kato, and N. Umehara, "Mechanical characterization and tribological evaluation of ion-beam-assisted sputter coatings of carbon with nitrogen incorporation," *Surface and Coatings Technology*, vol. 123, no. 2-3, pp. 177–184, 2000.

[28] P. Vlcak, F. Cerny, Z. Weiss et al., "The effect of nitrogen ion implantation on the surface properties of Ti6Al4V alloy coated by a carbon nanolayer," *Journal of Nanomaterials*, vol. 2013, Article ID 475758, 8 pages, 2013.

[29] P. Vlcak, "The effect of ion irradiation and elevated temperature on the microstructure and the properties of C/W/C/B multilayer coating," *Applied Surface Science*, vol. 365, pp. 306–313, 2016.

[30] P. Vlcak, J. Sepitka, T. Horazdovsky, I. Jirka, I. Gregora, and M. Nemec, "Nanomechanical testing of an a-C:N nanolayer prepared by ion beam assisted deposition on Ti6Al4V alloy," in *Proceedings of the 7th International Conference on Nanomaterials - Research and Application, NANOCON 2015*, pp. 68–72, cze, October 2015.

[31] P. Vlcak, J. Drahokoupil, P. Vertat, J. Sepitka, and J. Duchon, "Hardness response to the stability of a Ti(+N) solid solution in an annealed TiN/Ti(+N)/Ti mixture layer formed by nitrogen ion implantation into titanium," *Journal of Alloys and Compounds*, vol. 746, pp. 490–495, 2018.

[32] H. Schmidt, A. Schminke, M. Schmiedgen, and B. Baretzky, "Compound formation and abrasion resistance of ion-implanted Ti6Al4V," *Acta Materialia*, vol. 49, no. 3, pp. 487–495, 2001.

[33] P. Vlcak, F. Cerny, J. Drahokoupil, J. Sepitka, and Z. Tolde, "The microstructure and surface hardness of Ti6Al4V alloy implanted with nitrogen ions at an elevated temperature," *Journal of Alloys and Compounds*, vol. 620, pp. 48–54, 2015.

[34] P. Vlcak, T. Horazdovsky, R. Valenta, and J. Kovac, "Evolution of the nitrogen depth distribution in an implanted titanium alloy with a surface carbon nanolayer," *Chemical Physics Letters*, vol. 679, pp. 25–30, 2017.

[35] Z. Weiss and P. Vlcak, "Analysis of shallow depth profiles of titanium nitride and N-implanted titanium by GD-OES: The 'hydrogen effect' after the discharge startup and a correction thereof," *Journal of Analytical Atomic Spectrometry*, vol. 32, no. 12, pp. 2476–2484, 2017.

[36] M. M. Morshed, B. P. McNamara, D. C. Cameron, and M. S. J. Hashmi, "Stress and adhesion in DLC coatings on 316L stainless steel deposited by a neutral beam source," *Journal of Materials Processing Technology*, vol. 143-144, no. 1, pp. 922–926, 2003.

[37] Y. Funada, K. Awazu, K. Shimamura, and M. Iwaki, "Thermal properties of DLC thin films bombarded with ion beams," *Surface and Coatings Technology*, vol. 103-104, pp. 389–394, 1998.

[38] J. Robertson, "Diamond-like amorphous carbon," *Materials Science and Engineering: R: Reports*, vol. 37, pp. 129–282, 2002.

[39] J. Robertson, "Deposition mechanisms for promoting sp3 bonding in diamond-like carbon," *Diamond and Related Materials*, vol. 2, no. 5-7, pp. 984–989, 1993.

[40] P. A. Karaseov, O. A. Podsvirov, A. I. Titov et al., "Effect of ion bombardment on the phase composition and mechanical properties of diamond-like carbon films," *Journal of Surface Investigation. X-ray, Synchrotron and Neutron Techniques*, vol. 8, no. 1, pp. 45–49, 2014.

[41] P. Písařík, M. Jelínek, T. Kocourek et al., "Influence of diamond and graphite bonds on mechanical properties of DLC thin films," *Journal of Physics: Conference Series*, vol. 594, no. 1, Article ID 012008, 2015.

[42] L. Han, D. Liu, X. Chen, L. Yang, and Y. Zhao, "The deposition of a thick tetrahedral amorphous carbon film by argon ion bombardment," *Applied Surface Science*, vol. 258, no. 10, pp. 4794–4800, 2012.

[43] S. Wei, T. Shao, and J. Xu, "Effect of bombarding energy of N ions on composition, hardness and surface free energy of carbon nitride films," *Surface and Coatings Technology*, vol. 206, no. 19-20, pp. 3944–3948, 2012.

[44] S. Neuville and A. Matthews, "A perspective on the optimisation of hard carbon and related coatings for engineering applications," *Thin Solid Films*, vol. 515, no. 17, pp. 6619–6653, 2007.

[45] G. Popescu-Pelin, D. Craciun, G. Socol et al., "Investigations of pulsed laser deposited tin thin films for titanium implants," *Romanian Reports in Physics*, vol. 67, no. 4, pp. 1491–1502, 2015.

[46] D. M. Gordin, D. Busardo, A. Cimpean et al., "Design of a nitrogen-implanted titanium-based superelastic alloy with optimized properties for biomedical applications," *Materials Science and Engineering C: Materials for Biological Applications*, vol. 33, no. 7, pp. 4173–4182, 2013.

Hindawi
Journal of Nanomaterials
Volume 2018, Article ID 4718045, 11 pages
https://doi.org/10.1155/2018/4718045

*Research Article*

# Preparation and Drug Release Study of Novel Nanopharmaceuticals with Polysorbate 80 Surface Adsorption

**Xiaojun Tao,[1] Yu Li,[1] Qian Hu,[1] Li Zhu,[1] Zixuan Huang,[1] Jiajin Yi,[1] Xiaoping Yang,[1] Jianzhuo Hu,[2] and Xing Feng[1]**

[1]*Key Laboratory of Study and Discovery of Small Targeted Molecules of Hunan Province, School of Medicine, Hunan Normal University, Changsha 410013, China*
[2]*The First Hospital of University of Chinese Medicine, Changsha 410007, China*

Correspondence should be addressed to Xing Feng; fengxing01@hotmail.com

Received 13 December 2017; Revised 16 April 2018; Accepted 24 April 2018; Published 20 May 2018

Academic Editor: Mauro Pollini



Most free drugs that cross the blood–brain barrier are characterized by high liposolubility, but they often have limited clinical applications because of poor dissolution and poor bioavailability. In this study, we prepared donepezil drug-loaded nanoparticles (DZP) with cholesterol-modified pullulan (CHP) as the nanocarrier (DZP-CHP) and surface modified the drug-loaded nanoparticles to improve the water solubility of donepezil while enhancing its targeting and sustained release. We determined the drug loading and encapsulation efficiency of DZP-CHP nanoparticles at different feed ratios. The mean ± SD drug loading and entrapment efficiency were high: $13.52 \pm 2.03$ and $86.54 \pm 1.31$. On dynamic light-scattering measurement, mean ± SD particle size was $260.7 \pm 1.76$ nm, polydispersity index $0.123 \pm 0.004$, and zeta potential $-5.75 \pm 0.64$ mV. DZP-CHP nanoparticles prepared with the optimal feed ratio (DZP : CHP = 1 : 5) were coated with polysorbate 80, and the adsorption process was determined by isothermal titration calorimetry. We found good affinity between polysorbate 80 and DZP-CHP, with mean ± SD coverage $2.7 \pm 0.372$. The mean ± SD drug loading and entrapment efficiency of polysorbate 80-emulsified DZP-CHP nanoparticles were $8.25 \pm 1.80$ and $91.28 \pm 4.57$, respectively, and the proportion of drug released by 72 h was 42.71%. Compared to DZP-CHP alone, PS-DZP-CHP can enhance the release of donepezil.

## 1. Introduction

Research hot topics in the drug field are to design drug preparations with high-efficiency delivery [1–3]. Oral solid drugs released from the formulation and dissolved in body fluid is the premise of absorption, so with poor dissolution, drug absorption in vivo is slow and with low bioavailability, therefore not reaching the therapeutic level of plasma concentration and poor clinical treatment [4, 5]. Fat-soluble drugs more easily cross the blood–brain barrier for a pharmacological effect [6]. In preparing conventional formulations for craniocerebral diseases, increasing the drug solubility often requires a number of drug additions, which results in toxicity. Currently, about 40% of clinically used drugs have limited use because of poor dissolution [7, 8].

In recent years, the emergence of nanoformulations for injection has brought hope to solving the problem of drug delivery of fat-soluble drugs. Nanoparticles (NPs) represent a micropectin system composed of nanospheres or nanocapsules with particle size typically $<1\,\mu$m [9] Because of the small particle size and large specific surface area of NPs, the solubility and dissolution rate of insoluble drugs can be increased after drug loading [10]. Also, with the preparation and surface modification of biomaterials with specific properties, the NPs can feature long circulation and controlled release [11, 12]. Targeted delivery and reduced dose ensure efficacy and reduce side effects.

In this study, we used donepezil, a clinically important drug for treating Alzheimer's disease, with poor solubility [13] to develop a new type of nanostructured drug. Donepezil is fat-soluble, poorly dissolved in the body, and generally taken orally; with poor drug absorption and low bioavailability, the drug has no tissue-specific, toxic side effects on the peripheral nervous system, and its clinical application is

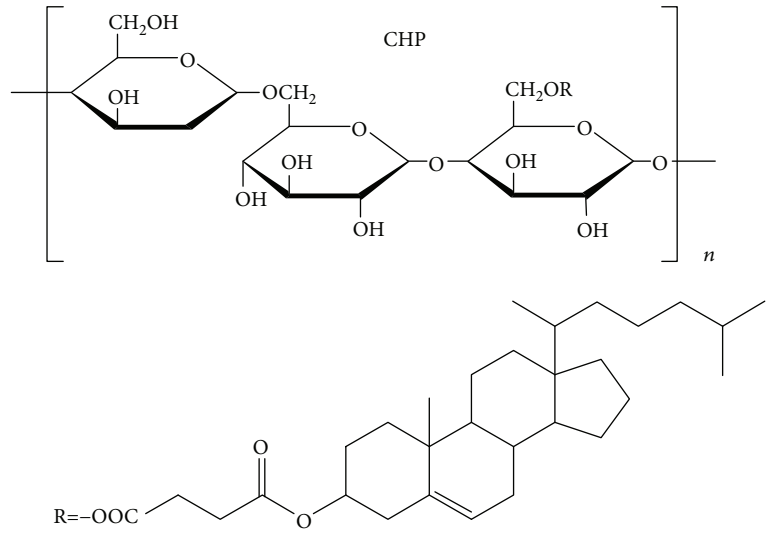


Figure 1: The chemical structure of CHP.

limited. In addition, conventional Aricept should be taken daily to maintain the therapeutic effect. However, in Alzheimer's patients, with the progression of the disease to a certain stage, the lack of memory of daily medication on a daily basis is an obstacle to the use of donepezil. We need new types of preparations to overcome these deficiencies.

Pullulan, an exopolysaccharide produced by budding short sporophore enzymes, is nontoxic and biodegradable [14, 15]. Cholesterol hydrophobically modified pullulan (CHP) is an amphipathic substance that self-assembles in aqueous solution into nanostructures with a shell of cholesteric hydrophobe and sugar-chain hydrophilicity [16] (Figure 1). CHP NPs can form a complex with A$\beta$ protein, effectively preventing protein aggregation, and can be quickly cleared from cells, which strongly inhibit cytotoxicity and provide a basis for the selection of nanomaterials [17]. Donepezil, as a strong hydrophobic drug, can be loaded into the hydrophobic center of CHP NPs to form a donepezil nanopreparation (DZP-CHP). Although nanopharmaceutical formulations have some passive targeting due to their small-size properties, the surface must be modified to achieve precise, tissue-specific targeting.

Polysorbate 80 is a common nonionic surfactant. The fatty acid chain (hydrophobic) and ethylene oxide units (hydrophilic) provide its amphiphilic properties. Polysorbate 80 has features of hydrophilicity, nonionicity, biodegradability, and nontoxicity to cells at low concentration and is easy to obtain. Therefore, it is widely used for the distribution of substances in food and drug products [18–20]. Numerous studies have found that it can be applied to the NP surface and can cross the blood–brain barrier through receptor-mediated endocytosis or other mechanisms and enhance drug-targeted delivery to the central brain for an enhanced targeted therapeutic effect [21–23]. In addition, the hydrophilic and hydrophobic portions of the nonionic surfactant from the polysorbate family are involved in the interaction, and their coating directly inhibits the reticuloendothelial system and thus helps to prolong the circulation time of NPs in the body [24, 25]. Polysorbate 80 also has a sustained-release effect [26].

Here we investigated the use of CHP NPs loaded with donepezil, then added polysorbate 80, and used isothermal titration calorimetry (ITC) to confirm that polysorbate 80 can be successfully adsorbed on the CHP NP surface and achieve the desired rate of adsorption. We aimed to provide the experimental basis for the research of new dosage forms of drugs for Alzheimer's disease.

## 2. Materials and Methods

*2.1. Materials.* The materials used are the following: constant temperature magnetic stirrer (IKA RCT basic, Germany), vacuum freeze dryer (Maxi Dry Lyo, Heto-Holten), transmission electron microscope (TEM) (JIEM-100S Japan), nanoparticle size and zeta potential analyzer (Malvern ZS-90, Britain); UV-vis spectrophotometer (JASCO V-560, USA); isothermal titration calorimeter (VP-ITC, Microcal Inc., Northampton, MA), dialysis bags (molecular weight cutoff 8 to 12 KDa, Germany), cholesterol hydrophobic modified pullulan (homemade), donepezil (Donepezil, Shanghai Ziqi Biological Technology Co. Ltd.), polysorbate 80 (Polysorbate-80, Tianjin Fuchen Reagent Institute). The remainder of the reagents was domestic analytical reagent.

*2.2. Methods*

*2.2.1. Dialysis Preparation of CHP and DZP-CHP NPs.* As we previously described [27, 28], dialysis was used to prepare NPs. We used 20 mg graft polymer CHP polymer dissolved in 2 ml DMSO solvent. The solution was transferred to a dialysis bag (MWCO 8–12 kDa) and placed in 1 l distilled water. The water was changed every 3 h in the first 12 h of dialysis and every 6 h in the 12 h after dialysis for a total of 24 h.

4 mg DZP and 20 mg CHP were dissolved in an appropriate amount of DMSO and triethylamine (TEA/DZP = 2, mmol/mmol) was added; the drug and the material solution

were thoroughly mixed in a ratio of 1 : 5, using the above method to prepare drug-loaded NPs. When the DMSO dialysis was clean, the solution was removed, then was treated with an ultrasound probe (50 W) for 2 min, and volume fixed in a 10 ml volumetric flask, then filtered with a 0.45 $\mu$m filter to obtain CHP and DZP-CHP NPs, which were stored at 4°C.

*2.2.2. Preparation of the Standard Curve of the Donepezil.* 5 mg reference substance of donepezil was accurately weighed and added to the solution, dissolved with DMSO and diluted to 1 $\mu$g/ml. The maximal ultraviolet absorption wavelength was detected by scanning in the 200 to 400 nm wavelength range with DMSO as a blank control.

An amount of 1 mg donepezil was added to a 10 ml volumetric flask, dissolved, and fixed to scale with DMSO, to obtain 100 $\mu$g/ml standard stored solution. An appropriate amount was diluted with DMSO to 5, 10, 15, 20, and 25 $\mu$g. With the DMSO solution as the control, the absorbance was measured at the maximum absorption wavelength, with absorbance $A$ as the ordinate and concentration $C$ as the abscissa to obtain a regression equation.

*2.2.3. Isothermal Titration Calorimetry (ITC).* A concentration of polysorbate 80 solution was dropped into the DZP-CHP NP solution, and the isothermal droplet calorimeter was used to measure its thermal change. An amount of 80 ml polysorbate was injected into the NP titration pool containing DZP-CHP for titration 20 times, 4 ml each. The temperature of the droplet was set to 25°C, and the thermodynamic parameters and connection curves were obtained by 20 times titration.

*2.2.4. Polysorbate 80 Emulsification of DZP-CHP NPs.* A concentration of DZP-CHP was placed in a 10 ml beaker and aspirated into a polysorbate 80 (PS) emulsifier beaker containing 0.7 mmol for 1 h. The mixed solution was placed in the EP tube, then treated for 3 min with the ultrasound probe (output power: 100, intermittent pulse working mode: pulse width 2.0 s, intermittent time 2.0 s), with repeated operation three times until uniform dispersion, then filtered with a filtration membrane to remove impurities and obtain polysorbate 80-emulsified DZP-CHP NPs (PS-DZP-CHP).

*2.2.5. Measurement of NP Size, Zeta Potential, and Morphology Observation.* The size, polydispersity index (PDI), and zeta potential of CHP, DZP-CHP, and PS-DZP-CHP NPs were measured by use of the Malvern ZS-90 system. The morphology of the particles was evaluated by TEM, and the newly prepared CHP, DZP-CHP, and PS-DZP-CHP water solutions were dropped on a carbon-supporting copper net. After drying, dyeing with the phosphotungstic acid, and natural drying again, the sample was observed by using TECNAI Spirit (120 kV) TEM (FEL, Hong Kong). The freeze-dried NPs were dissolved in pure water, added to clean silicon wafers and dried at room temperature, and the surface structure was observed by scanning electron microscopy.

*2.2.6. Determination of the Drug Loading Capacity (LC) and Encapsulation Efficiency (EE) of DZP-CHP and PS-DZP-CHP.* The determination of the drug loading capacity (LC) and encapsulation efficiency (EE) of DZP-CHP and PS-DZP-CHP follows Tao et al. [16]. For 4 ml freshly prepared DZP-CHP and PS-DZP-CHP NPs, absorbance was determined at 312 nm by spectrophotometry. The same solvent with blank CHP was a control. The drug content was calculated according to the standard curve, then the loading and encapsulation rate were obtained as follows:

$$\text{Loading capacity (LC\%)} = \frac{\text{the amount of DZP in the NPs}}{\text{weight of NPs}},$$
$$\text{Encapsulation efficiency (EE\%)} = \frac{\text{the amount of DZP in the NPs}}{\text{total amount of DZP}}. \quad (1)$$

*2.2.7. Release of DZP-CHP and PS-DZP-CHP NPs In Vitro.* Using the dialysis bag diffusion technique [29] to measure the release of donepezil, 1 mg DZP-CHP and PS-DZP-CHP NPs were dissolved in 5 ml 0.01 M phosphate buffer solution (pbs, ph 7.4), then transferred to a dialysis bag (MWCO 8–12 kDa) and placed in the same PBS solution at 37°C with constant temperature and magnetic stirring. An amount of 4 ml solution was removed at 0, 0.5, 1, 2, 4, 8, 12, 24, 48, and 72 h. An amount of 4 ml fresh PBS was added with the same pH at the same time. UV-vis spectrophotometry was used to determine the absorbance of dialysis solution of different times at 312 nm; the content of the solution was determined by the standard curve, and the release test was repeated three times in vitro.

$$Q\% = \frac{\left(C_n \times V + V_n \sum_{i=0}^{i=n} C_i\right)}{W_{\text{drug loading}}}, \quad (2)$$

where $C_n$ is the sample concentration at $T_n$ ($\mu$g/ml), $V$ is the release volume of the medium at $T_i$ (ml), and $C_i$ is the sample concentration at $T_i$ ($\mu$g/ml).

In addition, we changed the PBS release media to FBS release media at a certain concentration and analyzed the drug release of PS-DZP-CHP NPs. An amount of FBS solution (0.1 mg/ml) was added to the dialysis bag to measure the drug release of PS-DZP-CHP NPs. A weight ratio of donepezil to FBS of 1 : 10 was prepared to obtain nanoparticle-drug-FBS complex, and the mixture solution was dialyzed against 1000 ml distilled solution for 6 h to remove free donepezil. Then, we measured the drug release as described previously.

*2.3. Statistical Analysis.* Data are presented as mean ± SD and were analyzed by Student $t$-test or ANOVA for multiple samples with the use of SPSS 12.0. $P < 0.5$ was considered statistically significant.

## 3. Results

*3.1. Determining the Standard Curve of Donepezil.* To determine the drug loading and entrapment efficiency of drug-loaded NPs, we established a standard curve for donepezil. UV scan 1 showed maximum absorption of donepezil at wavelengths 270 and 312 nm, and the larger value of 312 nm was selected as the detection wavelength to minimize

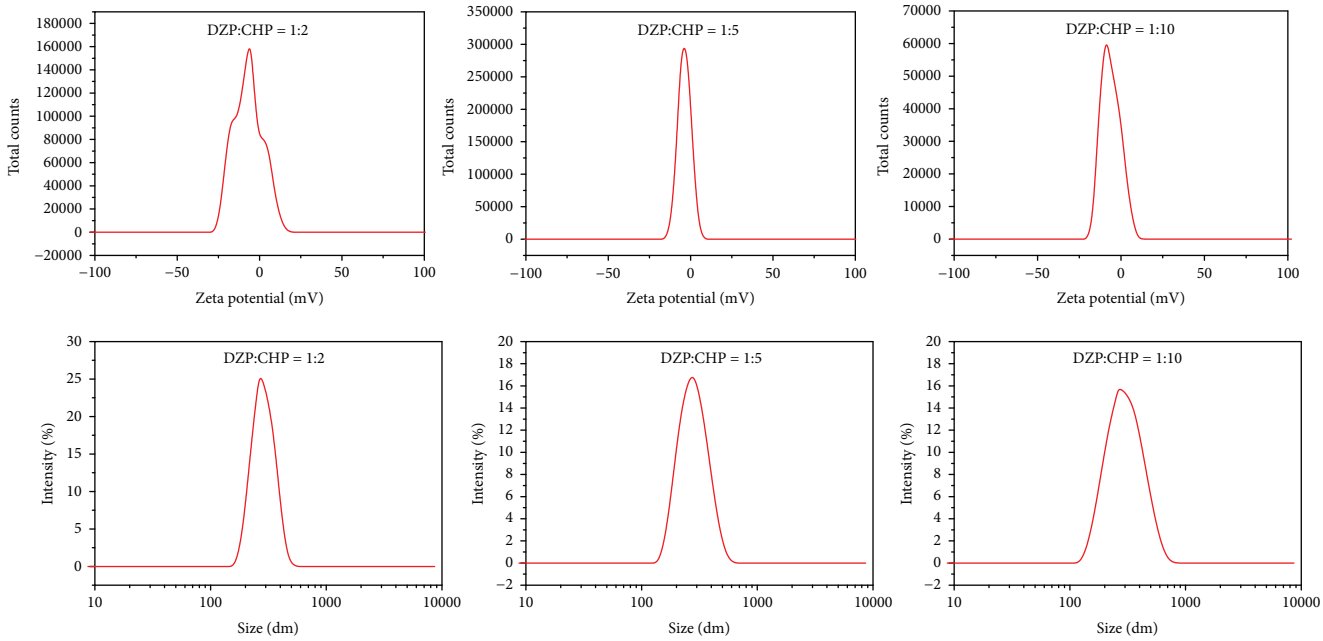


Figure 2: Potential change and particle size distribution of DZP-CHP NPs at different feed ratios.

Table 1: Particle size, polydispersity index (PDI), zeta potential, drug loading, and entrapment efficiency of CHP NPs at different feed ratios (1 : 2, 1 : 5, and 1 : 10).

| Feed ratio | Particle size (nm) | PDI | Zeta potential (mV) | Drug loading (%) | Encapsulation efficiency (%) |
|---|---|---|---|---|---|
| 1 : 2 | 273.3 ± 3.72 | 0.138 ± 0.013 | −6.20 ± 0.40 | 12.02 ± 1.90 | 42.00 ± 5.65 |
| 1 : 5 | 260.7 ± 1.76 | 0.123 ± 0.004 | −5.75 ± 0.64 | 13.42 ± 2.03 | 86.54 ± 1.31 |
| 1 : 10 | 266.8 ± 4.56 | 0.196 ± 0.019 | −9.30 ± 0.39 | 7.40 ± 1.72 | 59.71 ± 4.43 |

measurement errors. The standard curve was drawn with the concentration of donepezil standard solution as the abscissa and absorbance value as the ordinate, with standard curve equation $Y = -0.00373 + 0.01574X$. We found a linear relationship between concentration and absorbance in the concentration range of 0–30 $\mu$g/ml, with correlation coefficient 0.99885, which met the requirements.

*3.2. Relation between Particle Size, Zeta Potential, Drug Loading, and Entrapment Efficiency of DZP-CHP NPs and Feed Ratio.* The prepared CHP NPs were loaded with donepezil according to different feed ratios, and particle size and zeta potential were measured by dynamic light scattering. At feed ratios 1 : 2, 1 : 5, and 1 : 10, the mean ± SD NP size was 273.3 ± 3.72, 260.7 ± 1.76, 266.8 ± 4.56 nm, respectively, and PDI was 0.138 ± 0.013, 0.123 ± 0.004, 0.196 ± 0.019, respectively (Figure 2). The distribution of NP size was uniform, and the feed ratio was 1 : 5 with the smallest PDI and the most uniform distribution. The feed ratio 1 : 2 led to the largest NP size, which may be due to the too small amount of hydrophobic donepezil in the hydrophobic center of NPs and too weak hydrophobic interactions between the hydrophobic ends of the NPs and hydrophobic drugs during the self-assembly process, thereby resulting in the aggregation and a too large particle size. The results of particle size distribution are also consistent with this suggestion, showing the smallest NPs at feed ratio 1 : 5, which indicates that the formed NPs are more stable and uniform at this feed ratio.

We measured the absorbance of the drug-loaded NPs at 312 nm. The drug concentration was calculated by the standard curve of the concentration of donepezil to the absorbance, and the drug loading and entrapment efficiency of DZP-CHP NPs were calculated as described in Materials and Methods. With feed ratios of 1 : 2, 1 : 5, and 1 : 10, the mean ± SD drug loading of drug-loaded NPs was 12.02 ± 1.90%, 13.42 ± 2.03%, and 7.40 ± 1.72%, respectively, and the entrapment efficiency was 42.00 ± 5.65%, 86.54 ± 1.31%, and 59.71 ± 4.43%, respectively (Table 1). The drug loading and encapsulation efficiency of DZP-CHP NPs peaked at feed ratio 1 : 5. Therefore, this NP-loaded donepezil can provide better drug loading and encapsulation efficiency, with the best feed ratio about 1 : 5. The drug loading and entrapment efficiency of CHP NPs were saturated: when the mass ratio of drug to CHP NP exceeded a certain amount, the larger the feed ratio, the smaller the drug loading and entrapment efficiency of the NPs. Our results show an ideal feed ratio of CHP to donepezil of 1 : 5, so we chose DZP-CHP with a feed ratio of 1 : 5 for the next step.

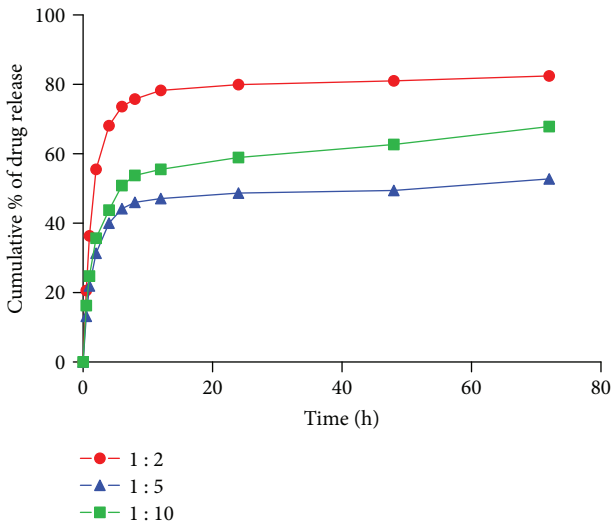


Figure 3: Release curves of donepezil from DZP-CHP NPs in phosphate buffered saline (PBS) at 37°C in vitro at different feed ratios. 1 : 2, 1 : 5, 1 : 10.

*3.3. Relation between Drug Release of DZP-CHP NPs In Vitro and Feed Ratio.* The dissolution curve of DZP-CHP NPs in distilled water at different feed ratios is shown in Figure 3. There are two stages in the drug release process of drug-loaded NPs: the initial stage with a rapid release (phase I), followed by a sustained long-term slow release (phase II). The possible reasons for this release characteristic are related to the presence of donepezil in DZP-CHP NPs. Some drugs are adsorbed on the surface of DZP-CHP self-aggregated NPs by a weak interaction, whereas most drugs and cholesterol in DZP-CHP molecules enter the hydrophobic core of NPs by hydrophobic interaction. The rapid release of the drug by the intermolecular hydrogen bonding on the surface sugar chain of CHP NPs causes the rapid release of phase I, whereas the slow diffusion of drug entrapped in the hydrophobic core of the particle leads to the slow release of phase II.

We observed different loading and encapsulation efficiency at different feed ratios. The drug entrapment in the NP core increases, and the drug adsorption on the surface decreases because the rapid release of drug phase I is weakened and the phase II slow release is enhanced. This is shown with DZP-CHP NPs at feed ratio 1 : 5 in Figure 4, which is consistent with its results of the highest entrapment efficiency. The particle size of NPs also affects the drug release rate. In general, with NPs with the same kind of carrier material, the smaller the particle size, the larger the interfacial area, and the release rate is higher. DZP-CHP (1 : 5) with the smallest particle size had the slowest release rate, whereas DZP-CHP (1 : 2) with the largest particle size had the fastest release rate. The possible reason is that DZP-CHP (1 : 5) with the strongest hydrophobic interaction, gathered closely, is in a more stable state, for slower internal drug release. The release rate of DZP-CHP (1 : 2) is the opposite, which is consistent with the previous results of particle size.

*3.4. Thermodynamic Analysis of the Effect of DZP-CHP NPs on Polysorbate 80.* ITC is often used to measure the connection properties of two substances. Because of the heat generated or absorbed during material binding, the change in the heat of the reaction system can be measured by titrating the polysorbate 80 into the solution of the DZP-CHP NPs to reflect the conjugation of the two. In Figure 5, 4 ml of Tween 80 was added to produce a corresponding endothermic peak; with an increase in number of drops, the peak gradually decreased. With the 15th drop, the peak value reversed and became an exothermic peak pointed downwards. Mean ± SD data are as follows: coverage, $2.70 \pm 0.372$; $K_A$ ($10^5$/M), $2.98 \pm 1.66$; $\triangle H$ (cal/mol), $1710 \pm 311.4$; and $\triangle S$ (cal/mol/deg), 30.8 (Table 2). During the dropping of polysorbate 80 molecules into the CHP NP solution, polysorbate 80 is adsorbed onto the surface of the CHP NP. Figure 5 shows that the adsorption of polysorbate 80 to the surface of DZP-CHP NPs is an endothermic process [13], and the faint exothermic peak at the tail may be due to polysorbate 80 reacting with donepezil adhered to the NP surface or some of the drug being released and dissolved in polysorbate 80 [18]. According to the Gibbs free energy formula, the result is $\triangle G < 0$, which indicates that the reaction is a spontaneous reaction. $K_A$ ($10^5$/M) was $2.98 \pm 1.66$, which indicates good affinity between the two. The coverage was $2.7 \pm 0.372$, so about 2.7 polysorbate 80 molecules could be adsorbed on the surface of one CHP. Since one CHP NP consisted of several CHPs, polysorbate 80 had better coverage on the surface of CHP NPs.

*3.5. Characterization of CHP, DZP-CHP, and PS-DZP-CHP NPs.* From TEM (×30000) (Figure 6), the prepared CHP, DZP-CHP, and PS-DZP-CHP NPs were uniform and spherical. From Table 3 and Figure 4, the mean ± SD diameter of DZP-CHP NPs before and after drug loading was $257.5 \pm 3.05$ and $266.3 \pm 4.46$, respectively, and the NP size was relatively uniform with mean ± SD dispersion index $0.169 \pm 0.020$ and $122 \pm 0.01$. The size of microspheres changed a little before and after drug loading, but the particle size was increased after emulsification, to a mean ± SD of $335.2 \pm 5.46$. Positively or negatively charged NPs exhibit more drug release than do neutral NPs [30]. The mean zeta potential increased from $-2.81 \pm 0.27$ to $-0.66 \pm 0.04$ mV; after that, CHP NPs encapsulate donepezil, which may be due to the molecular interaction between the polymer and donepezil. As compared with charged NPs, neutral NPs (zeta potential: ±10 mV) phagocytosed by macrophages are significantly reduced in vivo [31, 32], and phagocytosis is the main factor in removing NPs. Reducing phagocytosis may significantly extend the cycle time in the body [33]; therefore, DZP-CHP may have a longer cycle time in vivo than donepezil alone. Zeta potential decreased to $-2.22 \pm 0.86$ mV after polysorbate 80 was applied. The surface charge of bovine serum albumin is −5.6 mV, according to Paillard et al., and the potential of NPs decreases after adsorption on the surface of NPs [34]. Therefore, in this study, the potential reduction of NPs in 0.7 mmol polysorbate 80 emulsifier may also be related to the adsorption. Also, the increased particle size may lead to

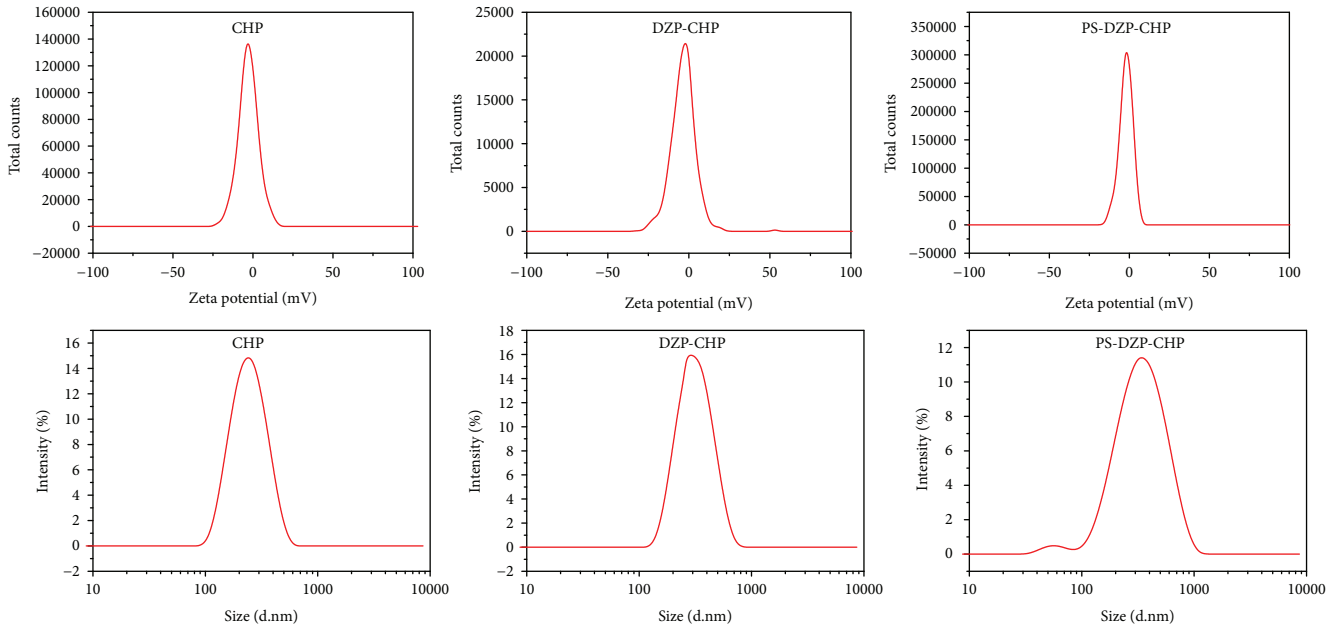


Figure 4: Particle size distribution and potential changes of NPs before and after drug loading. CHP: blank CHP NPs; DZP-CHP: donepezil-loaded CHP NPs; PS-DZP-CHP: polysorbate 80-emulsified DZP-CHP.

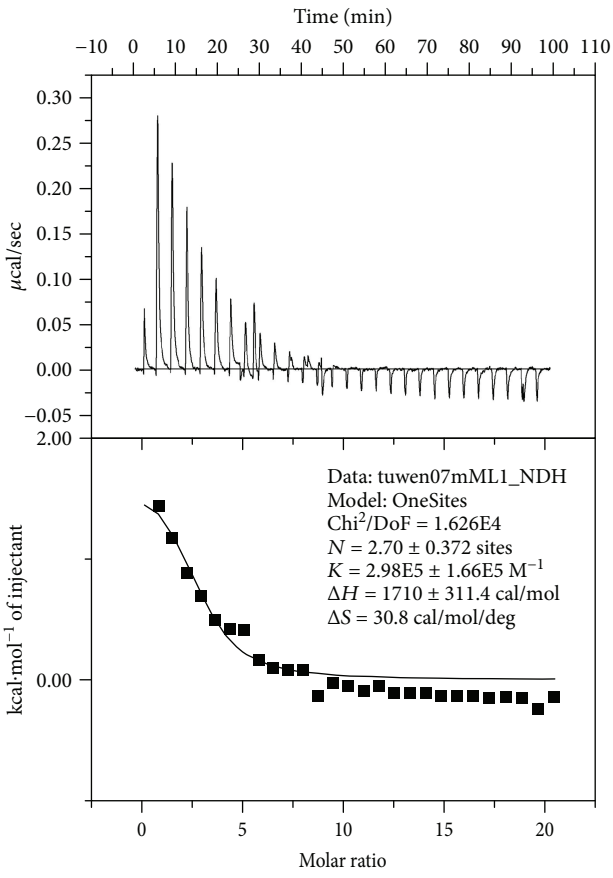


Figure 5: ITC data at 25°C for titration of polysorbate 80 into DZP-CHP NPs. The NP concentration in the cell (250 $\mu$l) was 7.7 $\mu$M and polysorbate 80 concentration in the syringe was 700 $\mu$M.

Table 2: Affinities ($K_A$), degree of coverage, and enthalpy changes upon binding when polysorbate 80 was titrated into nanoparticle solution at 25°C.

| Coverage | $K_A$ ($10^5$/M) | $\triangle H$ (cal/mol) | $\triangle S$ (cal/mol/deg) |
|---|---|---|---|
| 2.70 ± 0.372 | 2.98 ± 1.66 | 1710 ± 311.4 | 30.8 |

reduced surface charge density of NPs, thereby decreasing its zeta potential value or because of the shielding effect of the NPs on the surface charge with the adsorbed polysorbate 80 [1].

*3.6. In Vitro Drug Release of DZP-CHP NPs Coated and Uncoated by Polysorbate 80.* With donepezil alone (DZP), free drug release was complete within a very short time (Figure 7). With DZP-CHP NPs, the release was 55.12% in 72 h, for a controlled release effect. With PS-DZP-CHP NPs, the release was 42.71% in 72 h. With PS-DZP-CHP NP dialysis in fetal bovine serum (FBS), the drug release was 49.36% in 72 h. With PS-DZP-CHP NPs in FBS, the drug release was 31.21% in 72 h. When compared with the DZP-CHP NPs, the drug release of PS-DZP-CHP NPs is slower. The reason for the slow release of the PS-DZP-CHP NPs may be the presence of polysorbate 80 around the NPs; the hydrophobic regions of polysorbate 80 have strong adsorption properties for hydrophobic small-molecule drugs, thereby hampering the release of the drug to the media. And when compared with the PS-DZP-CHP NPs, the drug release of PS-DZP-CHP NPs in FBS is slower. The reason for the slow release of PS-DZP-CHP NPs in FBS can be that NPs were always adsorbed to plasma proteins in the blood circulation possibly the ApoE. After adsorption of plasma proteins, drug release can be reduced due to the steric hindrance of proteins. The release of PS-DZP-CHP NPs

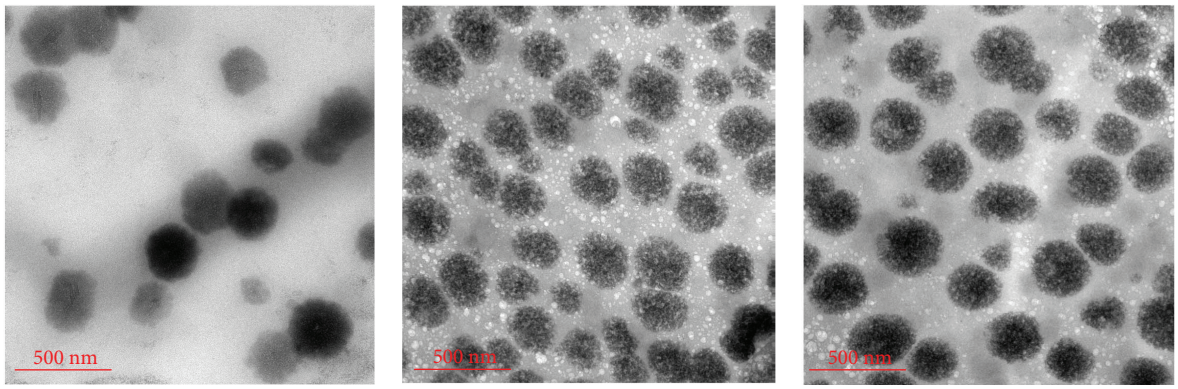


(a) (b) (c)

Figure 6: TEM of (a) CHP NPs, (b) DZP-CHP NPs, and (c) PS-DZP-CHP NPs.

Table 3: Particle size, polydispersity index (PDI), zeta potential, drug loading, and entrapment efficiency of the three kinds of CHP NPs.

| NPs | Particle size (nm) | PDI | Zeta potential (mV) | Drug loading (%) | Entrapment efficiency (%) |
|---|---|---|---|---|---|
| CHP | 257.5 ± 3.05 | 0.169 ± 0.02 | −2.81 ± 0.27 | — | — |
| DZP-CHP | 266.3 ± 4.46 | 0.122 ± 0.01 | −0.66 ± 0.04 | 14.78 ± 1.19 | 88.77 ± 2.60 |
| PS-DZP-CHP | 335.2 ± 5.46 | 0.138 ± 0.03 | −2.22 ± 0.86 | 8.25 ± 1.80 | 91.28 ± 4.57 |

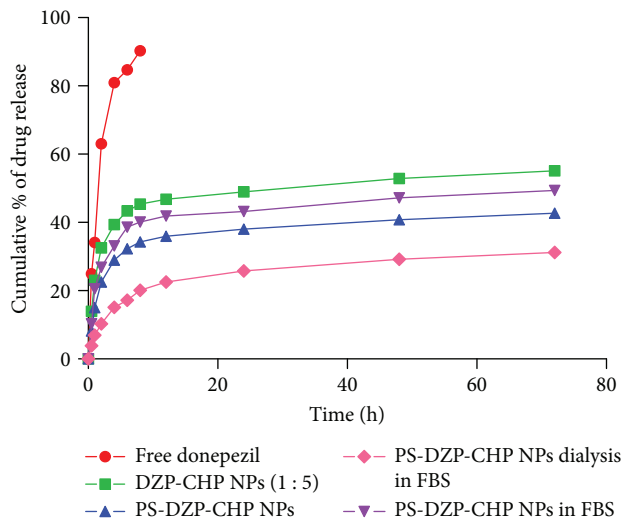


Figure 7: Release curves of donepezil from free donepezil, DZP-CHP NPs (1 : 5), PS-DZP-CHP NPs, and PS-DZP-CHP NP dialysis in FBS and PS-DZP-CHP NPs in FBS.

dialysis in FBS is faster than PS-DZP-CHP NPs. The reason for the fast release of PS-DZP-CHP NPs dialysis in FBS may be that the drug adsorption of plasma proteins out of the Visking dialysis tubing and the concentration difference have been expanded.

## 4. Discussion

We found that pullulan can be modified into an amphiphilic polymer by bonding hydrophobic small-molecule groups, which can be used in the field of biomedicine. Akiyoshi et al., Deguchi et al., and Lee and Akiyoshi's studies [35–38] used hexamethylene diisocyanate as a linker and found that the hydrophobic cholesteryl molecular-modified pullulan could obtain the amphiphilic cholesteryl base chitosan (CHP), which can form self-assembled NPs in water. The NP hydrophobic center can load epirubicin, mitoxantrone, paclitaxel [39], and other fat-soluble drugs to enhance their solubility. However, the hexamethylene diisocyanate itself is flammable and belongs to the body's exogenous substances and may have toxic effects on humans. Succinic anhydride is easily degradable in the body of the endogenous substances in the TCA cycle. Therefore, we used succinic anhydride as the connecting arm to graft cholesteryl onto the CHP NPs (Figure 8(a)), which is safer in theory as a drug carrier. The CHP self-polymerization group is a circular or oval hydrogel NP formed by the noncovalent hydrophobic interaction between the cholesterol groups [40]. Therefore, the greater the degree of substitution of grafted cholesterol, the stronger the hydrophobic interaction and the more stable the structure. However, because of strong hydrophobic action, a degree of substitution > 6% is not conducive to self-aggregation.

We used thermodynamic analysis of the adsorption of polysorbate 80 and DZP-CHP NPs. In general, the binding reaction results from hydrogen bonding, electrostatic interaction, hydrophobic interaction, and van der Waals force. Many scholars believe that when $\Delta H > 0$ and $\Delta S > 0$, the hydrophobic interaction is dominant. With $\Delta H < 0$ and $\Delta S < 0$, the hydrogen bond and van der Waals force are the main driving forces. With $\Delta H < 0$ and $\Delta S < 0$, the electrostatic force is the main force [41]. Therefore, according to our ITC findings, the hydrophobic interaction plays an

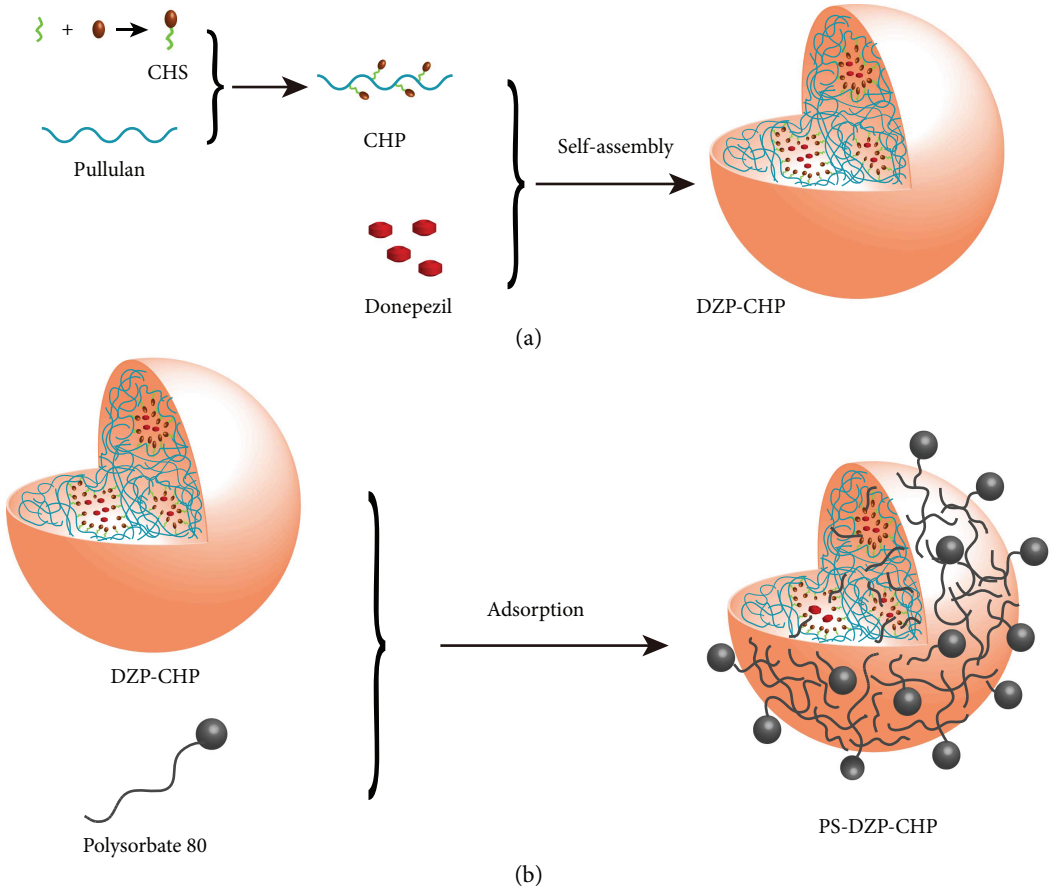


Figure 8: (a) CHP synthesis and self-assembly with donepezil into drug-loaded NPs; (b) polysorbate 80 adsorbed on the drug-loaded CHP NPs surface.

important role in the interaction between DZP-CHP NPs and polysorbate 80. According to Joshi et al. [42], polysorbate 80 may have structural changes in the initial phase of the adsorption of CHP NPs, and the acyl chain obtains a highly flexible structure. At the time of adsorption, the acyl chain ($-CH_2$) and ester group ($-C=O$) interacting with the CHP NPs under the hydrophobic interaction force dominate hydrogen bonding, so the polysorbate 80 molecule approaches the surface of the CHP NPs to result in the monolayer plane structure (Figure 8(b)), which is consistent with the experimental results.

Small particle size and other characteristics of the drug enhance its dissolution in the body and sustained release. In addition, studies have shown that NPs with polysorbate 80 coated on the surface are brain targeting and more permeable to the blood–brain barrier [43]. Polysorbate 80 is not cytotoxic and does not damage the blood–brain barrier of endothelial cells, making tight junctions appear to increase permeability for brain targeting [44]. The mechanism may be that polysorbate 80 coated on the surface of NPs can be used as an anchor point, and adsorption of apolipoproteins ApoB and ApoE occurs. The adsorption of apolipoprotein NPs mimics lipoprotein particles, which are absorbed by brain capillary endothelial cells via endocytosis mediated by the lipoprotein receptor low-density lipoprotein receptor and/or LRP [45–47]. In this case, the NPs traverse the blood–brain barrier as a Trojan horse bound to the drugs, and the drug is released into the endothelial cells, transported further into the brain by diffusion, or delivered to brain tissue by transcytosis to achieve brain targeting [48–50] or play the role of donepezil cholinesterase inhibitors to treat Alzheimer's disease [51, 52]. In addition, polysorbate 80 may also increase drug transport by hindering the specific exclusion of P-glycoprotein [53].

Polysorbate 80-coated NPs must be cross-linked to the blood–brain barrier with ApoB and ApoE proteins in the plasma. According to Ikai [54], polysorbate 80 is almost 1 : 1 bound to lipoprotein, and the binding is slow and tight. Both are in a stable state of reaction after 15 h, which is advantageous for the slow release of the new dosage form in vivo for efficacy. Polysorbate 80 and lipoprotein have a cross-linking reaction; the string-like structure of varying length can be seen on electron microscopy (the structure is also likely between CHP cross-linked, inserted in the middle). At the same time, polysorbate 80 does not affect the physical structure of ApoE and low-density lipoprotein and is safer.

However, the adsorption of NPs and proteins is also affected by many factors, such as the hydrophobicity of NPs, zeta potential, surface curvature, and surface roughness. The former two factors are the most important. The stronger the hydrophobicity, the stronger the adsorption

of protein and NPs. Since the material constituting the framework of the NP is a CHP molecule, the hydrophobic group is cholesteric and highly hydrophobic and easily interacts with the protein in the blood. Zeta potential also has an important effect on the adsorption of the two: in general, positively charged NPs preferentially adsorb proteins with isoelectric points < 5.5, such as albumin, whereas negatively charged NPs are the opposite and the adsorption between the surface charge density increases. We found that the absolute value of the zeta potential was larger for the drug-loaded NPs coated with than without polysorbate 80 and negatively charged, so polysorbate 80 may enhance NP–protein adsorption, and this novel NP should bind preferentially to ApoE in the blood (isoelectric points of three Apo subtypes E2, E3, and E4 are >5.5) as compared with albumin.

We found that PS-DZP-CHP has small molecular hydrophobic drug solubilization and good sustained-release effect. The release experiment in vitro showed that the CHP NPs emulsified by polysorbate 80 can release drugs at about 42.71% in 72 h, about 13% less than for nonemulsified NPs. In other words, the new NPs can be more stable in the blood, so they can maintain blood concentration longer, increase the medication interval, and improve patient compliance to treatment. Moreover, because of the increased stability, fewer drugs enter the systemic circulation and more NPs cross the blood–brain barrier before the release of the drug, thereby accumulating the drug in the brain and releasing it after targeting. The dosage can be reduced, as can the toxicity to the peripheral nervous system.

The controlled release of drug-loaded CHP NPs is an in vitro release behavior. When the NPs enter the body, the peripheral environment around the NPs is complicated and the release behavior is also complicated. However, due to the time and technical limitation, we did not confirm this theory by animal experiments, which needs further investigation.

## 5. Conclusion

The dose ratio of donepezil and nanomaterials has a certain effect on the drug loading, entrapment efficiency, and sustained-release features of CHP NPs, and the best feed ratio is 1 : 5. Surface modification of DZP-CHP NPs with polysorbate 80 showed good adsorption between polysorbate 80 and NPs on ITC. The CHP NPs have good drug loading, entrapment efficiency, and sustained-release effect, and the adsorption of polysorbate 80 further enhanced the sustained-release effect. CHP NPs after polysorbate 80 surface modification may be a new type of pharmaceutical preparation with a brain-targeting function in treating nervous system diseases.

## Conflicts of Interest

The authors declare no conflict of interests regarding the publication of this paper.

## Authors' Contributions

Xiaojun Tao and Yu Li contributed equally to this paper.

## Acknowledgments

This research was supported by the Hunan Provincial Natural Science Foundation of China (no. 2017JJ2188), Advanced Fund of Hunan Provincial Education Department (no. 16A128), and Changsha Science and Technology Bureau Project (no. kq1701052) (Xing Feng).

## References

[1] C. Riggio, E. Pagni, V. Raffa, and A. Cuschieri, "Nano-oncology: clinical application for cancer therapy and future perspectives," *Journal of Nanomaterials*, vol. 2011, Article ID 164506, 10 pages, 2011.

[2] Y. Ito, M. Yoshimura, T. Tanaka, and K. Takada, "Effect of lipophilicity on the bioavailability of drugs after percutaneous administration by dissolving microneedles," *Journal of Pharmaceutical Sciences*, vol. 101, no. 3, pp. 1145–1156, 2012.

[3] H. Lu, J. Wang, T. Wang, J. Zhong, Y. Bao, and H. Hao, "Recent progress on nanostructures for drug delivery applications," *Journal of Nanomaterials*, vol. 2016, Article ID 5762431, 12 pages, 2016.

[4] S. M. Wong, I. W. Kellaway, and S. Murdan, "Fast-dissolving microparticles fail to show improved oral bioavailability," *Journal of Pharmacy and Pharmacology*, vol. 58, no. 10, pp. 1319–1326, 2006.

[5] Q. Lv, X. Li, B. Shen et al., "A solid phospholipid-bile salts-mixed micelles based on the fast dissolving oral films to improve the oral bioavailability of poorly water-soluble drugs," *Journal of Nanoparticle Research*, vol. 16, no. 6, p. 2455, 2014.

[6] S. I. Rapoport, "Osmotic opening of the blood–brain barrier: principles, mechanism, and therapeutic applications," *Cellular and Molecular Neurobiology*, vol. 20, no. 2, pp. 217–230, 2000.

[7] C. W. Tzeng, F. L. Yen, T. H. Wu et al., "Enhancement of dissolution and antioxidant activity of kaempferol using a nanoparticle engineering process," *Journal of Agricultural and Food Chemistry*, vol. 59, no. 9, pp. 5073–5080, 2011.

[8] C. W. Lee, F. L. Yen, H. W. Huang et al., "Resveratrol nanoparticle system improves dissolution properties and enhances the hepatoprotective effect of resveratrol through antioxidant and anti-inflammatory pathways," *Journal of Agricultural and Food Chemistry*, vol. 60, no. 18, pp. 4662–4671, 2012.

[9] A. Albanese, P. S. Tang, and W. C. W. Chan, "The effect of nanoparticle size, shape, and surface chemistry on biological systems," *Annual Review of Biomedical Engineering*, vol. 14, no. 1, pp. 1–16, 2012.

[10] W. Li, X. Zhao, X. Sun, Y. Zu, Y. Liu, and Y. Ge, "Evaluation of antioxidant ability in vitro and bioavailability of *trans*-cinnamic acid nanoparticle by liquid antisolvent precipitate," *Journal of Nanomaterials*, vol. 2016, Article ID 9518362, 11 pages, 2016.

[11] X. Jiang, Y. S. Cheng, and H. D. C. Smyth, "Nanostructured aerosol particles: fabrication, pulmonary drug delivery, and controlled release," *Journal of Nanomaterials*, vol. 2011, Article ID 198792, 2 pages, 2011.

[12] R. Sakhtianchi, F. Atyabi, P. Yousef, E. Vasheghani-Farahani, M. Movahedi, and R. Dinarvand, "Targeted delivery of doxorubicin-utilizing chitosan nanoparticles surface-functionalized with anti-Her2 trastuzumab," *International Journal of Nanomedicine*, vol. 6, pp. 1977–1990, 2011.

[13] J. L. Molinuevo, M. L. Berthier, and L. Rami, "Donepezil provides greater benefits in mild compared to moderate Alzheimer's disease: implications for early diagnosis and treatment," *Archives of Gerontology and Geriatrics*, vol. 52, no. 1, pp. 18–22, 2011.

[14] I. Lynch, T. Cedervall, M. Lundqvist, C. Cabaleiro-Lago, S. Linse, and K. A. Dawson, "The nanoparticle–protein complex as a biological entity; a complex fluids and surface science challenge for the 21st century," *Advances in Colloid and Interface Science*, vol. 134-135, no. 21, pp. 167–174, 2007.

[15] P. Roach, D. Farrar, and C. C. Perry, "Surface tailoring for controlled protein adsorption: effect of topography at the nanometer scale and chemistry," *Journal of the American Chemical Society*, vol. 128, no. 12, pp. 3939–3945, 2006.

[16] X. Tao, Q. Zhang, K. Ling et al., "Effect of pullulan nanoparticle surface charges on HSA complexation and drug release behavior of HSA-bound nanoparticles," *PLoS One*, vol. 7, no. 11, article e49304, 2012.

[17] S. Boridy, H. Takahashi, K. Akiyoshi, and D. Maysinger, "The binding of pullulan modified cholesteryl nanogels to A$\beta$ oligomers and their suppression of cytotoxicity," *Biomaterials*, vol. 30, no. 29, pp. 5583–5591, 2009.

[18] G. Kaur and S. K. Mehta, "Developments of polysorbate (Tween) based microemulsions: preclinical drug delivery, toxicity and antimicrobial applications," *International Journal of Pharmaceutics*, vol. 529, no. 1-2, pp. 134–160, 2017.

[19] R. N. Alyaudtin, A. Reichel, R. Löbenberg, P. Ramge, J. Kreuter, and D. J. Begley, "Interaction of poly(butylcyanoacrylate) nanoparticles with the blood-brain barrierin vivoandin vitro," *Journal of Drug Targeting*, vol. 9, no. 3, pp. 209–221, 2001.

[20] R. G. Strickley, "Solubilizing excipients in oral and injectable formulations," *Pharmaceutical Research*, vol. 21, no. 2, pp. 201–230, 2004.

[21] G. B. Patil and S. J. Surana, "Bio-fabrication and statistical optimization of polysorbate 80 coated chitosan nanoparticles of tapentadol hydrochloride for central antinociceptive effect: in vitro–in vivo studies," *Artificial Cells, Nanomedicine, and Biotechnology*, vol. 45, no. 3, pp. 505–514, 2017.

[22] Y. Wang, C. Wang, C. Gong et al., "Polysorbate 80 coated poly (ε-caprolactone)–poly (ethylene glycol)–poly (ε-caprolactone) micelles for paclitaxel delivery," *International Journal of Pharmaceutics*, vol. 434, no. 1-2, pp. 1–8, 2012.

[23] H. Azhari, M. Strauss, S. Hook, B. J. Boyd, and S. B. Rizwan, "Stabilising cubosomes with tween 80 as a step towards targeting lipid nanocarriers to the blood–brain barrier," *European Journal of Pharmaceutics and Biopharmaceutics*, vol. 104, pp. 148–155, 2016.

[24] N. Watrous-Peltier, J. Uhl, V. Steel, L. Brophy, and E. Merisko-Liversidge, "Direct suppression of phagocytosis by amphipathic polymeric surfactants," *Pharmaceutical Research*, vol. 9, no. 9, pp. 1177–1183, 1992.

[25] S. D. Tröster, U. Müller, and J. Kreuter, "Modification of the body distribution of poly(methyl methacrylate) nanoparticles in rats by coating with surfactants," *International Journal of Pharmaceutics*, vol. 61, no. 1-2, pp. 85–100, 1990.

[26] G. Pamunuwa, V. Karunaratne, and D. N. Karunaratne, "Effect of lipid composition on in vitro release and skin deposition of curcumin encapsulated liposomes," *Journal of Nanomaterials*, vol. 2016, no. 9, Article ID 4535790, 9 pages, 2016.

[27] X. Tao, Q. Zhang, W. Yang, and Q. Zhang, "The interaction between human serum albumin and cholesterol-modified pullulan nanoparticle," *Current Nanoscience*, vol. 8, no. 6, pp. 830–837, 2012.

[28] S. Kim, K. M. Park, J. Y. Ko et al., "Minimalism in fabrication of self-organized nanogels holding both anti-cancer drug and targeting moiety," *Colloids and Surfaces B: Biointerfaces*, vol. 63, no. 1, pp. 55–63, 2008.

[29] G. Baier, C. Costa, A. Zeller et al., "BSA adsorption on differently charged polystyrene nanoparticles using isothermal titration calorimetry and the influence on cellular uptake," *Macromolecular Bioscience*, vol. 11, no. 5, pp. 628–638, 2011.

[30] X. Tao, Y. Xie, X. Qiu, Q. Zhang et al., "Cholesterol-modified comparative study of amino-pullulan nanoparticles as a drug carrier, cholesterol-modified carboxyethyl pullulan and pullulan nanoparticles," *Nanomaterials*, vol. 6, no. 5, pp. 165–180, 2016.

[31] S.-D. Li and L. Huang, "Pharmacokinetics and biodistribution of nanoparticles," *Molecular Pharmaceutics*, vol. 5, no. 4, pp. 496–504, 2008.

[32] T. S. Levchenko, R. Rammohan, A. N. Lukyanov, K. R. Whiteman, and V. P. Torchilin, "Liposome clearance in mice: the effect of a separate and combined presence of surface charge and polymer coating," *International Journal of Pharmaceutics*, vol. 240, no. 1-2, pp. 95–102, 2002.

[33] D. P. Speert, F. Eftekhar, and Puterman M. L., "Nonopsonic phagocytosis of strains of Pseudomonas aeruginosa from cystic fibrosis patients," *Infection and Immunity*, vol. 43, no. 3, pp. 1006–1011, 1984.

[34] A. Paillard, C. Passirani, P. Saulnier et al., "Positively-charged, porous, polysaccharide nanoparticles loaded with anionic molecules behave as 'stealth' cationic nanocarriers," *Pharmaceutical Research*, vol. 27, no. 1, pp. 126–133, 2010.

[35] K. Akiyoshi, S. Deguchi, N. Moriguchi, S. Yamaguchi, and J. Sunamoto, "Self-aggregates of hydrophobized polysaccharides in water. Formation and characteristics of nanoparticles," *Macromolecules*, vol. 26, no. 12, pp. 3062–3068, 1993.

[36] K. Akiyoshi, S. Deguchi, H. Tajima, T. Nishikawa, and J. Sunamoto, "Microscopic structure and thermoresponsiveness of a hydrogel nanoparticle by self-assembly of a hydrophobized polysaccharide," *Macromolecules*, vol. 30, no. 4, pp. 857–861, 1997.

[37] S. Deguchi, K. Kuroda, K. Akiyoshi, B. Lindman, and J. Sunamoto, "Gelation of cholesterol-bearing pullulan by surfactant and its rheology," *Colloids and Surfaces A: Physicochemical and Engineering Aspects*, vol. 147, no. 1-2, pp. 203–211, 1999.

[38] I. Lee and K. Akiyoshi, "Single molecular mechanics of a cholesterol-bearing pullulan nanogel at the hydrophobic interfaces," *Biomaterials*, vol. 25, no. 15, pp. 2911–2918, 2004.

[39] Z. Liu, Y. Jiao, Y. Wang, C. Zhou, and Z. Zhang, "Polysaccharides-based nanoparticles as drug delivery systems," *Advanced Drug Delivery Reviews*, vol. 60, no. 15, pp. 1650–1662, 2008.

[40] K. Akiyoshi, T. Nishikawa, Y. Mitsui, T. Miyata, M. Kodama, and J. Sunamoto, "Self-assembly of polymer amphiphiles: thermodynamics of complexation between bovine serum

albumin and self-aggregate of cholesterol-bearing pullulan," *Colloids and Surfaces A: Physicochemical and Engineering Aspects*, vol. 112, no. 2-3, pp. 91–95, 1996.

[41] P. D. Ross and S. Subramanian, "Thermodynamics of protein association reactions: forces contributing to stability," *Biochemistry*, vol. 20, no. 11, pp. 3096–3102, 1981.

[42] A. S. Joshi, A. Gahane, and A. K. Thakur, "Deciphering the mechanism and structural features of polysorbate 80 during adsorption on PLGA nanoparticles by attenuated total reflectance – Fourier transform infrared spectroscopy," *RSC Advances*, vol. 6, no. 110, pp. 108545–108557, 2016.

[43] Y. Chen and L. Liu, "Modern methods for delivery of drugs across the blood-brain barrier," *Advanced Drug Delivery Reviews*, vol. 64, no. 7, pp. 640–665, 2012.

[44] J. Kreuter, P. Ramge, V. Petrov et al., "Direct evidence that polysorbate-80-coated poly (butylcyanoacrylate) nanoparticles deliver drugs to the CNS via specific mechanisms requiring prior binding of drug to the nanoparticles," *Pharmaceutical Research*, vol. 20, no. 3, pp. 409–416, 2003.

[45] J. Kreuter, D. Shamenkov, V. Petrov et al., "Apolipoprotein-mediated transport of nanoparticle-bound drugs across the blood-brain barrier," *Journal of Drug Targeting*, vol. 10, no. 4, pp. 317–325, 2002.

[46] J. Kreuter, T. Hekmatara, S. Dreis, T. Vogel, S. Gelperina, and K. Langer, "Covalent attachment of apolipoprotein A-I and apolipoprotein B-100 to albumin nanoparticles enables drug transport into the brain," *Journal of Controlled Release*, vol. 118, no. 1, pp. 54–58, 2007.

[47] P. Aggarwal, J. B. Hall, C. B. Mcleland, M. A. Dobrovolskaia, and S. E. Mcneil, "Nanoparticle interaction with plasma proteins as it relates to particle biodistribution, biocompatibility and therapeutic efficacy," *Advanced Drug Delivery Reviews*, vol. 61, no. 6, pp. 428–437, 2009.

[48] J. Kreuter, "Mechanism of polymeric nanoparticle-based drug transport across the blood-br,ain barrier (BBB)," *Journal of Microencapsulation*, vol. 30, no. 1, pp. 49–54, 2012.

[49] K. Prabhakar, S. M. Afzal, G. Surender, and V. Kishan, "Tween 80 containing lipid nanoemulsions for delivery of indinavir to brain," *Acta Pharmaceutica Sinica B*, vol. 3, no. 5, pp. 345–353, 2013.

[50] A. E. Gulyaev, S. E. Gelperina, I. N. Skidan, A. S. Antropov, G. Y. Kivman, and J. Kreuter, "Significant transport of doxorubicin into the brain with polysorbate 80-coated nanoparticles," *Pharmaceutical Research*, vol. 16, no. 10, pp. 1564–1569, 1999.

[51] R. Stryjer, R. D. Strous, F. Bar et al., "Beneficial effect of donepezil augmentation for the management of comorbid schizophrenia and dementia," *Clinical Neuropharmacology*, vol. 26, no. 1, pp. 12–17, 2003.

[52] J. L. Cummings, P. A. Cyrus, F. Bieber et al., "Metrifonate treatment of the cognitive deficits of Alzheimer's disease," *Neurology*, vol. 50, no. 5, pp. 1214–1221, 1998.

[53] M. M. Nerurkar, P. S. Burton, and R. T. Borchardt, "The use of surfactants to enhance the permeability of peptides through Caco-2 cells by inhibition of an apically polarized efflux system," *Pharmaceutical Research*, vol. 13, no. 4, pp. 528–534, 1996.

[54] A. Ikai, "Extraction of the apo B cluster from human low density lipoprotein with tween 80," *The Journal of Biochemistry*, vol. 88, no. 5, pp. 1349–1357, 1980.

Hindawi
Journal of Nanomaterials
Volume 2018, Article ID 7805147, 8 pages
https://doi.org/10.1155/2018/7805147

*Review Article*

# The Recent Advances of Magnetic Nanoparticles in Medicine

**Ting Guo,[1] Mei Lin,[2] Junxing Huang,[3] Chenglin Zhou,[2] Weizhong Tian,[4] Hong Yu,[5] Xingmao Jiang,[6] Jun Ye,[1] Yujuan Shi,[1] Yanhong Xiao,[1] Xuefeng Bian,[1] and Xiaoqian Feng[1]**

[1]*Institute of Clinical Medicine, Taizhou People's Hospital Affiliated to Nantong University, Taizhou, Jiangsu 225300, China*
[2]*Clinical Laboratory, Taizhou People's Hospital Affiliated to Nantong University, Taizhou, Jiangsu 225300, China*
[3]*Oncology Department, Taizhou People's Hospital Affiliated to Nantong University, Taizhou, Jiangsu 225300, China*
[4]*Imaging Department, Taizhou People's Hospital Affiliated to Nantong University, Taizhou, Jiangsu 225300, China*
[5]*Pathology Department, Taizhou People's Hospital Affiliated to Nantong University, Taizhou, Jiangsu 225300, China*
[6]*School of Chemical Engineering and Pharmacy, Wuhan Institute of Technology, Wuhan, Hubei 430000, China*

Correspondence should be addressed to Mei Lin; l_mei@163.com

Received 28 December 2017; Accepted 16 April 2018; Published 29 April 2018

Academic Editor: Federica Paladini



With the progress of nanotechnology and molecular biology, nanoparticles have been widely studied and applied in biomedicine. Particularly, characterized by unique magnetic property, targeting, and biocompatibility, magnetic nanoparticles have become one of the research hotspots in the nanomedical field. Herein, we summarized the recent advances of magnetic nanoparticles in medicine, including the property, carrier function, MRI, and tumor magnetic inductive hyperthermia of magnetic nanoparticles.

## 1. Introduction

The constant development of medicine has rendered early diagnosis and precise treatment of its development direction. Nanotechnology has provided a new platform for medicine development. As a result of unique features, nanomaterials have been extensively studied and applied in the medical field [1]. As one kind of the nanomaterials, magnetic nanoparticles possess not only the general characteristics of nanoparticles but also the magnetic properties. After being modified surfacely, magnetic nanoparticles can possess excellent biocompatibility, which is suitable for medical application. For example, surface-modified magnetic nanoparticles can be used as vectors, allowing for drug or gene directional transportation under the action of the magnetic field to realize targeted therapy [2]. Moreover, under the action of applied magnetic field, magnetic nanoparticles have unique magnetic sensitivity, which can thus be applied in MRI [3]. Furthermore, the magnetocaloric effect of magnetic nanoparticles has also provided a new means for tumor treatment [4]. All in all, the application of magnetic nanoparticles will further promote the development of the medical field.

## 2. Category and Properties of Magnetic Nanoparticles

At present, magnetic nanoparticles (NPs) mainly include metal NPs, metal oxide NPs, and metal alloy NPs. The common NPs are gold [5], silver [6], iron, cobalt, and nickel. Metal oxide NPs mainly include iron oxides ($\gamma$-$Fe_2O_3$ and $Fe_3O_4$) and ferrites ($CoFe_2O_4$ and $Mn_{0.6}Zn_{0.4}Fe_2O_4$), and metal alloy NPs cover FeCo, FePt, and so on. Of them, metal oxide $Fe_2O_3$ and $Fe_3O_4$ magnetic nanoparticles are the most extensively used magnetic NPs [7], which can be handily prepared and easily controlled in particle size and shape [8]. Some metallic elements such as manganese (Mn) and Zn (Zn) can be added to nanosized iron oxide structure to prepare a variety of ferrite nanoparticles ($Mn_3Zn_7Fe_2O_4$, $Mn_{0.6}Zn_{0.4}Fe_2O_4$, and so on). These ferrite nanoparticles have a stronger magnetism and a higher relaxation rate, which contributes to their application for magnetic resonance imaging (MRI).

Magnetic NPs own the following properties. Firstly, magnetic nanometer materials have nonvirulence and nonimmunogenicity. Secondly, magnetic NPs possess the surface

Table 1: Frequently used compounds to surfacely modify magnetic NPs.

| Modified compounds | Advantages | Applications |
|---|---|---|
| PEG [12] | Enhanced water solubility of NPs, reduced RES phagocytosis, and increased blood circulation time | MRI, tumor diagnosis, and treatment |
| PEI | Good biocompatibility | Gene and drug vectors |
| Polyvinyl alcohol (PVA) | Elevated stability and reduced particle aggregation | MRI, vectors, and bioseparation |
| Glucan | Excellent stability and extended in vivo circulation time | Drug vectors |
| Chitosan [13] | Good stability and biocompatibility | Vector, thermotherapy |
| Liposome [14] | Good biocompatibility | Tumor treatment, thermotherapy, and MRI |
| FA [15] | Good biocompatibility, essential small-molecule vitamin for the human body | Targeted receptors, diagnosis, and treatment of tumors (breast cancer, cervical cancer, and ovarian cancer) |
| Gold [16, 17] | Biocompatibility can provide optical property and magnetism for biological application | Tumor diagnosis and MRI |

effect. In detail, they have great specific surface area, which is good for carrying a large amount of DNA fragments, drugs, and modified compounds. After modification, they can be used as vector. Thirdly, most modified magnetic NPs have excellent biocompatibility. Fourthly, some magnetic NPs have superparamagnetism.

General magnetic materials are a multimagnetic domain structure. When the size of magnetic materials is reduced to nanoscale, they have a single magnetic domain structure and their magnetism turns to paramagnetism [9]. Paramagnetic materials, in the external magnetic field, are macroscopically nonmagnetic, showing a very weak magnetic property. When the size of the magnetic material is smaller than the critical size (generally 20 nm), the magnetic spin of the magnetic nanomaterials will be disordered and superparamagnetic, which will be magnetized rapidly under the action of alternating magnetic field and can move in a directional manner with the magnetic field. But once the magnetic field is removed, the magnetization becomes zero, that is, it does not show magnetism when there is no external magnetic field [10]. The magnetic susceptibility of superparamagnetism in the presence of external magnetic field is much higher than that of general paramagnetic materials. Fifthly, magnetic NPs can be used for tumor thermotherapy since they can produce thermal effect under the action of alternating magnetic field (AMF). Sixthly, the magnetic NPs can be exploited for magnetic separation [11]. For instance, they can be served as vectors to bind biomolecules and then be separated from the biomolecules at the targeted area under the action of the magnetic field and thus used for targeted therapy or diagnosis. Since most PH outside tumor cells are usually low, most weak alkaline drugs can hardly enter the cells, showing drug resistance. In order to overcome such resistance, researchers have extensively studied the preparation and modification of multiple NPs. As superparamagnetic iron oxide (SPIO) NPs are being studied most extensively, $Fe_2O_3$ and $Fe_3O_4$ NPs have been widely applied in diagnosis and treatment for all kinds of tumors. Iron oxide NPs have many advantages such as excellent biodegradability, low cytotoxicity, the ability to be modified by multiple substances, the ability to bind with multiple targeted ligands or antibodies, and ease to prepare, and can enter cells through endocytosis. They have been used in MRI and tumor thermotherapy [7].

## 3. Modification of Magnetic Nanoparticles

As a result of the surface effect and interface effect of nanostructure, the exposed magnetic NPs are extremely unstable in structure and are apt to aggregation. After entering the human body, the magnetic NPs are subject to being absorbed with body proteins and phagocytosed by the vascular endothelial system. They thus cannot be applied in biomedicine. It has been confirmed that surface modification can better stabilize the nanostructure and improve the surface functionalization of nanoparticles. For instance, when coated by active material with hydroxyl and carboxyl, nanoparticles can bind DNA fragments, drugs, and proteins, thus exerting the function of transportation and targeted therapy. At present, numerous surface-modified compounds are available, including polyethylene glycol (PEG), polyethylenimine (PEI), folic acid (FA), liposome, noble metal, and inorganic materials (Table 1).

Surface modification can enhance the water solubility, biocompatibility, and stability of NPs; they thus can be served as vectors for drug delivery, gene transfer, MRI, and thermotherapy. Some surface-modified compounds such as PEG and carboxylated polyethyleneimine (PEI-COOH) have rendered favorable water solubility for magnetic NPs, leading to good application in MRI or other medical diagnosis and treatments [18, 19]. As one of the few polymers which can be used for *in vivo* injection, PEG has favorable water solubility, biocompatibility, and nontoxicity. It can bind onto the surface of NPs by end-group reactivity and thus be able to bind DNA fragments, drugs, and other biological fragments, extending the blood circulation time [20, 21]. PEG-modified ferrite NPs can enter cells through phagocytosis, which can suppress iron ion release when it is degraded in lysosome, lessening the binding of iron ion with catalase to reduce cell destruction [22]. PEI is a cationic polymer, which can carry gene fragments and drugs, thus carrying out drug or gene transfer. Tang et al. used PEI to modify Mn Zn ferrite and bound it with plasmid DNA. Agarose gel electrophoresis

(AGE) suggested a reliable binding of PEI/$Mn_{0.5}Zn_{0.5}Fe_2O_4$/DNA [23]. In the applied magnetic field, PEI-modified magnetic NPs have remarkably improved gene transfection efficiency [24]. Additionally, magnetic NPs receiving specific surface modification can specifically bind with target cell, thus being served as the vector for contrast medium of MRI or nanoprobe for the early diagnosis of tumor. Inert metal NPs also have aroused extensive attention. On the one hand, the gold nanocoating can bind with sulfhydryl-containing ligand, which can be used as vectors of biomolecules. On the other hand, the gold-coating surface can enhance its optical property and thus can be used to trace the NPs. Methacrylate- (PDEA-) coating magnetic NPs can resist the degradation of DNase I to the carried gene during the gene transfection of G2 cell hepatitis, thus improving gene transfection efficiency [25].

## 4. Application of Magnetic NPs in MRI

In recent years, tumor morbidity is increasing and early tumor diagnosis is of vital importance. MRI is one of the common methods for tumor diagnosis. With the development of nanotechnology, nanometer materials have been gradually applied for the diagnosis and treatment of tumor. Particularly, the combination of nanotechnology with MRI to detect tumor has attained satisfactory effects. In MRI, magnetic NPs have displayed unique sensitivity to the magnetic field in the presence of applied magnetic field. They can alter T1 or T2 relaxation time of MRI, which can thereby greatly enhance the diagnostic efficiency of MRI [26]. However, water solubility of magnetic NPs has to be enhanced in the meantime in preserving their magnetic property so that they can be extensively applied in clinics [27]. Research has indicated that PEG-modified NPs have excellent water solubility and biocompatibility, which can extend the blood circulation time and enhance the MRI effect [28].

The application of nanoprobe in MRI is one of research hotspots in molecular imaging field. After NPs coupled with ligands or antibodies enter the human body, they may be bound with the specific receptors or antibodies of tumor cells and thus be phagocytosed by tumor cells or bind onto the tumor cell surface, resulting in NPs aggregating in tumor tissues. Under such circumstances, magnetic nanomaterials will generate magnetism under the action of applied magnetic field, which allows for early diagnosis and detection of small lesion through MRI. MRI research on magnetic ferrite NPs coated with carboxylated PEG suggests that the MR transverse relaxation time T2 has reduced with the increase in NP concentration, while signals on MR T2-weighted image have enhanced [29].

Chitosan (CS), a surface modification of cationic polymer also can render excellent water solubility and stability for magnetic NPs. Lactobionic acid (LA) modification allows them to bind with hepatic cell surface receptor, thus being phagocytosed by hepatic cells. After superparamagnetic iron oxide NPs (CS-LA@SPION) modified with CS and LA together were injected into nude mice, MRI showed remarkably lowered T2-weighted image in the liver within 1 h after, which indicated they can be used as liver-targeted MRI contrast medium [30]]. Applying PEG to modify $Fe_3O_4$ NPs and then coupling them with chloride channel buthotoxin (CTX), Sun et al. prepared glioma nanoprobe. It was shown in MRI that such nanoprobe could effectively bind with glioma cells [31]. Another study showed that NP-PEG-CTX-Cy5.5 nanoprobe prepared by using $Fe_3O_4$ NPs as core and then coating the core with PEG, subsequently binding it with fluorescence molecules Cy5.5 and CTX, could not only be used for MRI of glioma but also could be detected by fluorescence microscopy [32]. Anbarasu et al. labeled the PEG-coated $Fe_3O_4$ NPs with monoclonal antibody and then planted it into the colon cancer mouse model. They successfully conducted targeted localization by MRI [33]. In addition, adding metallic elements such as Mn and Zn into the nanometer ferrite structure can change the properties of NPs [33], enhancing the magnetism of NPs (such as $Mn_{0.5}Zn_{0.5}Fe_2O_4$ and $Mn_{0.6}Zn_{0.4}Fe_2O_4$), increasing the transverse relaxation time of ferrite NPs, elevating the T2 MRI imaging contrast, darkening the T2-weighted image, and it thus can be better applied in MRI [34].

Stem cell has attracted extensive attention in research on biomedicine owing to its excellent proliferative capacity and differentiation potential. In this way, an effective, nontoxic and stable cell labeling is required to better investigate the treatment mechanism of stem cell and to monitor differentiation and migration of stem cells. Currently, there are two methods to label stem cells using the superparamagnetic NPs. One is cell surface labeling and the other one is intracellular labeling. It was discovered that cell surface labeling is likely to be eliminated by the reticuloendothelial system (RES). In comparison, intracellular labeling has certain requirements on the concentration of NPs. Its effective safe concentration was 20–25 mg/L [35]. In the glioma mouse experiment, after superparamagnetic NP-labeled stem cells were injected into the mouse, labeled stem cell migration could be observed in the mouse under MRI within 10 days after injection. Furthermore, cells injected into the tumor tissue were identified histologically to be the superparamagnetic NP-labeled stem cells. The function and activity of these cells are not affected, suggesting that superparamagnetic NPs can be used for labeling stem cells [36].

Currently, most research on targeted therapy for tumor is based on single point. But the therapy effect of most targeted therapy based on single point is poor. Therefore, it remains a challenge to research and develop multitarget therapy for tumor cell, so as to further improve the efficacy of such therapy on tumor. As we all know, tumor tissue is associated with exuberant angiogenesis. Consequently, combined application of targeted magnetic induction thermotherapy targeting tumor cell and tumor vascular hyperplasia endothelial cell may contribute to enhancing the efficacy. Additionally, some genes overexpress in multiple tumors. For instance, CD44 excessively expresses in tumors in the reproductive system, digestive system, and respiratory system. If general targeted molecular probe is designed, the development of research in the field of tumor molecular imaging diagnosis may be greatly promoted. However, there is still a long way to go for developing a general gene-targeted probe due to the mutagenicity of tumor cell.

## 5. Research on Magnetic NPs as Vectors

Gene therapy is a treatment by transferring the exogenous gene or gene fragment into the target gene of patient [37]. It is another novel treatment for tumor after traditional surgery, radiotherapy, and chemotherapy [38]. But gene transfer method with safety, efficiency, and controllability is the key for gene therapy [39]. DNA is extremely unstable inside and outside the cell and is likely to be degraded by nucleotidase. Stably transferring exogenous gene into target cell for gene therapy depends on the gene transfer system [40], and stable and effective gene vector is of importance to gene therapy [41].

Gene vectors can be classified into two types, the viral and nonviral vectors. Viral gene vectors, such as adenovirus, herpes simplex virus, and smallpox virus [42], can transfer the target gene into cell by viral vector for gene expression [43]. Viral vector is linked with high transfection efficiency. However, it has the drawbacks of immune response, limited number of genes carried by virus, unavoidable random insertion of viral vector into the host chromosome during gene transfer, and high expenses [44]. In Europe, one gene therapy using viral vector has been applied in clinics, but its treatment expenses are as high as 1 million dollars [45]. All these unfavorable factors have restricted the extensive application of viral vector. Therefore, nonviral gene vector research has attracted wide attentions.

The common nonviral gene vectors include cationic liposome, cationic polymer, and NPs. Liposome and polymer are two gene vectors that are extensively applied. The structure and size of cationic liposome binding with DNA are related to its transfection efficiency [46]. Most nonviral gene vectors have low transfection efficiency, which lack targeting. PEI is the common cationic liposome, and its positive charge can absorb DNA, thus forming the structure similar to core-shell, which can maintain DNA stability.

Nanocarriers have attracted increasing attention with the booming of nanotechnology. NPs can be easily modified and have excellent biocompatibility and little immune response. They are likely to enter tissue after coupling with related ligands or antibodies, thus binding with the cell surface-specific receptors or specific antigens. Alternatively, they can be phagocytosed by target cell and thereby enter the cell to realize DNA transfer. Studies have shown that some nanocarriers modified specifically have high gene transfer efficiency [47]. Magnetic NPs can carry out directional movement under the action of AMF, thereby enhancing the transfer efficiency. Moreover magnetic NPs can be used as vectors to bind with biomolecules by magnetic separation. These biomolecules can separate from vectors under the action of applied magnetic field, thus contributing to achieve the goal of targeted therapy.

It was discovered that doxorubicin magnetic NPs (DOX MNPs) can remarkably increase DOX uptake by glioma cells in the magnetic field. MTT assay revealed that death rate of tumor cells after DOX MNP uptake is notably higher than that after DOX uptake only [48].The Fe3O4 @Alg-GA NPs synthesized and modified by sodium alginate and D-galactosamine can enhance their uptake by human hepatoma cells under the action of AMF. Moreover, they can produce the heating effect and kill 95% cells [49]. A research on pancreatic cancer showed that chemotherapeutic DOX can be rapidly transferred and released in pancreatic cancer cells by using superparamagnetic iron oxide (SPIO) NPs as the vectors monitored under electron microscope, X-ray, and optical microscope [50]. As we all know, most chemotherapeutics cannot pass the blood brain barrier (BBB). But a novel administration route has been discovered in brain tumor animal experiment. When paclitaxel- and curcumin-targeted therapies were carried out in glioma mouse using the DL-lactic acid-glycolic acid (PLGA) magnetic NPs, the chemotherapeutics could rapidly pass the BBB by the vectors [51]. In a research on colon tumor, PEG was applied in modifying the uperparamagnetic ferrite core and then connected with the amino terminal fragment hATF of human recombinant protein, forming the targeted probe hATF-SPIO with the diameter of about 30 nm. It was demonstrated that the probe can specifically bind with uPAR-expressing tumor cells in vitro and develop in a targeted manner in the colon tumor animal models with moderately expressed uPAR [52]. With the development of nanosensor technology, hepatitis viruses in human blood can be quantitatively detected [53]. In the quantitative detection of tumor markers, immunosensor has considerable potential in the early detection of tumor [54].

With regard to the toxicity of magnetic NPs, many studies demonstrate that most superparamagnetic NPs have excellent biocompatibility. But some other studies indicate that NPs have toxicity to neurons and glial cells and the toxicity is related to the compounds modified on the surface of magnetic NPs [55].

## 6. Tumor-Targeted Thermotherapy of Magnetic Nanometer Materials

Thermotherapy is a method to kill tumor cells with thermal energy at a certain temperature. It can be applied alone and also can be used in combination with other therapies such as surgery, radiotherapy, and chemotherapy, exerting good synergistic effect [56]. It is reported that the therapeutic efficacy of paclitaxel can increase by 10–100 folds at 43°C for 30 min. In addition, the killing capacity of chemotherapeutics with low cytotoxicity under normal temperature can be doubled after heated [57]. Jordan et al. [58] first applied magnetic NPs in tumor thermotherapy and invented magnetic fluid thermotherapy (MFH). Magnetic fluid is a liquid magnetic material, which possesses magnetic properties as well as water solubility. It is appropriate for clinical application. Under an AMF, the nanoparticle core of magnetic fluid can transform the magnetic energy into thermal energy, which can stably elevate the temperature of tumor tissue, thus inhibiting tumor growth or killing tumor cell or inducing tumor cell apoptosis [59–61].

Generally, tumor tissue is associated with rapid angiogenesis, which may result in incomplete structure of the capillary wall, disordered branch and distorted structure and fragility. With the addition of tumor compression, the above factors may lead to circulation blocking. Moreover, during

magnetic thermotherapy for tumor, thermal dissipation is slow in tumor cells, which together with circulation blocking may give rise to local anaerobic metabolism. Consequently, the cancer cells are more sensitive to heat than normal cells [62]. Thermotherapy may kill tumor cells by reducing vascular endothelial cell regeneration to destroy vascular structure [63], reducing enzyme system activity on the tumor cell membrane, destroying mitochondrion resulting in energy supply disorder [64], inhibiting the activities of DNA polymerase and ligase in tumor cells resulting in DNA and RNA synthesis being disordered and regulating the expression of apoptosis-related genes to induce cell apoptosis [65]. Temperature at 42–45°C is considered to be the appropriate temperature for tumor thermotherapy, which can kill tumor cells, with no injury to normal tissues.

The magnetism of magnetic fluid depends on magnetic particles, among which $Fe_3O_4$ is the most extensively used magnetic fluid material. The magnetism of $Fe_3O_4$ nanoparticles can be enhanced by adding some metallic elements such Mn and Zn during preparation. By adjusting the proportion of Mn and Zn, the temperature-sensitive $Mn_xZn_{1-x}Fe_2O_4$ (Mn Zn ferrite) invented in Southeast University can transform magnetic energy into thermal energy below the Curie temperature under the action of AMF, thus elevating the temperature. But when the temperature arrives at the Curie temperature, it becomes a nonmagnetic material, stopping absorbing magnetic energy, thus decreasing the temperature. So cyclically, the temperature always maintains around the Curie temperature [66]. In this way, such Mn Zn ferrite NPs are endowed with the self-controlled temperature ability. Moreover, the Mn Zn ferrite NPs have numerous advantages during magnetic thermotherapy, such as thermal bystander effect, universality, high-characteristic absorption rate, constant temperature, and excellent biocompatibility. MFH can effectively destroy cancer cells, with no injury to normal cells. It is considered as one of the most promising cancer therapies. A study on the safety of Mn Zn ferrite NPs indicated that the hemolytic rate of Mn Zn ferrite magnetic fluid was 1.0429% and the $LD_{50}$ was 7.186 g/kg. The bone marrow micronucleus formation rate had no significant difference between the experimental group and the negative control group [67].

It is discovered in a hepatoma cell research that when the constructed P[5HRE] AFPp-p53/PEI-Fe304 magnetic NPs were used to mediate gene therapy combined with MFH, they could distinctly suppress the proliferative activity of hepatoma HepG2 cells. The effect was markedly superior to that in control the NP group and negative control group [68]. Xie et al. [69] modified Mn Zn ferrite NPs ($Mn_{0.5}Zn_{0.5}Fe_2O_4$) with PEG lipid molecules through hydrophobic interaction. Such nanoparticles with core-shell structure rendered high magnetism, strong alternating magnetothermal effect, and good biocompatibility. In the early symptom liver metastasis mouse model of colorectal cancer, the oleic acid-wrapped ferrite RGF polypeptide complex ($Fe_3O_4$@PMAO_RGD) was injected into the hepatic artery to bind with the surface $\alpha V\beta 3$ receptor of the tumor cell and then MFH was conducted under the action of AMF. It was found that the activity of colorectal cancer liver metastasis tumor cells was remarkably lowered [70]. Combined therapy of MFH with targeted chemotherapy and (or) gene therapy had shown a promising application prospect in the diagnosis and treatment for tumor. Using Mn0.5Zn0.5Fe2O4 as vector, Lin et al. combined radionuclide, suicide gene, and MFH organically to treat liver cancer. The results indicated an excellent effect, and the tumor inhibition rate of the combined therapy group was remarkably higher than that of any other single therapy [71]. Another research showed that magnetic $cAs_2O_3/Fe_2O_3$ nanocomposites adopted to thermochemotherapy for hepatoma had an evident higher effect than that of the single thermotherapy and the $As_2O_3$ chemotherapy alone and the equivalent dosage of chemotherapeutics was greatly lowed and has few side effects [72].

## 7. Problem and Prospect

With the development of nanoscience and nanotechnology, the research and application of magnetic NPs have made considerable progress in the biomedical field. For example, magnetic NPs have been extensively applied in biomolecule vectors, targeted localization, MRI, and thermotherapy. However, most studies remain at the laboratory research stage, and few have really been applied in clinics. Their toxicity, side effects, long-term efficacy, and in vivo metabolic mechanism still need to be further studied. A large amount of basic and clinical research needs to be done for their clinical application. Confidently, magnetic NPs will have a broad application prospect in the medical field, with the increasing development and the further intensive research of nanotechnology, biotechnology, and medicine.

## Conflicts of Interest

The authors declare that there is no conflict of interests.

## Acknowledgments

This work is financially supported by the National Natural Science Foundation of China (81571797), the 333 Plan Foundation of Jiangsu, China (BRA2017173), and the project of Taizhou People's Hospital (ZL201734).

## References

[1] R. Saini, S. Saini, and S. Sharma, "Nanotechnology: the future medicine," *Journal of Cutaneous and Aesthetic Surgery*, vol. 3, no. 1, pp. 32-33, 2010.

[2] T. Eslaminejad, S. N. Nematollahi-Mahani, and M. Ansari, "Glioblastoma targeted gene therapy based on pEGFP/p53-loaded superparamagnetic iron oxide nanoparticles," *Current Gene Therapy*, vol. 17, no. 1, pp. 59–69, 2017.

[3] Y. X. J. Wang, S. M. Hussain, and G. P. Krestin, "Superparamagnetic iron oxide contrast agents: physicochemical characteristics and applications in MR imaging," *European Radiology*, vol. 11, no. 11, pp. 2319–2331, 2001.

[4] P. Xue, L. Sun, Q. Li et al., "PEGylated polydopamine-coated magnetic nanoparticles for combined targeted chemotherapy and photothermal ablation of tumour cells," *Colloids and Surfaces B: Biointerfaces*, vol. 160, pp. 11–21, 2017.

[5] B. D. Chithrani, A. A. Ghazani, and W. C. W. Chan, "Determining the size and shape dependence of gold nanoparticle uptake into mammalian cells," *Nano Letters*, vol. 6, no. 4, pp. 662–668, 2006.

[6] M. Jeyaraj, G. Sathishkumar, G. Sivanandhan et al., "Biogenic silver nanoparticles for cancer treatment: an experimental report," *Colloids and Surfaces B: Biointerfaces*, vol. 106, pp. 86–92, 2013.

[7] Q. A. Pankhurst, J. Connolly, S. K. Jones, and J. Dobson, "Applications of magnetic nanoparticles in biomedicine," *Journal of Physics D: Applied Physics*, vol. 36, no. 13, pp. R167–R181, 2003.

[8] A. Akbarzadeh, M. Samiei, and S. Davaran, "Magnetic nanoparticles: preparation, physical properties, and applications in biomedicine," *Nanoscale Research Letters*, vol. 7, no. 1, pp. 144–156, 2012.

[9] S. Blundell and D. Thouless, "Magnetism in condensed matter," *American Journal of Physics*, vol. 71, no. 1, pp. 94-95, 2003.

[10] J. H. Kim, S. M. Kim, and Y. I. Kim, "Properties of magnetic nanoparticles prepared by co-precipitation," *Journal of Nanoscience and Nanotechnology*, vol. 14, no. 11, pp. 8739–8744, 2014.

[11] L. Borlido, A. M. Azevedo, A. C. A. Roque, and M. R. Aires-Barros, "Magnetic separations in biotechnology," *Biotechnology Advances*, vol. 31, no. 8, pp. 1374–1385, 2013.

[12] D. Jin, X. Jiang, X. Jing, and Z. Ou, "Effects of concentration, head group, and structure of surfactants on the degradation of phenanthrene," *Journal of Hazardous Materials*, vol. 144, no. 1-2, pp. 215–221, 2007.

[13] H. Jiang, H. Wu, Y. L. Xu, J. Z. Wang, and Y. Zeng, "Preparation of galactosylated chitosan/tripolyphosphate nanoparticles and application as a gene carrier for targeting SMMC7721 cells," *Journal of Bioscience and Bioengineering*, vol. 111, no. 6, pp. 719–724, 2011.

[14] P. Pradhan, J. Giri, F. Rieken et al., "Targeted temperature sensitive magnetic liposomes for thermo-chemotherapy," *Journal of Controlled Release*, vol. 142, no. 1, pp. 108–121, 2010.

[15] D. Chen, Q. Tang, W. Xue, J. Xiang, L. Zhang, and X. Wang, "The preparation and characterization of folate-conjugated human serum albumin magnetic cisplatin nanoparticles," *Journal of Biomedical Research*, vol. 24, no. 1, pp. 26–32, 2010.

[16] M. Kumagai, T. K. Sarma, H. Cabral et al., "Enhanced in vivo magnetic resonance imaging of tumors by PEGylated iron-oxide–gold core–shell nanoparticles with prolonged blood circulation properties," *Macromolecular Rapid Communications*, vol. 31, no. 17, pp. 1521–1528, 2010.

[17] I. Y. Goon, L. M. H. Lai, M. Lim, P. Munroe, J. J. Gooding, and R. Amal, "Fabrication and dispersion of gold-shell-protected magnetite nanoparticles: systematic control using polyethyleneimine," *Chemistry of Materials*, vol. 21, no. 4, pp. 673–681, 2009.

[18] M. Corti, A. Lascialfari, M. Marinone et al., "Magnetic and relaxometric properties of polyethylenimine-coated superparamagnetic MRI contrast agents," *Journal of Magnetism and Magnetic Materials*, vol. 320, no. 14, pp. e316–e319, 2008.

[19] Y. Zhang, L. Zhang, X. Song et al., "Synthesis of superparamagnetic iron oxide nanoparticles modified with MPEG-PEI via photochemistry as new MRI contrast agent," *Journal of Nanomaterials*, vol. 2015, Article ID 417389, 6 pages, 2015.

[20] E. C. Gryparis, M. Hatziapostolou, E. Papadimitriou, and K. Avgoustakis, "Anticancer activity of cisplatin-loaded PLGA-mPEG nanoparticles on LNCaP prostate cancer cells," *European Journal of Pharmaceutics and Biopharmaceutics*, vol. 67, no. 1, pp. 1–8, 2007.

[21] Z. Tu, B. Zhang, G. Yang et al., "Synthesis of poly(ethylene glycol) and poly(vinyl pyrrolidone) co-coated superparamagnetic iron oxide nanoparticle as a pH-sensitive release drug carrier," *Colloids and Surfaces A: Physicochemical and Engineering Aspects*, vol. 436, pp. 854–861, 2013.

[22] M. Yu, S. Huang, K. J. Yu, and A. M. Clyne, "Dextran and polymer polyethylene glycol (PEG) coating reduce both 5 and 30 nm iron oxide nanoparticle cytotoxicity in 2D and 3D cell culture," *International Journal of Molecular Sciences*, vol. 13, no. 5, pp. 5554–5570, 2012.

[23] Q.-S. Tang, D.-S. Zhang, N. Gu, X.-M. Cong, M.-L. Wan, and L.-Q. Jin, "Synthesis and in vitro study of PEI-coated Mn-Zn ferrite: a novel gene vector," *Journal of Functional Materials*, vol. 38, no. 8, pp. 1268–1272, 2007.

[24] Y. B. Zhou, Z. Tang, C. Shi, S. Shi, Z. Qian, and S. Zhou, "Polyethylenimine functionalized magnetic nanoparticles as a potential non-viral vector for gene delivery," *Journal of Materials Science: Materials in Medicine*, vol. 23, no. 11, pp. 2697–2708, 2012.

[25] H. W. Sun, X. Zhu, L. Zhang et al., "PDEA-coated magnetic nanoparticles for gene delivery to Hep G2 cells," *Biotechnology and Bioprocess Engineering*, vol. 18, no. 4, pp. 648–654, 2013.

[26] H. Shokrollahi, A. Khorramdin, and G. Isapour, "Magnetic resonance imaging by using nano-magnetic particles," *Journal of Magnetism and Magnetic Materials*, vol. 369, no. 11, pp. 176–183, 2014.

[27] X. Y. Shi, S. H. Wang, S. D. Swanson et al., "Dendrimer-functionalized shell-crosslinked iron oxide nanoparticles for in-vivo magnetic resonance imaging of tumors," *Advanced Materials*, vol. 20, no. 9, pp. 1671–1678, 2008.

[28] Z. Li, L. Wei, M. Y. Gao, and H. Lei, "One-pot reaction to synthesize biocompatible magnetite nanoparticles," *Advanced Materials*, vol. 17, no. 8, pp. 1001–1005, 2005.

[29] A. H. Rezayan, M. Mousavi, S. Kheirjou, G. Amoabediny, M. S. Ardestani, and J. Mohammadnejad, "Monodisperse magnetite ($Fe_3O_4$) nanoparticles modified with water soluble polymers for the diagnosis of breast cancer by MRI method," *Journal of Magnetism and Magnetic Materials*, vol. 420, pp. 210–217, 2016.

[30] G. Jin, D. Li, L. Xia, Y. Long, Y. Liu, and J. Quan, "Preparation of chitosan-lactose acid-SPION and its application in MR imaging in vivo," *Journal of Medical Science Yanbian University*, vol. 37, no. 4, pp. 268–270, 2014.

[31] C. Sun, O. Veiseh, J. Gunn et al., "In vivo MRI detection of gliomas by chlorotoxin-conjugated superparamagnetic nanoprobes," *Small*, vol. 4, no. 3, pp. 372–379, 2008.

[32] O. Veiseh, C. Sun, J. Gunn et al., "Optical and MRI multifunctional nanoprobe for targeting gliomas," *Nano Letters*, vol. 5, no. 6, pp. 1003–1008, 2005.

[33] M. Anbarasu, M. Anandan, E. Chinnasamy, V. Gopinath, and K. Balamurugan, "Synthesis and characterization of polyethylene glycol (PEG) coated $Fe_3O_4$ nanoparticles by chemical co-precipitation method for biomedical applications," *Spectrochimica Acta Part A: Molecular and Biomolecular Spectroscopy*, vol. 135, no. 25, pp. 536–539, 2015.

[34] H.-J. Chen, Z. H. Zhang, L. J. Luo, and S. Z. Yao, "Surface-imprinted chitosan-coated magnetic nanoparticles modified multi-walled carbon nanotubes biosensor for detection of bovine serum albumin," *Sensors and Actuators B: Chemical*, vol. 163, no. 1, pp. 76–83, 2012.

[35] I. K. Ko, H. T. Song, E. J. Cho, E. S. Lee, Y. M. Huh, and J. S. Suh, "In vivo MR imaging of tissue-engineered human mesenchymal stem cells transplanted to mouse: a preliminary study," *Annals of Biomedical Engineering*, vol. 35, no. 1, pp. 101–108, 2007.

[36] S. J. Kim, B. Lewis, M. S. Steiner, U. V. Bissa, C. Dose, and J. A. Frank, "Superparamagnetic iron oxide nanoparticles for direct labeling of stem cells and in vivo MRI tracking," *Contrast Media & Molecular Imaging*, vol. 11, no. 1, pp. 55–64, 2016.

[37] G. K. Y. Wong and A. T. Chiu, "Gene therapy, gene targeting and induced pluripotent stem cells: applications in monogenic disease treatment," *Biotechnology Advances*, vol. 28, no. 6, pp. 715–724, 2010.

[38] C. Fu, L. Lin, H. Shi et al., "Hydrophobic poly (amino acid) modified PEI mediated delivery of rev-casp-3 for cancer therapy," *Biomaterials*, vol. 33, no. 18, pp. 4589–4596, 2012.

[39] D. W. Pack, A. S. Hoffman, S. Pun, and P. S. Stayton, "Design and development of polymers for gene delivery," *Nature Reviews Drug Discovery*, vol. 4, no. 7, pp. 581–593, 2005.

[40] G. Xiaoxiao, D. Baoji, L. Yunhui, G. Ying, L. Dan, and W. Erkang, "Vectors based on nanomaterials for gene delivery," *Progress in Chemistry*, vol. 27, no. 8, pp. 1093–1101, 2015.

[41] L. Naldini, "Gene therapy returns to centre stage," *Nature*, vol. 526, no. 7573, pp. 351–360, 2015.

[42] C.-Y. Chen, C.-Y. Lin, G.-Y. Chen, and Y. C. Hu, "Baculovirus as a gene delivery vector: recent understandings of molecular alterations in transduced cells and latest applications," *Biotechnology Advances*, vol. 29, no. 6, pp. 618–631, 2011.

[43] S. Huang and M. Kamihira, "Development of hybrid viral vectors for gene therapy," *Biotechnology Advances*, vol. 31, no. 2, pp. 208–223, 2013.

[44] J. R. Viola, S. El-Andaloussi, I. I. Oprea, and C. I. E. Smith, "Non-viral nanovectors for gene delivery: factors that govern successful therapeutics," *Expert Opinion on Drug Delivery*, vol. 7, no. 6, pp. 721–735, 2010.

[45] C. Morrison, "$1-million price tag set for Glybera gene therapy," *Nature Biotechnology*, vol. 33, no. 3, pp. 217-218, 2015.

[46] T. A. Balbino, A. A. M. Gasperini, C. L. P. Oliveira, A. R. Azzoni, L. P. Cavalcanti, and L. G. de la Torre, "Correlation of the physicochemical and structural properties of pDNA/cationic liposome complexes with their in vitro transfection," *Langmuir*, vol. 28, no. 31, pp. 11535–11545, 2012.

[47] J. Hewinson, J. F. R. Paton, and S. Kasparov, "Viral gene delivery: optimized protocol for production of high titer lentiviral vectors," *Methods in Molecular Biology*, vol. 998, pp. 65–75, 2013.

[48] I. Venugopal, S. Pernal, A. Duproz, J. Bentley, H. Engelhard, and A. Linninger, "Magnetic field-enhanced cellular uptake of doxorubicin loaded magnetic nanoparticles for tumor treatment," *Materials Research Express*, vol. 3, no. 9, 2016.

[49] S. Liao, C. Liu, B. P. Bastakoti et al., "Functionalized magnetic iron oxide/alginate core-shell nanoparticles for targeting hyperthermia," *International Journal of Nanomedicine*, vol. 10, pp. 3315–3328, 2015.

[50] M. P. Arachchige, S. S. Laha, A. R. Naik, K. T. Lewis, R. Naik, and B. P. Jena, "Functionalized nanoparticles enable tracking the rapid entry and release of doxorubicin in human pancreatic cancer cells," *Micron*, vol. 92, pp. 25–31, 2017.

[51] Y. Cui, M. Zhang, F. Zeng, H. Jin, Q. Xu, and Y. Huang, "Dual-targeting magnetic PLGA nanoparticles for codelivery of paclitaxel and curcumin for brain tumor therapy," *ACS Applied Materials & Interfaces*, vol. 8, no. 47, pp. 32159–32169, 2016.

[52] S. Zhang, L. Wang, L. Chen et al., "Molecular image of superparamagnetic iron oxide nanopariticle labeled with hATF in colon tumor models," *Journal of Biomedical Engineering*, vol. 32, no. 5, pp. 1067–1074, 2015.

[53] W. Chakraborty, R. Ray, N. Samanta, and C. RoyChaudhuri, "Quantitative differentiation of multiple virus in blood using nanoporous silicon oxide immunosensor and artificial neural network," *Biosensors and Bioelectronics*, vol. 98, pp. 180–188, 2017.

[54] H. Afsharan, F. Navaeipour, B. Khalilzadeh et al., "Highly sensitive electrochemiluminescence detection of p53 protein using functionalized Ru–silica nanoporous@gold nanocomposite," *Biosensors and Bioelectronics*, vol. 80, pp. 146–153, 2016.

[55] C. Costa, F. Brandão, M. J. Bessa et al., "In vitro cytotoxicity of superparamagnetic iron oxide nanoparticles on neuronal and glial cells. Evaluation of nanoparticle interference with viability tests," *Journal of Applied Toxicology*, vol. 36, no. 3, pp. 361–372, 2016.

[56] M. Lin, J. X. Huang, J. Zhang et al., "The therapeutic effect of PEI-$Mn_{0.5}Zn_{0.5}Fe_2O_4$ nanoparticles/pEgr1-HSV-TK/GCV associated with radiation and magnet-induced heating on hepatoma," *Nanoscale*, vol. 5, no. 3, pp. 991–1000, 2013.

[57] Y. Tang and A. J. McGoron, "Increasing the rate of heating: a potential therapeutic approach for achieving synergistic tumour killing in combined hyperthermia and chemotherapy," *International Journal of Hyperthermia*, vol. 29, no. 2, pp. 145–155, 2013.

[58] A. Jordan, P. Wust, R. Scholz et al., "Cellular uptake of magnetic fluid particles and their effects on human adenocarcinoma cells exposed to AC magnetic fields in vitro," *International Journal of Hyperthermia*, vol. 12, no. 6, pp. 705–722, 1996.

[59] W. Chen, P. Yi, Y. Zhang, L. Zhang, Z. Deng, and Z. Zhang, "Composites of aminodextran-coated $Fe_3O_4$ nanoparticles and graphene oxide for cellular magnetic resonance imaging," *ACS Applied Materials & Interfaces*, vol. 3, no. 10, pp. 4085–4091, 2011.

[60] K. Hayashi, K. Ono, H. Suzuki et al., "High-frequency, magnetic-field-responsive drug release from magnetic nanoparticle/organic hybrid based on hyperthermic effect," *ACS Applied Materials & Interfaces*, vol. 2, no. 7, pp. 1903–1911, 2010.

[61] S. Laurent, S. Dutz, U. O. Häfeli, and M. Mahmoudi, "Magnetic fluid hyperthermia: focus on superparamagnetic iron oxide nanoparticles," *Advances in Colloid and Interface Science*, vol. 166, no. 1-2, pp. 8–23, 2011.

[62] F. K. Storm, W. H. Harrison, R. S. Elliott, and D. L. Morton, "Normal tissue and solid tumor effects of hyperthermia in animal models and clinical trials," *Cancer Research*, vol. 39, no. 6, Part 2, pp. 2245–2251, 1979.

[63] X. Liang, H. Zhou, X. Liu et al., "Effect of local hyperthermia on lymphangiogenic factors VEGF-C and -D in a nude mouse xenograft model of tongue squamous cell carcinoma," *Oral Oncology*, vol. 46, no. 2, pp. 111–115, 2010.

[64] T. J. Vogl, P. Farshid, N. N. N. Naguib, and S. Zangos, "Thermal ablation therapies in patients with breast cancer liver metastases: a review," *European Radiology*, vol. 23, no. 3, pp. 797–804, 2013.

[65] C. S. Muenyi, A. R. Pinhas, T. W. Fan, G. N. Brock, C. W. Helm, and J. C. States, "Sodium arsenite ± hyperthermia sensitizes p53-expressing human ovarian cancer cells to cisplatin by modulating platinum-DNA damage responses," *Toxicological Sciences*, vol. 127, no. 1, pp. 139–149, 2012.

[66] H. Ni, D. Zhang, N. Gu et al., "Preparation and characterization of Mn-Zn ferrite magnetic nanoparticles for tumor hyperthermia," *Journal of Chinese Electron Microscopy Society*, vol. 25, no. 1, pp. 66–70, 2006.

[67] J. Liu, J. Zhang, L. Wang, Y. T. Li, and D. S. Zhang, "Biocompatibility study of $Mn_{0.5}Zn_{0.5}Fe_2O_4$ magnetic nanoparticles," *Key Engineering Materials*, vol. 483, pp. 552–558, 2011.

[68] C. Zhao, C. Yuan, and G. Wu, "p[5HRE]AFPp-p53/PEI-$Fe_3O_4$ magnetic nanoparticle combined with magnetic fluid hyperthermia inhibit hepatoma cells," *Chinese Journal of Cancer Biotherapy*, vol. 23, no. 1, pp. 44–51, 2016.

[69] J. Xie, Y. Zhang, C. Yan et al., "High-performance PEGylated Mn–Zn ferrite nanocrystals as a passive-targeted agent for magnetically induced cancer theranostics," *Biomaterials*, vol. 35, no. 33, pp. 9126–9136, 2014.

[70] O. K. Arriortua, E. Garaio, B. Herrero de la Parte et al., "Antitumor magnetic hyperthermia induced by RGD-functionalized $Fe_3O_4$ nanoparticles, in an experimental model of colorectal liver metastases," *Beilstein Journal of Nanotechnology*, vol. 7, pp. 1532–1542, 2016.

[71] M. Lin, J. Huang, X. Jiang et al., "A combination hepatoma-targeted therapy based on nanotechnology: pHRE-Egr1-HSV-TK/$^{131}$I-antiAFPMcAb-GCV/MFH," *Scientific Reports*, vol. 6, no. 1, article 33524, 2016.

[72] Z. Y. Wang, J. Song, and D. S. Zhang, "Nanosized $As_2O_3$/$Fe_2O_3$ complexes combined with magnetic fluid hyperthermia selectively target liver cancer cells," *World Journal of Gastroenterology*, vol. 15, no. 24, pp. 2995–3002, 2009.

Hindawi
Journal of Nanomaterials
Volume 2018, Article ID 8950143, 9 pages
https://doi.org/10.1155/2018/8950143

*Review Article*

# Surface Disinfections: Present and Future

**Matteo Saccucci**,[1] **Erika Bruni**,[2] **Daniela Uccelletti**,[2] **Agnese Bregnocchi**,[3] **Maria Sabrina Sarto**,[3] **Maurizio Bossù**,[1] **Gabriele Di Carlo**,[1] **and Antonella Polimeni**[1]

[1]*Department of Oral and Maxillofacial Sciences, Sapienza University of Rome, Viale Regina Elena 287a, 00161 Rome, Italy*
[2]*Department of Biology and Biotechnology "Charles Darwin", Sapienza University of Rome, Piazzale Aldo Moro 5, 00185 Rome, Italy*
[3]*Department of Aerospace, Electrical and Energy Engineering, Sapienza University of Rome, Via Eudossiana 18, 00184 Rome, Italy*

Correspondence should be addressed to Matteo Saccucci; matteo.saccucci@uniroma1.it

Received 27 December 2017; Accepted 7 March 2018; Published 16 April 2018

Academic Editor: Mauro Pollini



The propagation of antibiotic resistance increases the chances of major infections for patients during hospitalization and the spread of health related diseases. Therefore finding new and effective solutions to prevent the proliferation of pathogenic microorganisms is critical, in order to protect hospital environment, such as the surfaces of biomedical devices. Modern nanotechnology has proven to be an effective countermeasure to tackle the threat of infections. On this note, recent scientific breakthroughs have demonstrated that antimicrobial nanomaterials are effective in preventing pathogens from developing resistance. Despite the ability to destroy a great deal of bacteria and control the outbreak of infections, nanomaterials present many other advantages. Moreover, it is unlikely for nanomaterials to develop resistance due to their multiple and simultaneous bactericidal mechanisms. In recent years, science has explored more complex antimicrobial coatings and nanomaterials based on graphene have shown great potential in antibacterial treatment. The purpose of this article is to deepen the discussion on the threat of infections related to surface disinfection and to assess the state of the art and potential solutions, with specific focus on disinfection procedures using nanomaterials.

## 1. Introduction

One of the most important routine practices in dental units is the chemical disinfection of surfaces and instruments for infection control. When it comes to selecting disinfectants, it is crucial to take into account several aspects, such as timing, disinfection methods, the risks posed by using germicides, and factors affecting their effectiveness [1]. Chemical disinfectants are essentially active substances in aqueous solutions, engaged in different forms according to their final purpose: immersion, sterilization, disinfection, and decontamination of medical equipment, such as sprays to disinfect the surfaces. Sterilizing and disinfectant products are classified in three levels: high, intermediate, and low, according to the pathogens they are able to kill [2–5]. However, it should be remembered that sterilization with sterilizing by means of chemical products, for critical and semicritical items, is always the second choice in terms of process to be implemented on thermosensitive material (for which sterilizing with heat is not advised). The correct use of disinfectants should take into account the fact that the biocide property is influenced by the concentration, time of contact, and potential traces of interfering material or substances (e.g., organic fluids, soap, metallic ions, and pH) [6–8]. Ideally, the perfect disinfectant should possess a complete antimicrobial spectrum, act rapidly and persistently, lack toxicity to humans and the environment, be compatible with the material to treat, be chemically stable, and be economical and easy to use. Actually, no product meets all these requirements; therefore, we need to find the best possible compromise to achieve the ideal result, minimizing the disadvantages related to their use [9]. In order to reach this target, all the details and information written in the technical sheet and safety documents provided by the manufacturer must be carefully analysed. All the chemical and physical features are listed in this documentation, and there are instructions for the correct usage and disposal in order to prevent the equipment from being damaged and protect the worker's safety at the same time. Once a disinfectant passes the cell wall, it is able to act on the pathogen organism through coagulation mechanisms and protein oxidation of microbial cells and by denaturalizing bacterial enzymes. If these substances are

compatible, they can be used in association and produce a synergetic action that enhances the technical features of the final product [10]. There are several compounds that can be divided into groups according to the basic compound they originate from. There is a wide range of disinfectants available on the market, including halogen compounds like sodium hypochlorite, alcohols, peroxygen compounds like hydrogen peroxide, and aldehydes like glutaraldehyde, all of which have a broad efficacy spectrum if used appropriately. Other types of disinfectants such as phenols, quaternary ammonium compounds, and biguanides (including chlorhexidine) are mostly ineffective with nonenveloped viruses and bacterial spores, and most of them have limited ability to kill mycobacteria [11, 12]. Chemical products like disinfectant, germicide, microbiocide, and biocide are often confused, and many of their synonyms imply a broad spectrum of efficiency against multiple microbial pathogens. Nevertheless, a certain product may potentially be effective only against one class of microorganism. The main target of the disinfection process is to interrupt the transmission of pathogens from an infected subject to a susceptible host. Chemical disinfection is generally limited to the use of liquid germicides on equipment and environmental surfaces. Surface contamination of a pathogen shed into the environment can occur directly or by means of settled aerosols. Environmental factors such as temperature, relative humidity, the specific nature of the pathogen, and its suspending medium determine the survival of these organisms. Their lifespan ranges from a few minutes to weeks and even months. During this period of time, contact with the contaminated item can lead to direct inoculation of a susceptible host or, more commonly, contamination of another vehicle, like the hands, through which indirect inoculation occurs. Disinfectants may prove effective in preventing the survival of pathogens and their transfer to subordinate vehicles and ultimately to susceptible hosts [13]. Nevertheless, chemical disinfection should only be employed when heat sterilization is not possible. In some cases however, it is necessary to perform a high-level chemical disinfection of the medical instruments after each use [14]. Evaluating the patients' and staff's risk exposure to potentially contaminated surfaces (directly or from settled aerosols), such as frequently contacted surfaces, is crucial to determining the need to disinfect environmental surfaces. There are three basic principles, of equal importance, that must be followed to achieve a successful result. It is important to choose a good product since poor disinfectants will fail even if properly applied. Applying the correct protocol for the selected product is also very important because even using a good product may prove ineffective if the method of application is not good contact with the contaminated surface/s. Disinfection presents a duality within its nature. A disinfectant is a powerful substance engineered to kill and can pose a serious threat if used frequently or improperly [15]. Resistance to germicides is extremely rare and, yet, lately there has been significant interest in the fact that there are some mechanisms of bacterial resistance that overlap between germicides and antibiotics, which in either way are bacterial toxins. Thus, the exposure to sublethal concentrations of germicides may trigger antibiotic resistance.

## 2. Antibiotic Resistance

At the beginning of the twentieth century, infectious diseases were the main cause of death in the world and only with the introduction of antibiotics was it possible to reduce the mortality rate caused by them. These molecules revolutionized modern medicine, saving millions of lives and containing many serious infections. They were considered as "wonder drugs" because of their nature: these are chemical compounds produced by actinomycetes, fungi, or bacteria capable of acting on other microorganisms inhibiting growth (bacteriostatic effect) or killing them (bactericidal effect). Antibiotics have many modes of action, such as inhibiting the synthesis of a bacterial cell wall, biosynthesis of proteins, RNA, DNA, and disrupting membrane organization. The use of antibiotics began with the commercial production of penicillin at the end of 1940 and was a great success until the development of newer more effective molecules in the 1980s [16]. In the last decade, these medicines remained one of the most commonly prescribed classes of drugs, with 70 billion of doses consumed [17]. An unforeseen aspect, after discovery of antibiotics, was their widespread use, abuse, and misuse in various forms and in different parts of the world. The level of antibiotic-resistant infections was found to be strongly linked to the increase of antibiotic consumption [18]. Over the next five decades since the introduction of these drugs, there has been an unprecedented natural selection in evolutionary history that had led to an increasing number of resistant strains [19]. The discovery of new molecules and the chemical modification of existing ones, however, did not overcome the problem. In addition, the development of antimicrobial drugs gave a low return on investment, so since the late 1980s, it was possible to observe a gap in the production of antimicrobials, which was abandoned in favour of medicines that allowed for a greater profit. This had further contributed to the current crisis in the fight against drug-resistant pathogens [20]. Antibiotic-resistant organisms are known as "superbugs," which are no longer sensitive to antibiotic and continue to multiply in its presence. The World Health Organization estimated 25,000 deaths due to drug-resistant infections every year only in Europe, while in the United States, more than 63,000 patients die every year from hospital-acquired bacterial infections that cost about $35 billion to society, causing discomforts also economically [16]. The first serious clinical threat in fighting infectious diseases occurred with Enterococcus Vancomycin-resistant strains (VRE), which possess intrinsic resistance to many of the commonly used antibiotics and, perhaps more importantly, the ability to gain resistance to many antibiotics present on the market [21]. Among other things, recent American studies have found that more than 40% of *Staphylococcus aureus* strains collected in hospitals resulted in being resistant to methicillin (strains of *S. aureus* methicillin-resistant, MRSA) and some of them also to vancomycin (multidrug-resistance), unfortunately a recent molecule [22]. Antibiotic resistance is a natural process that occurs via gene level mutation and for this reason it is impossible to overcome or prevent its development. Indeed, a simple selective pressure and an imperfect chromosome replication lead to acquiring one or more mutations in the

protein or gene target of the antibiotic that prevents binding (transforming the target into insensitive variants) [23]. The new antibiotic capability by bacteria is acquired de novo by genetic mutations or obtained from an external source. In fact bacteria are able to transfer and interchange genetic material directly between each other by transferring plasmids. This mechanism is known as horizontal gene transfer (HGT) and it is common among bacteria, even among those that are phylogenetically distant [24]. It is considered as one of the most important reasons in the evolution of drug resistance that acts in association with natural selection. Resistant bacteria can also spread in the environment thanks to the presence of human and animal excrements, as in the case of farms and wastewaters, which are able to convey such microorganisms, spreading them elsewhere. Antibiotic-resistant species and traces of drugs can pass through the intestines of humans and animals, contaminating subsequently waters and soils: in fact, rivers and lands cultivated with the use of organic fertilizers coming from animals fed with antibiotics would be able to induce the proliferation of bacteria resistant to them [25]. Bacteria that are not annihilated by antibiotics resist their action and continue to multiply, creating increasingly resistant strains which, after being fortified, may reach our organism by passing through the aquifers or the food grown on contaminated soils. Nowadays water resources are among the major sources of hyperresistant bacteria [26, 27]. Resistant bacteria are involved in the high incidence of healthcare-acquired infections (HAIs), recognized as critical emergence in hospitals and clinics around the world. Infected patients disseminate and release many multidrug-resistant Gram-negative and Gram-positive species to other ones and to healthy people: such bacteria share the ability to survive on various hospital surfaces for long periods and for this reason they are difficult to eradicate by cleaning and chemical disinfection. From surfaces, pathogens may infect patients by direct contact or indirectly, by means of the hands of medicals and healthcare workers. Thus cleaning and surface disinfection are very important in order to limit their transfer and reduce their diffusion [28]. The efficacy of cleaning practices can be affected by many factors, which can compromise the disinfectant action itself. Many studies report that different types of surfaces prepossess the bacteria removal properties [29]. Besides, an inadequate use of disinfectants and incorrect contact times result in low surface disinfection. If manufacturer's instructions are not followed, contaminations of sanitiser solutions may also occur worsening the situation [30]. In addition, the use of disinfectant wipes with a poor germicide activity and composed of a considerable quantity of cellulose or cotton (which can sequestrate quaternary ammonium molecules) may decrease their efficaciousness and serve conversely as means for microbes [31, 32]. New disinfectants, antimicrobial surfaces, automated dispersal systems, UV irradiation, hydrogen peroxide decontamination, and steam treatments could represent novel overtures in contrast with the traditional and often ineffective cleaning methods; however, they are more expensive than usual ones [33].

So with the aim of preventing and controlling infectious diseases caused by multidrug-resistant bacteria, we need continually to develop new strategies and therapeutic innovations to contribute to the fight against antibiotic resistance. For this reason, during the last years, a great importance was given to the research of novel substances and compounds with antimicrobial activity. In this regard, nanomaterials and nanoscience seem to be a good solution in solving this public health problem.

## 3. Graphene-Based Nanomaterials as Novel Antimicrobial Drugs

A new perspective in the treatment of bacterial infections is offered by the use of nanomaterials and nanoparticles as novel and nontraditional antibacterial agents [34–37]. In particular, more recently, graphene has been proposed as a novel antimicrobial material. Graphene is a single-layer sheet of carbon atoms that are packed closely in a two-dimensional (2D) honeycomb lattice. It has unique physicochemical properties including a high surface area, extraordinary electrical and thermal conductivity, and strong mechanical strength [38–40]. Graphene and its derivatives (like graphene nanoplatelets, multilayer graphene flakes, graphene oxide, and reduced graphene oxide) are considered graphene-based nanomaterials (GFNs) and have been studied extensively in material science, chemistry, biotechnology, and nanomedicine for a wide range of applications including biosensing/bioimaging, disease diagnostics, drug delivery, and photothermal therapy [41–46]. GFNs vary in shape, size, surface area, layer number, lateral dimensions, surface chemistry, stiffness, defect density or quality of the individual graphene sheets, and purity; and all these properties significantly influence the interaction of GFNs with biological systems [47]. Generally, GFNs with small size, sharp edges, and rough surfaces easily internalize into the cell as compared to larger, smooth GFNs [48]. GFNs, particularly monolayer graphene, have the theoretical maximum surface area because every atom lies on the surface, providing an extremely high capacity for drug delivery [49, 50]. In particular, more recently, graphene has been proposed as a novel antimicrobial material, with a strong cytotoxic effect on both Gram-positive and Gram-negative bacteria and fungi [48–52] but a very low cytotoxic effect on human cells and animal models [53, 54]. In general, with respect to carbon nanotubes, graphene-based nanomaterials are preferable due to the lower production cost and ease of manipulation. With reference to antimicrobial application, graphene-based materials are preferred with respect to carbon nanotube due to their better efficiency against bacteria and ease of use [51]. Reports indicate that GFNs exert cytotoxicity in both in vitro and in vivo studies in various types of bacteria, mammalian cells, and animal models [53]. Among them, graphene oxide (GO) has good antibacterial effect against *Pseudomonas aeruginosa* and *Staphylococcus aureus* compared to benzalkonium chloride one, a common surface disinfectant. Reduced GO (rGO) can be also used as an antibacterial surface when it is activated by solar near-infrared irradiation that gives it the ability to kill the majority of airborne bacteria on contact, proving to be a very efficient coating nanomaterial [55]. It has been shown that these nanostructures also have

a remarkable antimicrobial activity against some multidrug-resistant bacteria such as *Klebsiella pneumoniae*, *Escherichia coli*, and *P. aeruginosa* [56]. Most published studies have evaluated graphene oxide (GO) and reduced GO (rGO) due to their better solubility/dispersibility/stability in water and under physiological conditions compared to other GFNs. However, it is demonstrated that GO and rGO induce formation of reactive oxygen species (ROS), which are representative of an induced oxidative stress on the cell. On the contrary, it is demonstrated that multilayer graphene flakes and graphene nanoplatelets have cytotoxic effect on bacteria cell but without induction of ROS [53]. Like in other types of nanocompound, the antimicrobial effect of graphene derivatives is defined by mechanical interactions damaging cell walls and by its chemical oxidation that lead to the generation of reactive oxygen species (ROS) [57]. Several works report the development and production of graphene-based nanomaterials, zinc-oxide nanostructures, and zinc-oxide-decorated graphene nanoplatelets [58, 59] for use as severe antibacterial and antibiofilm agents [60–62] (Figure 1) but without exerting relevant cytotoxic effect on human cells in vitro. Physical interaction between nanomaterial and bacterial cell leads to a direct damage of the cell wall, whereas chemical interaction leads primarily to formation of reactive oxygen species (ROS), which are representative of an induced oxidative stress on the cell. In particular, this developed nanomaterial does not induce ROS production on the cell, and for this reason it can produce a cytotoxic effect on bacteria and fungi but not on human cells and animal models [60]. In general, the antibacterial action of nanomaterials and nanoparticles involves both physical and chemical effects. The interaction mechanisms that can be considered as the main cause of the antimicrobial effects of nanoparticles and graphene-based materials cannot be understood or expected without taking into consideration the fact that phenomena intrinsic to the nanoscale are governed by quantum effects and by the domain of the phenomena of surface and interface. It is known that nanostructures and nanoparticles are characterized by an increasing ratio between surface and volume atoms, as their size decreases. Therefore, nanoparticles are characterized by a much stronger surface interaction capability with other objects than microsized particles. In graphene, volume approaches zero and surface area infinity; it is thus understood that nanostructures have a much higher probability to get in touch and interact strongly with bacterial cell than microparticles [63]. There are several interaction mechanisms between nanomaterials and cell walls. Among them is bacterial wrapping: this mechanism characterizes the interaction, for example, of graphene nanoplatelets with bacteria, as shown in Figure 2. The D-nanostructure adheres to the bacterium surface and induces mechanical stress [64–66]. Several results report on the important role of 2D basal planes rather than edges in antimicrobial properties, in which completely flat Langmuir–Blodgett films act against bacterial cells having few contacts with sheet edges [67, 68]. This antimicrobial mechanism is a valuable alternative to biocide-releasing surfaces that uses antibiotics or silver, which are depleted from the surface over time [69]. Antimicrobial GFN surfaces also avoid the release of toxic biocides, relevant in the design of antimicrobial surfaces for environmental applications [70].

Another antimicrobial mechanism is based on membrane punctuation: nanostructures adhere to the cell wall and penetrate through the membrane with their sharp edges as shown in Figure 3. This mechanism is a characteristic of both D and 1D nanostructures (like GNPs and ZnO-NRs) [71] and it is particularly effective in case of GNPs decorated with ZnO-NRs (ZNGs), because the 2D shape of the supporting GNP enables the 1D ZnO-NRs decorating its surface to penetrate the cell wall [72]. Strategy to decorate GO nanosheets with structure-featured metal oxides was also addressed [73]. In fact, these nanomaterials took advantage of the large specific surface area and morphological features from graphene, but also introduced the bacterial activities of metal oxides simultaneously. Recently, the synthesis of Zn–CuO@GO nanosheets to apply as disinfectants has been carried out and demonstrated their activities to combat against multi-drug-resistant bacteria strains, such as a *E. coli* multidrug-resistant strain and a methicillin-resistant *S. aureus* strain [74]. The nanosheets, inhibiting bacterial growth via physical damage, function as effective antibacterial agents. In this way, possible genetic mutation and development of other drug-resistant mechanisms might not be applicable.

Graphene is also able to induce antiadhesion of the bacterial cells over the substrate for biofilm formation and it is particularly effective in order to prevent biofilm formation, as shown in Figure 4 [61].

The mechanism based on ROS generation does not seem to be activated by the nanostructures shown in Figure 1, because graphene is fully reduced and ZnO is a biocompatible material. This limits the cytotoxicity induced on human cells *in vitro* or on animal models like *Caenorhabditis elegans* [60] as it was observed in the case of GO [75–77].

Moreover, the development of bacterial resistance to such nanomaterials is improbable because of their multiple and simultaneous bactericidal mechanisms [78, 79]. Various medical devices such as synthetic fibers, venous catheters, and surgical instruments have already been treated with nanoantimicrobial coatings, using silver nanoparticles in order to fight nosocomial infections and subsequent bacterial resistance [80].

## 4. Conclusions

Health associated diseases are the main unwanted consequence of the spread of antibiotic resistance, so that, during hospitalization, the risk of serious infections for a patient is increasing. This suggests finding innovative and functional remedies to curb the propagation of pathogenic microorganisms from the surface of biomedical devices to the surrounding hospital environment. With this purpose, nowadays nanotechnology proves to be an excellent weapon in the struggle against infection. One of the recent efforts is the discovery of antimicrobial nanomaterials, so that pathogens may not be able to develop resistance. They have several advantages besides the ability to control infections and kill many bacteria: unlike the common antibiotics and detergents, nanoparticles are not toxic, stable for long periods, and

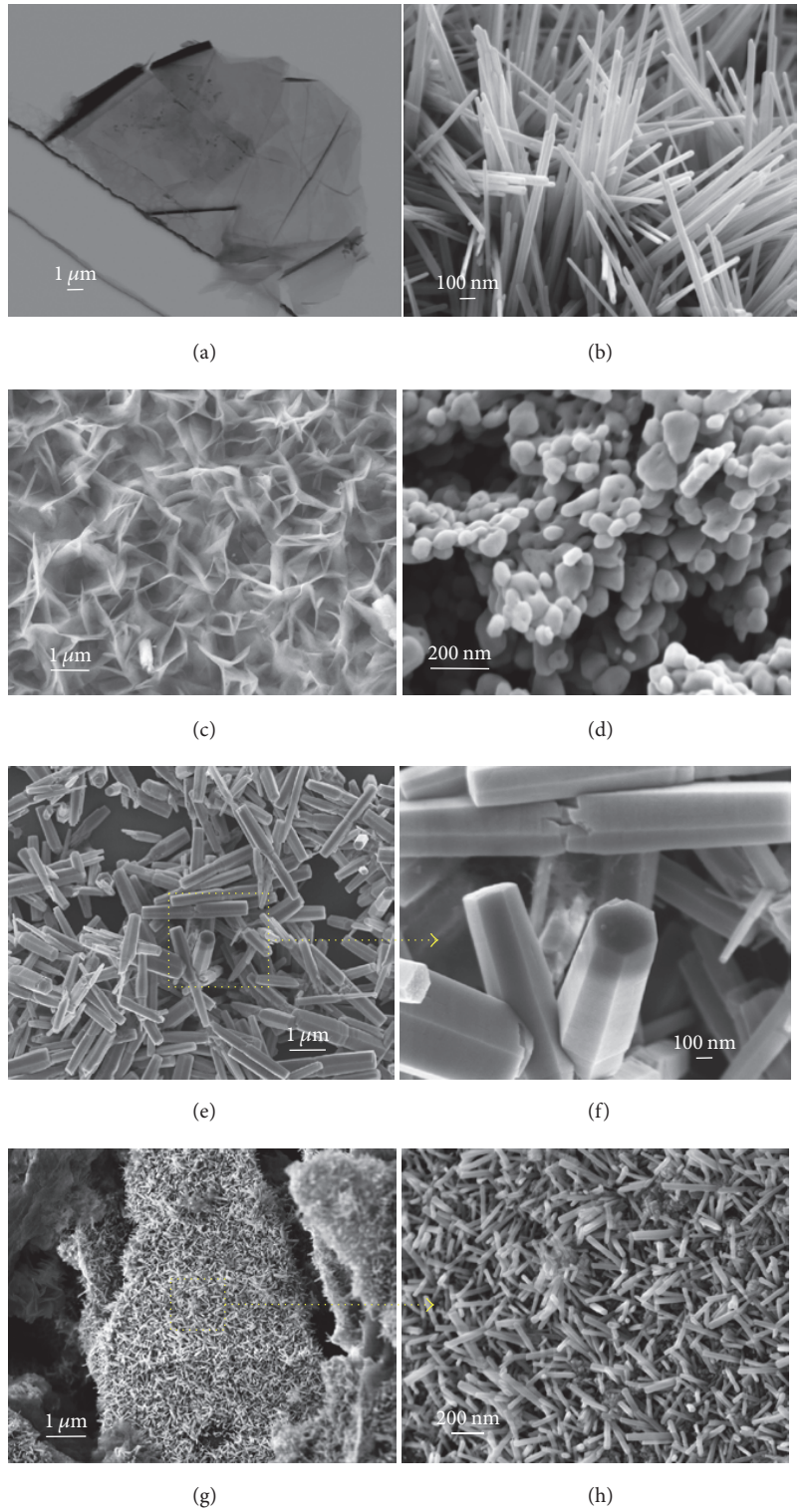


Figure 1: Original FE-SEM images showing the morphology of different nanomaterials produced at Sapienza-CNIS-DIAEE: (a) graphene nanoplatelets (GNPs); (b-c) zinc-oxide nanowalls (ZnO-NWs); (d) zinc-oxide nanoparticles (ZnO-NPs); (e-f) zinc-oxide microrods (ZnO-MRs); and (g-h) zinc-oxide-decorated GNPs (ZNGs).

simple to produce. Moreover, many chemical disinfectants have positive but above all negative aspects: there is no disinfectant with maximum effectiveness against a wide spectrum of pathogens; each case requires the choice of the most appropriate disinfectant, which depends on several factors, such as concentration, time of action, and the type of surface and microorganism. Many detergents could be contaminated by a wrong method of conservation and they could cause

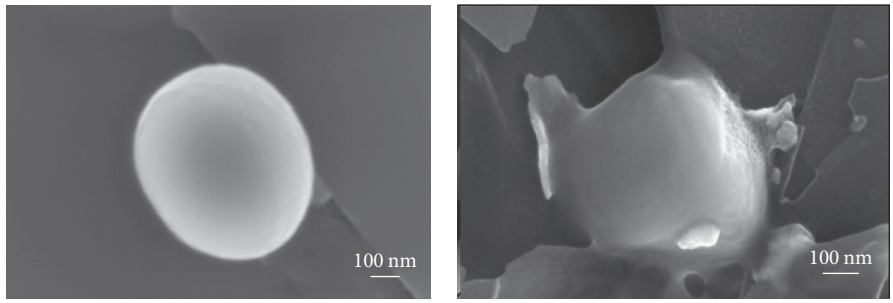


(a) (b)

Figure 2: Original FE-SEM images of *Staphylococcus aureus* (a) wrapped by a GNP (b).

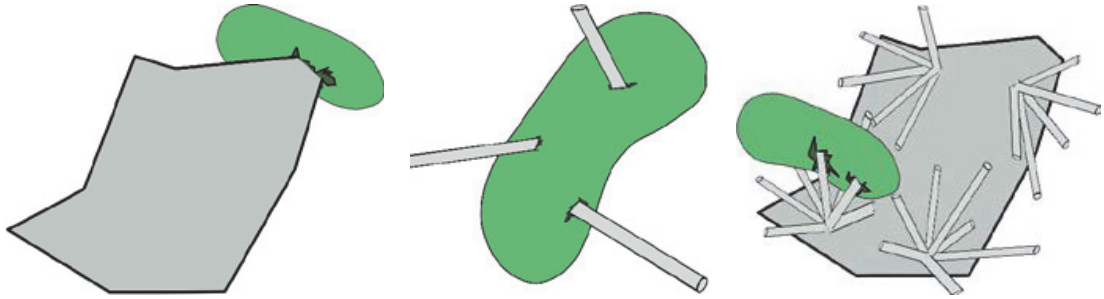

(a) (b) (c)

Figure 3: Mechanical damage of cell wall produced by sharp edges in 2D (a) or 1D (b) or hybrid 1D-2D (c) nanostructures.

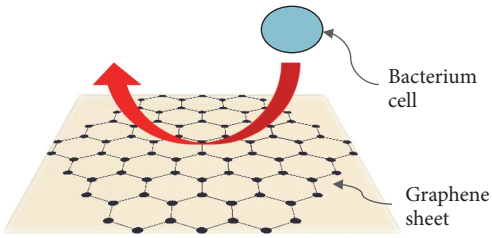


Figure 4: Inhibition of cell adhesion over a substrate induced by graphene.

hardening of plastics and a long-term deterioration of the treated materials. Therefore new generation nanomaterials may allow overcoming all these limitations and allow us to exploit only the positive aspects offered by these innovative applications. In the last years, more elaborated antimicrobial coatings were investigated and graphene-based nanomaterial emerged as promising antibacterial treatment. Layers of graphene-based nanomaterial can be employed as a novel surface coating resin or as a new fabrication material for medical devices and common objects touched by patients and hospital staff that require good disinfection and particular sanitation in the resistant-antibiotic era.

## Conflicts of Interest

The authors declare that there are no conflicts of interest regarding the publication of this paper.

## Acknowledgments

The authors would like to thank INAIL Association for the Project INAIL BRIC 2016, NanoDisp.

## References

[1] S. Springthorpe, "Disinfection of surfaces and equipment," *Journal of the Canadian Dental Association*, vol. 66, no. 10, pp. 558–560, 2000.

[2] W. A. Rutala and D. J. Weber, "Disinfection and sterilization in health care facilities: an overview and current issues," *Infectious Disease Clinics of North America*, vol. 30, no. 3, pp. 609–637, 2016.

[3] D. J. Weber, S. A. Consoli, and W. A. Rutala, "Occupational health risks associated with the use of germicides in health care," *American Journal of Infection Control*, vol. 44, no. 5, pp. e85–e89, 2016.

[4] W. A. Rutala and D. J. Weber, "The benefits of surface disinfection," *American Journal of Infection Control*, vol. 32, no. 4, pp. 226–231, 2004.

[5] W. A. Rutala and D. J. Weber, "Surface disinfection: should we do it?" *Journal of Hospital Infection*, vol. 48, pp. S64–S68, 2001.

[6] S. J. Dancer, "Dos and don'ts for hospital cleaning," *Current Opinion in Infectious Diseases*, vol. 29, no. 4, pp. 415–423, 2016.

[7] W. A. Rutala and D. J. Weber, "Disinfection, sterilization, and antisepsis: an overview," *American Journal of Infection Control*, vol. 44, no. 5, pp. e1–e6, 2016.

[8] W. A. Rutala and D. J. Weber, "Disinfection and sterilization: an overview," *American Journal of Infection Control*, vol. 41, no. 5, pp. S2–S5, 2013.

[9] P. Zunino, *La Disinfezione in Ambito Odontoiatric*, Zanichelli, Ed., Bologna, Italy, 2013.

[10] J. M. Boyce, "Modern technologies for improving cleaning and disinfection of environmental surfaces in hospitals," *Antimicrobial Resistance and Infection Control*, vol. 5, no. 5, pp. 1–10, 2016.

[11] D. J. Weber, W. A. Rutala, M. B. Miller, K. Huslage, and E. Sickbert-Bennett, "Role of hospital surfaces in the transmission of emerging health care-associated pathogens: norovirus, clostridium difficile, and acinetobacter species," *American Journal of Infection Control*, vol. 38, no. 5, pp. S25–S33, 2010.

[12] D. Jeffrey, "Chemicals used as disinfectants: active ingredients and enhancing additives," *Revue Scientifique et Technique de l'OIE*, vol. 14, no. 1, pp. 57–74, 1995.

[13] A. P. Fraise, P. A. Lambert, and J. Maillard, *Russell, Hugo & Ayliffe's Principles and Practice of Disinfection, Preservation & Sterilization*, Blackwell Publishing Ltd, Oxford, UK, 3rd edition, 1999.

[14] M. Saccucci, G. Ierardo, C. Protano, M. Vitali, and A. Polimeni, "How to manage the biological risk in a dental clinic: current and future perspectives," *Minerva Stomatol*, vol. 66, no. 5, pp. 232–239, 2017.

[15] G. Dvorak, "Disinfection," *Center for Food Security and Public Health Iowa state University*, vol. 1, no. 1, pp. 1–20, 2008.

[16] S. B. Zaman, M. A. Hussain, R. Nye, V. Mehta, K. T. Mamun, and N. Hossain, "A Review on Antibiotic Resistance: Alarm Bells are Ringing," *Cureus*, vol. 9, no. 6, pp. 1–10, 2017.

[17] T. P. Van Boeckel, S. Gandra, A. Ashok et al., "Global antibiotic consumption 2000 to 2010: an analysis of national pharmaceutical sales data," *The Lancet Infectious Diseases*, vol. 14, no. 8, pp. 742–750, 2014.

[18] N. Khardori, "Antibiotics-past, present, and future," *Medical Clinics of North America*, vol. 90, no. 6, pp. 1049–1076, 2006.

[19] S. B. Levy, "Active efflux mechanisms for antimicrobial resistance," *Antimicrobial Agents and Chemotherapy*, vol. 36, no. 4, pp. 695–703, 1992.

[20] A. J. Huh and Y. J. Kwon, "'Nanoantibiotics': a new paradigm for treating infectious diseases using nanomaterials in the antibiotics resistant era," *Journal of Controlled Release*, vol. 156, no. 2, pp. 128–145, 2011.

[21] E. Rubinstein and Y. Keynan, "Vancomycin-resistant enterococci," *Critical Care Clinics*, vol. 29, no. 4, pp. 841–852, 2013.

[22] B. Périchon and P. Courvalin, "VanA-type vancomycin-resistant *Staphylococcus aureus*," *Antimicrobial Agents and Chemotherapy*, vol. 53, no. 11, pp. 4580–4587, 2009.

[23] N. Waglechner and G. D. Wright, "Antibiotic resistance: it's bad, but why isn't it worse?" *BMC Biology*, vol. 15, no. 84, pp. 1–10, 2017.

[24] J. L. Martinez, "General principles of antibiotic resistance in bacteria," *Drug Discovery Today: Technologies*, vol. 11, no. 1, pp. 33–39, 2014.

[25] A. Tello, B. Austin, and T. C. Telfer, "Selective pressure of antibiotic pollution on bacteria of importance to public health," *Environmental Health Perspectives*, vol. 120, no. 8, pp. 1100–1106, 2012.

[26] B. L. Coleman, M. Louie, M. I. Salvadori et al., "Contamination of Canadian private drinking water sources with antimicrobial resistant Escherichia coli," *Water Research*, vol. 47, no. 9, pp. 3026–3036, 2013.

[27] S. Akturk, S. Dincer, and S. Toroglu, "Determination of microbial quality and plasmid-mediated multidrug resistant bacteria in fountain drinking water sources in Turkey," *Journal of Environmental Biology*, vol. 33, no. 6, pp. 1127–1136, 2012.

[28] K. G. Torkar and S. Ivić, "Surveillance of bacterial colonisation on contact surfaces in different medical wards," *Archives of Industrial Hygiene and Toxicology*, vol. 68, no. 2, pp. 116–126, 2017.

[29] S. Ali, G. Moore, and A. P. R. Wilson, "Effect of surface coating and finish upon the cleanability of bed rails and the spread of Staphylococcus aureus," *Journal of Hospital Infection*, vol. 80, no. 3, pp. 192–198, 2012.

[30] D. J. Weber, W. A. Rutala, and E. E. Sickbert-Bennett, "Outbreaks associated with contaminated antiseptics and disinfectants," *Antimicrobial Agents and Chemotherapy*, vol. 51, no. 12, pp. 4217–4224, 2007.

[31] J. L. Cadnum, K. N. Hurless, S. Kundrapu, and C. J. Donskey, "Transfer of clostridium difficile spores by nonsporicidal wipes and improperly used hypochlorite wipes: practice + product = perfection," *Infection Control and Hospital Epidemiology*, vol. 34, no. 4, pp. 441-442, 2013.

[32] K. Engelbrecht, D. Ambrose, L. Sifuentes, C. Gerba, I. Weart, and D. Koenig, "Decreased activity of commercially available disinfectants containing quaternary ammonium compounds when exposed to cotton towels," *American Journal of Infection Control*, vol. 41, no. 10, pp. 908–911, 2013.

[33] S. J. Dancer, "Controlling hospital-acquired infection: focus on the role of the environment and new technologies for decontamination," *Clinical Microbiology Reviews*, vol. 27, no. 4, pp. 665–690, 2014.

[34] A. Kumar, P. K. Vemula, P. M. Ajayan, and G. John, "Silver-nanoparticle-embedded antimicrobial paints based on vegetable oil," *Nature Materials*, vol. 7, no. 3, pp. 236–241, 2008.

[35] C. Wei, W.-Y. Lin, Z. Zalnal et al., "Bactericidal activity of $TiO_2$ photocatalyst in aqueous media: toward a solar-assisted water disinfection system," *Environmental Science & Technology*, vol. 28, no. 5, pp. 934–938, 1994.

[36] O. Akhavan and E. Ghaderi, "Toxicity of graphene and graphene oxide nanowalls against bacteria," *ACS Nano*, vol. 4, no. 10, pp. 5731–5736, 2010.

[37] S. Liu, T. H. Zeng, M. Hofmann et al., "Antibacterial activity of graphite, graphite oxide, graphene oxide, and reduced graphene oxide: membrane and oxidative stress," *ACS Nano*, vol. 5, no. 9, pp. 6971–6980, 2011.

[38] A. K. Geim and K. S. Novoselov, "The rise of graphene," *Nature Materials*, vol. 6, no. 3, pp. 183–191, 2007.

[39] K. S. Novoselov, A. K. Geim, S. V. Morozov et al., "Electric field in atomically thin carbon films," *Science*, vol. 22, no. 306, pp. 666–669, 2004.

[40] M. J. Allen, V. C. Tung, and R. B. Kaner, "Honeycomb carbon: a review of graphene," *Chemical Reviews*, vol. 110, no. 1, pp. 132–145, 2010.

[41] G. De Bellis, A. Tamburrano, A. Dinescu, M. L. Santarelli, and M. S. Sarto, "Electromagnetic properties of composites containing graphite nanoplatelets at radio frequency," *Carbon*, vol. 49, no. 13, pp. 4291–4300, 2011.

[42] M. S. Sarto, A. G. D'Aloia, A. Tamburrano, and G. De Bellis, "Synthesis, modeling, and experimental characterization of graphite nanoplatelet-based composites for EMC applications," *IEEE Transactions on Electromagnetic Compatibility*, vol. 54, no. 1, pp. 17–27, 2012.

[43] A. Tamburrano, F. Sarasini, G. De Bellis, A. G. D'Aloia, and M. S. Sarto, "The piezoresistive effect in graphene-based polymeric composites," *Nanotechnology*, vol. 24, no. 46, Article ID 465702, 2013.

[44] L. Paliotta, G. De Bellis, A. Tamburrano et al., "Highly conductive multilayer-graphene paper as a flexible lightweight electromagnetic shield," *Carbon*, vol. 89, pp. 260–271, 2015.

[45] S. Syama and P. V. Mohanan, "Safety and biocompatibility of graphene: a new generation nanomaterial for biomedical application," *International Journal of Biological Macromolecules*, vol. 86, pp. 546–555, 2016.

[46] H. Y. Mao, S. Laurent, W. Chen et al., "Graphene: promises, facts, opportunities, and challenges in nanomedicine," *Chemical Reviews*, vol. 113, no. 5, pp. 3407–3424, 2013.

[47] V. C. Sanchez, A. Jachak, R. H. Hurt, and A. B. Kane, "Biological interactions of graphene-family nanomaterials: an interdisciplinary review," *Chemical Research in Toxicology*, vol. 25, no. 1, pp. 15–34, 2012.

[48] Y. Li, H. Yuan, A. von dem Bussche et al., "Graphene microsheets enter cells through spontaneous membrane penetration at edge asperities and corner sites," *Proceedings of the National Acadamy of Sciences of the United States of America*, vol. 110, no. 30, pp. 12295–12300, 2013.

[49] H. Yue, W. Wei, Z. Yue et al., "The role of the lateral dimension of graphene oxide in the regulation of cellular responses," *Biomaterials*, vol. 33, no. 16, pp. 4013–4021, 2012.

[50] M. L. Schipper, N. Nakayama-Ratchford, C. R. Davis et al., "A pilot toxicology study of single-walled carbon nanotubes in a small sample of mice," *Nature Nanotechnology*, vol. 3, no. 4, pp. 216–221, 2008.

[51] H. Ji, H. Sun, and X. Qu, "Antibacterial applications of graphene-based nanomaterials: Recent achievements and challenges," *Advanced Drug Delivery Reviews*, vol. 105, pp. 176–189, 2016.

[52] B. Zhang, P. Wei, Z. Zhou, and T. Wei, "Interactions of graphene with mammalian cells: Molecular mechanisms and biomedical insights," *Advanced Drug Delivery Reviews*, vol. 105, pp. 145–162, 2016.

[53] L. Ou, B. Song, H. Liang et al., "Toxicity of graphene-family nanoparticles: a general review of the origins and mechanisms," *Particle and Fibre Toxicology*, vol. 13, no. 57, pp. 1–24, 2016.

[54] C. R. Chandraiahgari, G. De Bellis, P. Ballirano et al., "Synthesis and characterization of ZnO nanorods with a narrow size distribution," *RSC Advances*, vol. 5, no. 62, pp. 49861–49870, 2015.

[55] L. Hui, J. T. Auletta, Z. Huang et al., "Surface disinfection enabled by a layer-by-layer thin film of polyelectrolyte-stabilized reduced graphene oxide upon solar near-infrared irradiation," *ACS Applied Materials & Interfaces*, vol. 7, no. 19, pp. 10511–10517, 2015.

[56] X. Wu, S. Tan, Y. Xing, Q. Pu, M. Wu, and J. X. Zhao, "Graphene oxide as an efficient antimicrobial nanomaterial for eradicating multi-drug resistant bacteria in vitro and in vivo," *Colloids and Surfaces B: Biointerfaces*, vol. 157, pp. 1–9, 2017.

[57] M. Yousefi, M. Dadashpour, M. Hejazi et al., "Anti-bacterial activity of graphene oxide as a new weapon nanomaterial to combat multidrug-resistance bacteria," *Materials Science and Engineering C: Materials for Biological Applications*, vol. 74, pp. 568–581, 2017.

[58] C. R. Chandraiahgari, G. De Bellis, S. K. Balijepalli et al., "Control of the size and density of ZnO-nanorods grown onto graphene nanoplatelets in aqueous suspensions," *RSC Advances*, vol. 6, no. 86, pp. 83217–83225, 2016.

[59] I. Rago, C. R. Chandraiahgari, M. P. Bracciale et al., "Zinc oxide microrods and nanorods: different antibacterial activity and their mode of action against Gram-positive bacteria," *RSC Advances*, vol. 4, no. 99, pp. 56031–56040, 2014.

[60] E. Zanni, S. De Palma, C. R. Chandraiahgari et al., "In vitro toxicity studies of zinc oxide nano- and microrods on mammalian cells: a comparative analysis," *Materials Letters*, vol. 179, pp. 90–94, 2016.

[61] A. Bregnocchi, E. Zanni, D. Uccelletti et al., "Graphene-based dental adhesive with anti-biofilm activity," *Journal of Nanobiotechnology*, vol. 15, no. 1, pp. 1–22, 2017.

[62] E. Zanni, C. R. Chandraiahgari, G. De Bellis et al., "Zinc oxide nanorods-decorated graphene nanoplatelets: a promising antimicrobial agent against the cariogenic bacterium Streptococcus mutans," *Nanomaterials*, vol. 6, no. 10, pp. 1–18, 2016.

[63] C. Bruzeam, I. Ivan, B. Pacheco, and R. Kevin, "Nanomaterials and nanoparticles: sources and toxicity," *Biointerphases*, vol. 2, no. 4, pp. MR17–MR71, 2007.

[64] I. Rago, A. Bregnocchi, E. Zanni et al., "Antimicrobial activity of graphene nanoplatelets against Streptococcus mutans," in *Proceedings of the 15th IEEE International Conference on Nanotechnology (IEEE-NANO '15)*, pp. 9–12, July 2015.

[65] O. Akhavan, E. Ghaderi, and A. Esfandiar, "Wrapping bacteria by graphene nanosheets for isolation from environment, reactivation by sonication, and inactivation by near-infrared irradiation," *The Journal of Physical Chemistry B*, vol. 115, no. 19, pp. 6279–6288, 2011.

[66] M. Olivi, M. Alfè, V. Gargiulo et al., "Antimicrobial properties of graphene-like nanoparticles: coating effect on Staphylococcus aureus," *Journal of Nanoparticle Research*, vol. 18, no. 12, article 358, 2016.

[67] L. Hui, J.-G. Piao, J. Auletta et al., "Availability of the basal planes of graphene oxide determines whether it is antibacterial," *ACS Applied Materials & Interfaces*, vol. 6, no. 15, pp. 13183–13190, 2014.

[68] J. D. Mangadlao, C. M. Santos, M. J. L. Felipe, A. C. C. De Leon, D. F. Rodrigues, and R. C. Advincula, "On the antibacterial mechanism of graphene oxide (GO) Langmuir-Blodgett films," *Chemical Communications*, vol. 51, no. 14, pp. 2886–2889, 2015.

[69] J. Liu and R. H. Hurt, "Ion release kinetics and particle persistence in aqueous nano-silver colloids," *Environmental Science & Technology*, vol. 44, no. 6, pp. 2169–2175, 2010.

[70] I. Banerjee, R. C. Pangule, and R. S. Kane, "Antifouling coatings: recent developments in the design of surfaces that prevent fouling by proteins, bacteria, and marine organisms," *Advanced Materials*, vol. 23, no. 6, pp. 690–718, 2011.

[71] N. Lin, P. Berton, C. Moraes, R. D. Rogers, and N. Tufenkji, "Nanodarts, nanoblades, and nanospikes: Mechano-bactericidal nanostructures and where to find them," *Advances in Colloid and Interface Science*, vol. 252, no. 1, pp. 55–68, 2018.

[72] E. Zanni, E. Bruni, C. R. Chandraiahgari et al., "Evaluation of the antibacterial power and biocompatibility of zinc oxide nanorods decorated graphene nanoplatelets: new perspectives for antibiodeteriorative approaches," *Journal of Nanobiotechnology*, vol. 15, no. 1, article 57, pp. 1–20, 2017.

[73] R. Rajeswari and H. G. Prabu, "Synthesis characterization, antimicrobial, antioxidant, and cytotoxic activities of zno nanorods on reduced graphene oxide," *Journal of Inorganic and Organometallic Polymers and Materials*, vol. 1, no. 1, pp. 1–15, 2017.

[74] L. Zhang, J. Lou, W. Zhang, C. Wu, and Z. Jin, "Bacteria killing in ICU associated infections: antibacterial nanosheets as disinfectant," *RSC Advances*, vol. 8, no. 1, pp. 278–283, 2018.

[75] L. Q. Chen, P. P. Hu, L. Zhang, S. Z. Huang, L. F. Luo, and C. Z. Huang, "Toxicity of graphene oxide and multi-walled carbon nanotubes against human cells and zebrafish," *SCIENCE CHINA Chemistry*, vol. 55, no. 10, pp. 2209–2216, 2012.

[76] T. Tanveer, P. Zahid, H. Hasan et al., "In vitro toxic effects of reduced graphene oxide nanosheets on lung cancer cells," *Nanotechnology*, vol. 28, no. 50, pp. 504001–504016, 2017.

[77] M. Pelin, L. Fusco, V. León et al., "Differential cytotoxic effects of graphene and graphene oxide on skin keratinocytes," *Scientific Reports*, vol. 7, Article ID 40572, 2017.

[78] R. Y. Pelgrift and A. J. Friedman, "Nanotechnology as a therapeutic tool to combat microbial resistance," *Advanced Drug Delivery Reviews*, vol. 65, no. 13-14, pp. 1803–1815, 2013.

[79] N. Beyth, Y. Houri-Haddad, A. Domb, W. Khan, and R. Hazan, "Alternative antimicrobial approach: nano-antimicrobial materials," *Evidence-Based Complementary and Alternative Medicine*, vol. 2015, Article ID 246012, 16 pages, 2015.

[80] M. Polívková, T. Hubáček, M. Staszek, V. Švorčík, and J. Siegel, "Antimicrobial treatment of polymeric medical devices by silver nanomaterials and related technology," *International Journal of Molecular Sciences*, vol. 15, no. 18, pp. 1–24, 2017.

Hindawi
Journal of Nanomaterials
Volume 2018, Article ID 2058613, 9 pages
https://doi.org/10.1155/2018/2058613

*Review Article*

# Carbon Nanomaterials for Breast Cancer Treatment

**M. L. Casais-Molina**,[1] **C. Cab**,[1] **G. Canto**,[2] **J. Medina**,[1] **and A. Tapia**[1]

[1]*Facultad de Ingeniería, Universidad Autónoma de Yucatán (UADY), Av. Industrias no Contaminantes por Periférico Norte, Apdo. Postal 150, Cordemex, 97310 Mérida, YUC, Mexico*
[2]*Centro de Investigaciones en Corrosión, Universidad Autónoma de Campeche (UAC), Av. Agustín Melgar S/N entre Calle 20 y Juan de la Barrera, Col. Buenavista, 24039 San Francisco de Campeche, CAM, Mexico*

Correspondence should be addressed to M. L. Casais-Molina; melissa.casais@correo.uady.mx

Received 8 September 2017; Accepted 14 February 2018; Published 26 March 2018

Academic Editor: Federica Paladini



Currently, breast cancer is considered as a health problem worldwide. Furthermore, current treatments neither are capable of stopping its propagation and/or recurrence nor are specific for cancer cells. Therefore, side effects on healthy tissues and cells are common. An increase in the efficiency of treatments, along with a reduction in their toxicity, is desirable to improve the life quality of patients affected by breast cancer. Nanotechnology offers new alternatives for the design and synthesis of nanomaterials that can be used in the identification, diagnosis, and treatment of cancer and has now become a very promising tool for its use against this disease. Among the wide variety of nanomaterials, the scientific community is particularly interested in carbon nanomaterials (fullerenes, nanotubes, and graphene) due to their physical properties, versatile chemical functionalization, and biocompatibility. Recent scientific evidence shows the potential uses of carbon nanomaterials as therapeutic agents, systems for selective and controlled drug release, and contrast agents for diagnosing and locating tumors. This generates new possibilities for the development of innovative systems to treat breast cancer and can be used to detect this disease at much earlier stages. Thus, applications of carbon nanomaterials in breast cancer treatment are discussed in this article.

## 1. Introduction

Cancer is one of the main causes of human death and a major public health concern worldwide [1, 2]. Cancer refers to the uncontrolled growth and propagation of cells. It appears in almost any part of the body when a cell accumulates a set of mutations, generally during various years [3, 4]. Growth promoting genes in normal cells are duplicated several times in cancer cells and often become unstable acquiring lethal characteristics as they multiply [5]. The American Cancer Society estimates about 1,735,350 new cancer cases diagnosed and 609,640 cancer deaths in the US by 2018 [6]. According to the World Health Organization (WHO), there were about 14 million of new cancer cases and 8.2 million cancer-related deaths worldwide in 2012, and it is expected that annual cancer cases will rise from 14 million to 22 within the next two decades [3]. Breast cancer is the second most frequent cancer with 1.7 million diagnosed cases worldwide [2, 4] and is currently the main cause of death in women with an annual increase of 1 million new cases which lead to 450,000 deaths per year [2]. Breast cancer is an uncontrolled growth of cells that starts in the breast tissues and affects both women and, very rarely, men (less than 1% of all breast cancer cases) [7, 8].

In its initial stages, breast cancer can be detected by means of image studies (mammography, ultrasound, and magnetic resonance imaging) or, less often, clinical trials of palpable tumors. Recently, strategies to mitigate breast cancer have focused on prevention and its early detection and treatment. Breast cancer treatment depends on the type of cancer [9] and its grade, that is, size and extension of the tumor [7]. Surgery, radiotherapy, chemotherapy, and hormonal therapy are the main types of cancer treatments [7, 10].

Although survival rates of breast cancer patients are higher than to those of other types of cancer, in general, current treatments are not entirely effective in stopping the spread and/or recurrence of breast cancer. Furthermore, they are not specific and harm healthy tissues and cells [11–14]. Finding a solution to this problem would have a great repercussion on patient's lifestyle, especially for those suffering metastatic breast cancers.

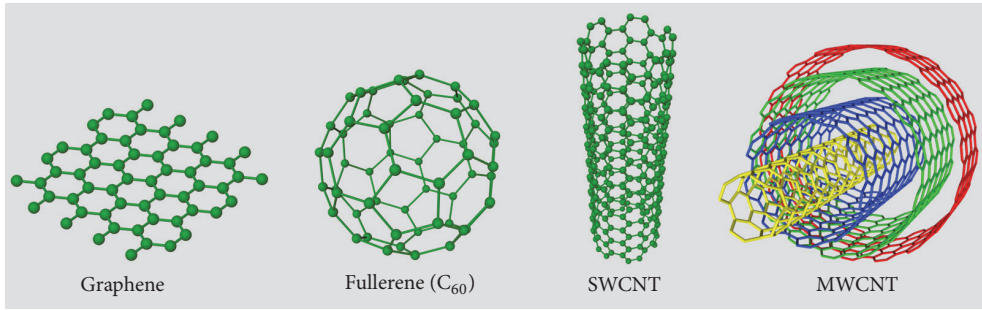


Figure 1: Structural representation of some allotropic forms of carbon.

In recent years, it has been observed that thanks to the nanotechnology advancements, it has been possible to improve the efficiency of conventional breast cancer treatments. One example of this is the release of chemotherapeutic drugs using nanomaterials [15–17]. Nanotechnology is considered one of the great emerging areas in science and technology that promises to make considerable advances in health. Nanotechnology can be defined as the science and engineering involved in the study, design, creation, synthesis, characterization, manipulation, and application of materials, devices, and functional systems through the control of matter at a nanoscale, that is, at the scale of atoms and molecules [18]. This also implies the use of phenomena and properties of matter at the nanoscale. According to the European Commission, the term "nanomaterial" refers to a natural, incidental, or manufactured material containing particles, in an unbound state or as an aggregate or as an agglomerate and where, for 50% or more of the particles in the number size distribution, one or more external dimensions is in the size range 1–100 nm [19].

Nanomaterials are promising tools that have been investigated for the advancement of current breast cancer treatment. Among these, carbon nanomaterials, fullerenes, nanotubes, and graphene, are of particular interest to the scientific community due to their unique physicochemical and biological properties. Many properties of carbon nanomaterials, such as size, shape, surface structure and charge, chemical composition, aggregation and/or agglomeration, and solubility, can greatly influence their interactions with biomolecules and cells. For example, carbon nanomaterials have been employed to produce exceptional images of tumor sites [20, 21], impressive potential as high-efficiency delivery transporters for drugs and/or biomolecules into cells [20, 22, 23]. Therefore, the main emphasis of this article focuses on the discussion of carbon nanomaterials and their current applications in the identification, diagnosis, and treatment of breast cancer.

## 2. Carbon Nanomaterials

Nanomaterials have interesting physicochemical and biological properties which depend on their structural characteristics. They have several uses for different biomedical applications [24], such as the development of innovative systems to treat breast cancer. There is a wide variety of nanomaterials synthesized and currently studied in the biology field; however, the scientific community is particularly interested on carbon nanomaterials due to their physical properties, chemical functionalization, versatility, and biocompatibility [16]. Although the properties of diamond and graphite have been extensively analyzed, other allotropic forms of carbon such as fullerene, carbon nanotubes (CNT), or graphene are of recent interest (Figure 1).

The first carbon nanostructure in closed cage-shaped (fullerenes) was discovered in 1985 by Kroto et al. (Nobel Prize in Chemistry 1996) by irradiating a graphite disc with a laser beam and mixing the resulting carbon gas with helium [25]. The fullerenes are either ellipsoidal or spherical, like a soccer ball (Figure 1), and are the third most stable carbon form after diamond and graphite. Fullerene ($C_{60}$) is better known as buckminsterfullerene in honor of Buckminster Fuller, an architect who successfully used the geodesic dome in architecture [25].

Although CNTs were observed decades ago, it was not seriously considered until the discovery of fullerene ($C_{60}$) [25] and the theoretical studies of other possible similar nanostructures. The attribution of the discovery of CNTs is controversial as a 1976 document reports the multilayer tubular structures identified with an electron microscope [26]. However, they were first experimentally observed in 1991 by Iijima, who used an insoluble material derived from the implementation of the arc-discharge synthesis technique [27].

CNTs have geometric structures which can be generated from graphite sheets. Graphene is defined as a single graphite layer (bidimensional), of finite size, constituted by a multitude of carbon atoms located in the vertices of a hexagonal net.

The structural formation of a CNT can be conceptualized as the envelopment of one graphite layer (graphene) resulting in a Single-Walled CNT (SWCNT). Multiple rolled layers of graphene result in a Multi-Walled CNT (MWCNT) (Figure 1). The diameter, internal geometry, and physicochemical properties of the CNTs depend on how the graphite layers are rolled (chirality vector dependence) [27] (Figure 2).

Currently, graphene is considered as the structural base of all the allotropic forms of carbon found since 1985 (Figure 1) and was synthesized in 2004 by Geim and Novoselov et al. (Nobel Prize in Physics 2010) by means of a very simple process which consisted in the exfoliation of graphite to obtain graphene layers using cellophane tape [28].

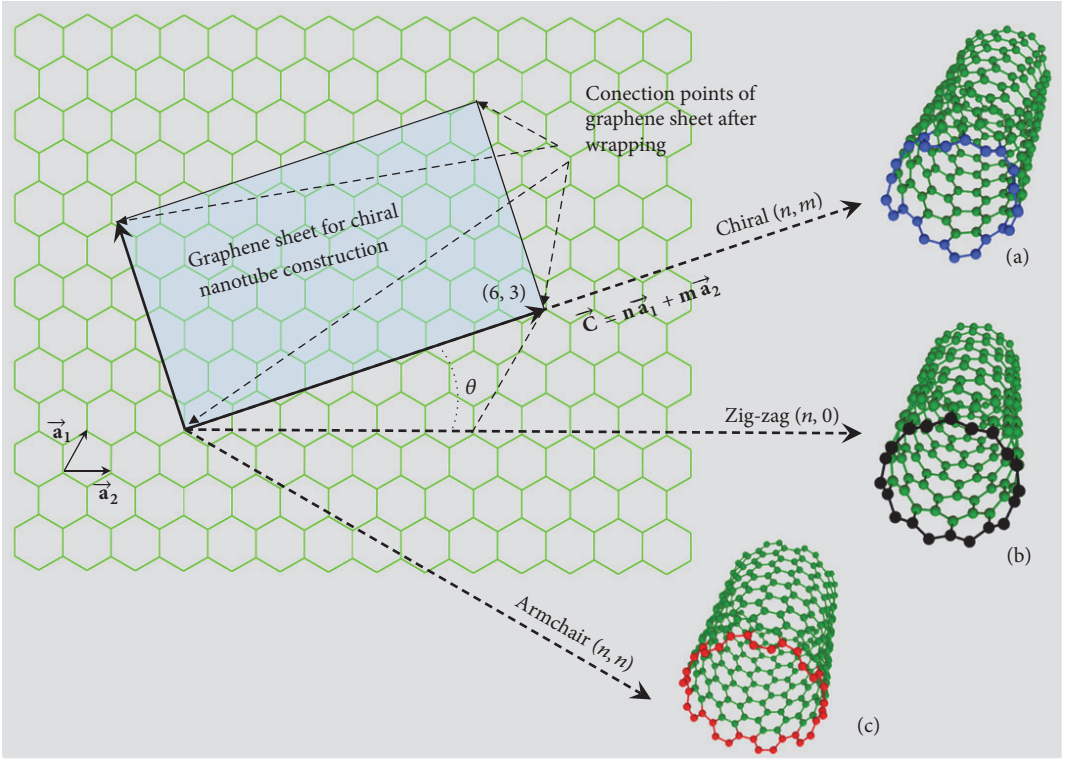


Figure 2: Representation of the chirality vector dependence with the generation of CNT species or types: (a) chiral, (b) zig-zag, and (c) armchair.

## 3. Studies Regarding Carbon Nanomaterials and Breast Cancer

The physicochemical properties and novel techniques of the synthesis of fullerenes, CNTs, and graphene have originated new research fields in biomedicine which aim to study and treat pathologies such as cancer with these carbon nanomaterials [16]. Several reports towards the application of carbon nanomaterials to diagnose and treat cancer (especially breast cancer) have been performed. Figure 3 shows the number of articles reporting the implementation of carbon nanomaterials for different applications to diagnose and treat cancer, such as breast cancer. The dates in the figure below are the results of a query in the Thomson Reuters database (Web of Science™ website) including studies from 2001 and 2017.

As indicated in Figure 3, the number of studies on the implementation of carbon nanomaterials for diagnosing and treating cancer worldwide has an exponential growth trend. There were more than 968 publications on breast cancer treatment until 2017, representing 14.4% of all the international publications on cancer until that year.

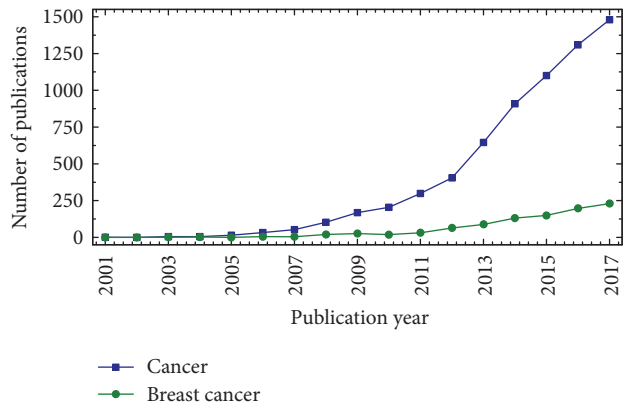


Figure 3: Annual trend in the number of international scientific publications related to the use of carbon nanomaterials for different applications to diagnose and treat cancer, such as breast cancer. Source: authors' calculations based on the data obtained in the Thomson Reuters database (Web of Science) in the period from 2001 to 2017.

## 4. Advances towards the Application of Carbon Nanomaterials for Breast Cancer Treatment

Literature data taken from the Thomson Reuters database (Web of Science website) suggest that carbon nanomaterials have potential uses as devices for selective and controlled drug delivery and/or release, contrast agents for diagnosing and locating breast tumors, and biosensors. They have also applications in photodynamic therapy.

*4.1. Drug Release.* Chemotherapy and hormonal therapy are the main cancer treatments used to destroy or control cancer cells in the entire body [7, 10]. Chemotherapy refers to the intravenous or oral administration of chemotherapeutic drugs. Although their very high efficiency, chemotherapeutic

drugs are not specific for cancer cells and, therefore, diverse side effects may emerge during treatment including hair loss, nausea, vomiting, fatigue, and risk of developing infections [13]. Anthracyclines (doxorubicin and epirubicin) and taxanes (paclitaxel and docetaxel) are the most common chemotherapeutic drugs [7]. About 60–70% of all breast cancer cases receive hormonal therapy, which refers to the blocking of hormones that promote the growth of cancer cells by means of pharmaceuticals [10] such as estrogen. The efficiency of this type of treatment depends on the biological characteristics of patients with hormone receptor-positive (estrogen-receptor-positive or ER+). Tamoxifen (TAM), aromatase inhibitors, and fulvestrant [7, 12–14] are common pharmaceuticals. TAM is an "antiestrogen", that is, a Selective Estrogen Receptor Modulator (SERM) that binds to estrogen receptors of cancer cells in the breast, blocking the action of this hormone. Currently, most of the ER+ breast cancers are treated with TAM whose efficiency has been tested during the initial and advanced stages in women of all ages [12, 13]. However, TAM has also side effects [12, 13].

One of the main problems associated with conventional drugs for breast cancer treatment is the unfavorable pharmacokinetics of their solubility, their limited biodistribution, their lack of selectivity, and the harm they produce to tissues. These drawbacks could be avoided if drugs were positioned in specific regions of the body. This would allow for reducing the drugs dosage, their concentrations on sites that are not of interest, and the side effects associated with chemotherapy and hormonal therapy [15, 16]. In this regard, carbon nanomaterials with potential uses for the administration of drugs against cancer and breast cancer are being analyzed [17, 22, 23, 29–31]; they are considered as advantageous systems to control drug release in the organism and increase the efficiency of treatments and reduce their toxicity [17, 32, 33]. However, carbon nanomaterials have some disadvantages including their lack of solubility and low reproduction rate through their chemical functionalization and structural characterization. Furthermore, their use in medicine is widely tested due to their potential toxicity [32–39].

Carbon nanomaterials have a very low solubility in aqueous or biological media when they are in their native form or are not chemically functionalized. In the latter case, the nanomaterial lacks the molecular aggregates (simple or complex) that provide its specific activities. Insolubility is very relevant in toxicology studies as the excessive accumulation of conventional drugs inside of biological environment, along with a high stability to enzymatic oxidation, hinders their elimination from the body. Therefore, the increase in chemical functionalization of carbon nanomaterials (fullerenes, CNTs, and graphene) favors their solubility and reduces the toxicity in the organism, increasing their viability for the administration and delivery of drugs (Figure 4) [40, 41].

CNTs are particularly of scientific interest due to their chemical stability, mechanic resistance, high electrical and thermal conductivity, high surface area, and tubular structure, as well as their ability to pass through the membranes of endothelial, vascular, and tumor cells [32, 38, 42–44]. The surface and high electrical and thermal conductivity of CNTs

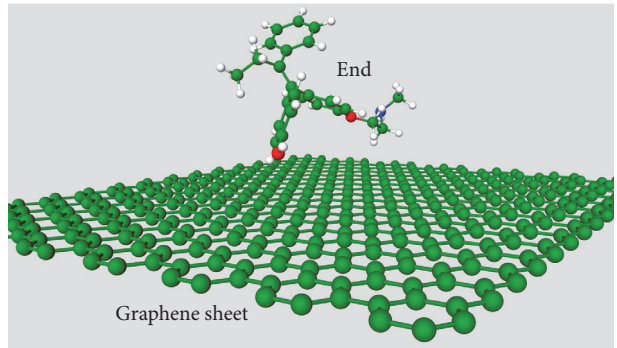


Figure 4: Schematic representation of graphene sheet functionalization with a chemotherapeutic drug (endoxifen).

allow other molecules (drugs, peptides, and nucleic acids) to be attached to their walls and extremities. Therefore, CNTs are considered as a viable alternative for the administration and delivery of drugs. Even chemical functionalization can increase the solubility of the extreme insoluble and hydrophobic fullerene. For instance, cationic-functionalized fullerenes have a stable solubility and are more able to bind anionic residues of cancer cells, which enable a targeted and controlled delivery of drugs [45, 46].

Graphene is a bidimensional carbon nanomaterial characterized by its simple synthesis [28]. It can be easily functionalized due to its high surface area and has a high electrical and thermal conductivity and a high flexibility and mechanical resistance [47, 48]. However, recent research shows that graphene is a very hard nanomaterial to be manipulated and synthesized in a controlled way. Furthermore, in the context of biomedical applications, graphene is lower toxic than CNTs and fullerenes [49].

Recent studies in nanomedicine concluded that fullerenes, CNTs, and graphene have favorable properties for the carriage, targeted, and controlled delivery of chemotherapeutical drugs including taxol (paclitaxel), docetaxel (DTX), doxorubicin (DOX), and others [22, 29, 31, 32, 44, 50–53]. Raza et al. [22] reported that the system conformed by the fullerene $C_{60}$ and DTX ($C_{60}$/DXT) is able to improve up to 4.2 times the bioavailability of DTX and decreases the clearance of DTX by 50%. In addition, $C_{60}$/DXT system showed an effective controlled release of ~84.32% of DTX during a period of 120 hours, as well as compatibility with erythrocytes. Furthermore, an in vitro cytotoxicity assay revealed that, compared to free DTX, $C_{60}$/DTX system exhibits significantly increased cytotoxicity on human breast cancer cell lines (MCF-7 and MDA-MB-231). Zhang et al. [54] developed a multifunctional tumor-targeting drug delivery system (HA-MWCNTs/Tf@ART) for the in vitro treatment of breast cancer cells (MCF-7), by means of hyaluronic acid functionalized MWCNTs as drug carrier (HA-MWCNTs), with the transferrin as the targeting ligand (Tf) and the artemisinin (ART) as the drug, that showed synergistic antitumor efficacy due to the enhanced intracellular accumulation of ART in cancer cells and the simultaneous delivery of Tf and ART. Also, under radiation, this nanomaterial led to improved inhibition efficacy against tumors.

On the other hand, there is even experimental evidence of their pharmacokinetics and toxicity profiles which are favored when carbon nanomaterials are functionalized [22, 44, 45, 51]. Hence, carbon nanomaterials have biochemical characteristics that allow them to pass through cell membranes and release the drugs in specific tissues [43, 45].

*4.2. Contrast Agent.* Currently, the timely identification of breast cancer tumors is relevant for medical community as it allows, in the vast majority of cases, the eradication of the disease. The contrast agent technique has been of particular interest since it enables real-time identification of breast tumors. This technique uses specific antibodies for recognizing antigens which are expressed in the surface of certain tumors. These specific antibodies are added to fluorescent molecules or fluorophores which enable them to absorb electromagnetic radiation (light) under specific wavelengths and emit it under longer wavelengths. However, common contrast agents (CAs) used in the magnetic resonance imaging (MRI), such as gadolinium complexes and superparamagnetic iron oxides, generally cannot pass through the cell membrane. In this sense, the packaging of CAs onto or inside of carbon nanomaterials enables them to be internalized by cells. Even though gadolinium is the most used contrast agent in MRI, in recent years, research has focused on reducing the side effects and needed dose of this lanthanide metal, as well as enhancing the selectivity of desired organs and tissues. It has been shown that carbon nanomaterials could be more effective than common CAs by 2–100 times in their activity and lead to dose reductions by 1-2 orders of magnitude [55]. Moreover, carbon nanomaterials can penetrate cell membranes as well as couple with drugs. Therefore, the development of efficient contrast agents coupled with powerful medical imaging techniques is needed for increasing the sensitivity and specificity in breast cancer diagnosis.

Carbon nanomaterials have been found to be an excellent scaffold for contrast agents since they can be used to carry imaging agents, such as fluorescent labels and radionuclides, contributing to the generation of high-quality images and the early detection of breast cancer [20, 21, 49, 56–58]. Experiments have demonstrated that CNT can carry imaging agents [57] and demonstrated great potential of using functionalized MWCNT as efficient cell probes for MRI [59]. In vivo MRI on mice showed that CNTs functionalized with Gd (Gd-CNTs) have the ability to act as a good contrast agent [60]. Moreover, when CNT is functionalized with phospholipids, the biocompatibility increases, making it more stable while circulating in the reticuloendothelial system [61, 62].

In recent years, fullerene and their derivatives have been considered as one of the most promising agents for cancer imaging due to their specific physicochemical properties. In this regard, polyhydroxy fullerenes (PHF) have shown their potential use for cancer imaging [63]. In addition, it was observed that PHF nanoparticles functionalized with amines (PHF-$NH_2$) were soluble in water and exhibited green emission with a quantum yield of ~17%. Also, due to their high surface charge, PHF-$NH_2$ nanoparticles present excellent fluorescence properties and are able to easily penetrate cell lines, such as breast cancer cells (MCF-7) in vitro [64]. Furthermore, endohedral fullerenes (enclosed cage-shaped carbon structures that contain simple or complex molecules) have been successfully implemented as contrast agents for MRI [58].

Chelates are common in MRI studies due to their good contrast properties. These compounds have heavy metal ions in their structures such as gadolinium ($Gd^{+3}$). However, they frequently lose the metal or suffer transmetalation processes (release of $Gd^{+3}$ in the organism), which severely affects patients with renal or hepatic dysfunctions [65, 66]. Recent studies indicate that this can be avoided by introducing the $Gd^{+3}$ molecules inside the cavity of the fullerene cage and then functionalize it. This allows for a good solubility and a low toxicity of the chelate contained in the nanomaterial [67]. One of these fullerenes, the metallofullerenol $Gd@C_{82}(OH)_{22}$ is a potent activating agent of T Lymphocytes of the immune system when used as contrast agent in MRI. Metallofullerenol can efficiently inhibit the growth of tumors and is less toxic than some usual antitumor drugs to treat breast cancer such as taxol (paclitaxel) [57, 67].

Through their functionalization, fullerenes, graphenes, and CNTs are capable of carrying imaging agents or chemotherapeutic drugs for diagnosing and treating breast cancer [20, 67, 68]. This confers these systems an additional advantage and allows them to contribute to cancer detection and also to the targeted and controlled administration of drugs.

*4.3. Photodynamic Therapy.* Surgery and radiotherapy are breast cancer treatments commonly used to remove, eliminate, or control cancer cells in a specific area [7, 10]. Surgery allows for identifying the extension of the tumor and is commonly used to extirpate the part of the breast containing the cancerous tumor (breast-conserving surgery) or the whole breast (mastectomy) [7], unlike radiotherapy (destruction of cancer cells by means of high-energy rays or particles) which is usually recommended after surgery to reduce the risk of recurrence [7]. However, both surgery and radiotherapy are treatments that require invasive procedures; therefore, side effects are common.

Photodynamic therapy (PDT) is a clinically approved, minimally invasive treatment that can exert a selective cytotoxic activity towards malignant cells. PDT requires light, a photosensitizer, and molecular oxygen. The procedure involves the topically or intravenously administration of a photosensitizer to cancerous cells, followed by irradiation with a light of specific wavelength (inside of absorbance band of the sensitizer). The electronically excited photosensitizer transfers energy to ground state of molecular oxygen to produce excited singlet oxygen, which is cytotoxic, thus leading to direct tumor cell death via apoptosis or necrosis and damage of the tumor microvasculature and dramatic changes in tumor microenvironment [69].

Recently, the properties of carbon nanomaterials and their potential applications in PDT have been analyzed in an attempt to substitute current invasive thermal procedures that remove tumors or cancer cells of breast cancer [70–81]. Due to the carbon nanomaterials presence in the PDT,

cancer cells accumulate light-sensitive molecules (carbon nanomaterials) which, in the presence of oxygen, absorb the radiation of an infrared camera and turn it into heat. This induces cytotoxic effects that lead to an irreversible photodamage of cancer cells [71–74, 77]. In this regard, carbon nanomaterials have been used successfully to cause thermal ablation of solid tumors in breast cancer studies [16, 68, 74–76, 79–82]. Ogbodu et al. [74] reported for the first time the synthesis, photophysical properties, and PDT activity of ZnMCPPc-spermine-SWCNT (zinc monocarboxy phenoxy phthalocyanine upon conjugation to spermidine, as a targeting molecule, and then adsorbed onto SWCNT) on breast cancer cells (MCF-7). The in vitro cytotoxicity test of ZnMCPPc-spermine-SWCNT in cancer cells (MCF-7) proved to be relatively nontoxic in the absence of light. In addition, the results showed that the presence at 40 mM of spermine improves the effect of PDT, with up to 97% decrease in cell viability. Shi et al. [80] developed a multifunctional system based on the fullerene $C_{60}$, iron oxide nanoparticles, polyethylene glycol, and folic acid that offers a combination of advantages including cancer diagnosis, radiofrequency-assisted thermal therapy, PDT, and magnetic targeting applications. Furthermore, experimental results did not reveal any remarkable toxicity in vitro or in vivo. On the other hand, Nurunnabi et al. [81] developed a carboxyl functionalized graphene nanodots that act as a potential agent for the imaging of cancer in deep tissue/organs through a noninvasive technique and can efficiently kill breast cancer cells (>70% of MDA-MB231 cell line) through combined photodynamic and photothermal effects.

The results of the above studies reveal the potential uses of carbon nanomaterials in the photodynamic therapy and there were several challenges that must be overcome before being used as a standard technique for breast cancer treatment.

*4.4. Biosensors.* The generation of biosensors capable of detecting cancer tumors is very important, particularly for breast cancer whose detection during the early stage is a key factor for its eradication. Biosensors are able to identify tumor markers at such a low concentration (traces) where other techniques, such as image studies, may fail. Therefore, the numbers of studies towards the use of carbon nanomaterials as biosensors have increased [16, 82–84].

Engineers of the University of California in San Diego developed a graphene sensor capable of detecting mutations and early-stage breast cancer [85]. Also, researchers at the University of Manchester found that graphene oxide is not toxic to healthy cells and can act as an anticancer agent selectively targeting cancer stem cells [86]. Although these techniques are still new, their results are promising for preventing and treating breast cancer.

## 5. Conclusion

The study, design, creation, synthesis, manipulation, and application of carbon nanomaterials are an emerging technology with promising applications in the biomedicine field, particularly for detecting, diagnosing, and treating breast cancer. However, there is no carbon nanomaterial that presents simultaneously the desirable traits for therapeutic use in humans (nontoxic, good solubility, high specificity, easy functionalization, targeted and controlled delivery system, etc.). Furthermore, more research is needed to avoid potential side effects. Currently, the studies on toxicological properties and biomedical applications of carbon nanomaterials have a trend to increase, but these studies are still inconclusive for the implementation in human's traits. Research findings commented here are part of human efforts that contribute to the future implementation of nanotechnology-assisted solutions to treat breast cancer, the control of propagation and recurrence of breast cancer, and the reduction of toxic effects of conventional treatments.

## Conflicts of Interest

All authors declare that they do not have any conflicts of interest to report.

## Acknowledgments

The authors acknowledge the Facultad de Ingeniería of the Universidad Autónoma de Yucatán (FIUADY) for easing this work and the Consejo Nacional de Ciencia y Tecnología (CONACYT) of Mexico, for its support under Projects FOMIX-170297 and 255571 of the CB2015.

## References

[1] B. W. Stewart and C. P. Wild, *World Cancer Report*, WHO, IARC, 2014.

[2] R. Siegel, J. Ma, Z. Zou, and A. Jemal, "Cancer statistics, 2014," *CA: A Cancer Journal for Clinicians*, vol. 64, no. 1, pp. 9–29, 2014.

[3] S. G. Zelle and R. M. Baltussen, "Economic analyses of breast cancer control in low- and middle-income countries: A systematic review," *Systematic Reviews*, vol. 2, no. 1, article no. 20, 2013.

[4] World Health Organization. Media Centre, http://www.who.int/entity/mediacentre/factsheets/fs297/en/.

[5] V. A. Senra, *El Cáncer: Epidemiologia, Etiología, Diagnóstico y Prevención*, Harcourt, Madrid, 2002.

[6] American Cancer Society. Cancer Facts Figures, https://www.cancer.org/content/dam/cancer-org/research/cancer-facts-and-statistics/annual-cancer-facts-and-figures/2018/cancer-facts-and-figures-2018.pdf.

[7] C. Girish, P. Vijayalakshmi, R. Mentham, C. B. Rao, and S. Nama, "A review on breast cancer," *International Journal of Pharma and Bio Sciences*, vol. 4, no. 2, pp. 47–54, 2014.

[8] N. H. Chávez-Hernández and M. Salamanca-García, "Epidemiología del cáncer de mama en hombres atendidos en el Centro Médico Nacional 20 de noviembre," *Revista de Especialidades Médico Quirúrgicas*, vol. 19, pp. 267-71, 2014.

[9] E. Villarreal-Ríos, V. Escorcia-Reyes, L. Martínez-González et al., "Historia natural del proceso diagnóstico del cáncer de mama," *Revista Panamericana de Salud Publica*, vol. 35, no. 3, pp. 172–178, 2014.

[10] M. K. Vanitha, D. Sakthisekaran, and P. Anandakumar, "Breast cancer: types, epidemiology and aetiology- A review," *Advanced Journal of Pharmacie and Life science Research*, vol. 2, no. 4, pp. 29–38, 2014.

[11] S. Darby, P. McGale, C. Correa et al., "Effect of radiotherapy after breast-conserving surgery on 10-year recurrence and 15-year breast cancer death: meta-analysis of individual patient data for 10 801 women in 17 randomised trials," *The Lancet*, vol. 378, no. 9804, pp. 1707–1716, 2011.

[12] Early Breast Cancer Trialists' Collaborative Group (EBCTCG), "Relevance of breast cancer hormone receptors and other factors to the efficacy of adjuvant tamoxifen: patient-level meta-analysis of randomised trials," *The Lancet*, vol. 378, no. 9793, pp. 771–784, 2011.

[13] M. Clarke, R. Collins, S. Darby et al., "Effects of radiotherapy and of differences in the extent of surgery for early breast cancer on local recurrence and 15-year survival: an overview of the randomised trials," *The Lancet*, vol. 366, no. 9503, pp. 2087–2106, 2005.

[14] Early Breast Cancer Trialists' Collaborative Group, "Adjuvant bisphosphonate treatment in early breast cancer: Meta-analyses of individual patient data from randomised trials," *The Lancet*, vol. 386, no. 10001, pp. 1353–1361, 2015.

[15] N. K. Mehra and S. Palakurthi, "Interactions between carbon nanotubes and bioactives: A drug delivery perspective," *Drug Discovery Today*, vol. 21, no. 4, pp. 585–597, 2016.

[16] D. Chen, C. A. Dougherty, K. Zhu, and H. Hong, "Theranostic applications of carbon nanomaterials in cancer: Focus on imaging and cargo delivery," *Journal of Controlled Release*, vol. 210, pp. 230–245, 2015.

[17] B. Singh, S. Beg, S. Lohan, and K. Raza, "Carbon nanotubes (CNTs) and their application in drug delivery system," *Recent Trends Biotechnology, Houston*, 2015.

[18] M. Mir, S. Ishtiaq, S. Rabia et al., "Nanotechnology: from In Vivo Imaging System to Controlled Drug Delivery," *Nanoscale Research Letters*, vol. 12, article no. 500, 2017.

[19] D. R. Boverhof, C. M. Bramante, J. H. Butala et al., "Comparative assessment of nanomaterial definitions and safety evaluation considerations," *Regulatory Toxicology and Pharmacology*, vol. 73, no. 1, pp. 137–150, 2015.

[20] A. Al Faraj, A. S. Shaik, R. Halwani, and A. Alfuraih, "Magnetic Targeting and Delivery of Drug-Loaded SWCNTs Theranostic Nanoprobes to Lung Metastasis in Breast Cancer Animal Model: Noninvasive Monitoring Using Magnetic Resonance Imaging," *Molecular Imaging and Biology*, vol. 18, no. 3, pp. 315–324, 2016.

[21] W. Ding, C. Lou, J. Qiu et al., "Targeted Fe-filled carbon nanotube as a multifunctional contrast agent for thermoacoustic and magnetic resonance imaging of tumor in living mice," *Nanomedicine: Nanotechnology, Biology and Medicine*, vol. 12, no. 1, pp. 235–244, 2016.

[22] K. Raza, N. Thotakura, P. Kumar et al., "C60-fullerenes for delivery of docetaxel to breast cancer cells: A promising approach for enhanced efficacy and better pharmacokinetic profile," *International Journal of Pharmaceutics*, vol. 495, no. 1, pp. 551–559, 2015.

[23] F. Nasrollahi, J. Varshosaz, A. A. Khodadadi, S. Lim, and A. Jahanian-Najafabadi, "Targeted Delivery of Docetaxel by Use of Transferrin/Poly(allylamine hydrochloride)-functionalized Graphene Oxide Nanocarrier," *ACS Applied Materials & Interfaces*, vol. 8, no. 21, pp. 13282–13293, 2016.

[24] S. Goenka, V. Sant, and S. Sant, "Graphene-based nanomaterials for drug delivery and tissue engineering," *Journal of Controlled Release*, vol. 173, no. 1, pp. 75–88, 2014.

[25] H. W. Kroto, J. R. Heath, S. C. O'Brien, R. F. Curl, and R. E. Smalley, "$C_{60}$: Buckminsterfullerene," *Nature*, vol. 318, no. 6042, pp. 162-163, 1985.

[26] A. Oberlin, M. Endo, and T. Koyama, "Filamentous growth of carbon through benzene decomposition," *Journal of Crystal Growth*, vol. 32, no. 3, pp. 335–349, 1976.

[27] S. Iijima, "Helical microtubules of graphitic carbon," *Nature*, vol. 354, no. 6348, pp. 56–58, 1991.

[28] K. S. Novoselov, A. K. Geim, S. V. Morozov et al., "Electric field in atomically thin carbon films," *Science*, vol. 306, no. 5696, pp. 666–669, 2004.

[29] J. Shi, B. Wang, L. Wang et al., "Fullerene (C60)-based tumor-targeting nanoparticles with "off-on" state for enhanced treatment of cancer," *Journal of Controlled Release*, vol. 235, pp. 245–258, 2016.

[30] A. Ortega-Guerrero, J. M. Espinosa-Duran, and J. Velasco-Medina, "TRPV1 channel as a target for cancer therapy using CNT-based drug delivery systems," *European Biophysics Journal*, vol. 45, no. 5, pp. 423–433, 2016.

[31] A. Al Faraj, A. P. Shaik, and A. S. Shaik, "Magnetic single-walled carbon nanotubes as efficient drug delivery nanocarriers in breast cancer murine model: Noninvasive monitoring using diffusion-weighted magnetic resonance imaging as sensitive imaging biomarker," *International Journal of Nanomedicine*, vol. 10, pp. 157–168, 2014.

[32] K. H. Son, J. H. Hong, and J. W. Lee, "Carbon nanotubes as cancer therapeutic carriers and mediators," *International Journal of Nanomedicine*, vol. 11, pp. 5163–5185, 2016.

[33] Y. Zhang, D. Petibone, Y. Xu et al., "Toxicity and efficacy of carbon nanotubes and graphene: The utility of carbon-based nanoparticles in nanomedicine," *Drug Metabolism Reviews*, vol. 46, no. 2, pp. 232–246, 2014.

[34] N. Kobayashi, H. Izumi, and Y. Morimoto, "Review of toxicity studies of carbon nanotubes," *Journal of Occupational Health*, vol. 59, no. 5, pp. 394–407, 2017.

[35] Z. Chen, L. Ma, Y. Liu, and C. Chen, "Applications of functionalized fullerenes in tumor theranostics," *Theranostics*, vol. 2, no. 3, pp. 238–250, 2012.

[36] L. Ou, B. Song, H. Liang et al., "Toxicity of graphene-family nanoparticles: A general review of the origins and mechanisms," *Particle and Fibre Toxicology*, vol. 13, no. 1, article no. 57, 2016.

[37] A. B. Seabra, A. J. Paula, R. De Lima, O. L. Alves, and N. Durán, "Nanotoxicity of graphene and graphene oxide," *Chemical Research in Toxicology*, vol. 27, no. 2, pp. 159–168, 2014.

[38] Z. Chen, A. Zhang, X. Wang et al., "The Advances of Carbon Nanotubes in Cancer Diagnostics and Therapeutics," *Journal of Nanomaterials*, vol. 2017, pp. 1–13, 2017.

[39] J. Yang, Y. Wu, Y. Shen et al., "Enhanced Therapeutic Efficacy of Doxorubicin for Breast Cancer Using Chitosan Oligosaccharide-Modified Halloysite Nanotubes," *ACS Applied Materials & Interfaces*, vol. 8, no. 40, pp. 26578–26590, 2016.

[40] R. Singh, D. Pantarotto, L. Lacerda et al., "Tissue biodistribution and blood clearance rates of intravenously administered carbon nanotube radiotracers," *Proceedings of the National Acadamy of Sciences of the United States of America*, vol. 103, no. 9, pp. 3357–3362, 2006.

[41] M. Lucafò, M. Gerdol, A. Pallavicini et al., "Profiling the molecular mechanism of fullerene cytotoxicity on tumor cells by RNA-seq," *Toxicology*, vol. 314, no. 1, pp. 183–192, 2013.

[42] A. Bianco, K. Kostarelos, and M. Prato, "Applications of carbon nanotubes in drug delivery," *Current Opinion in Chemical Biology*, vol. 9, no. 6, pp. 674–679, 2005.

[43] S. K. S. Kushwaha, S. Ghoshal, A. K. Rai, and S. Singh, "Carbon nanotubes as a novel drug delivery system for anticancer therapy: A review," *Brazilian Journal of Pharmaceutical Sciences*, vol. 49, no. 4, pp. 629–643, 2013.

[44] W. Shao, A. Paul, B. Zhao, C. Lee, L. Rodes, and S. Prakash, "Carbon nanotube lipid drug approach for targeted delivery of a chemotherapy drug in a human breast cancer xenograft animal model," *Biomaterials*, vol. 34, no. 38, pp. 10109–10119, 2013.

[45] S. Foley, C. Crowley, M. Smaihi et al., "Cellular localisation of a water-soluble fullerene derivative," *Biochemical and Biophysical Research Communications*, vol. 294, no. 1, pp. 116–119, 2002.

[46] Y.-Y. Huang, S. K. Sharma, R. Yin, T. Agrawal, L. Y. Chiang, and M. R. Hamblin, "Functionalized fullerenes in photodynamic therapy," *Journal of Biomedical Nanotechnology*, vol. 10, no. 9, pp. 1918–1936, 2014.

[47] Y. Shao, J. Wang, H. Wu, J. Liu, I. A. Aksay, and Y. Lin, "Graphene based electrochemical sensors and biosensors: a review," *Electroanalysis*, vol. 22, no. 10, pp. 1027–1036, 2010.

[48] P. G. Campbell, M. A. Worsley, A. M. Hiszpanski, T. F. Baumann, and J. Biener, "Synthesis and functionalization of 3D nanographene materials: Graphene aerogels and graphene macro assemblies," *Journal of Visualized Experiments*, vol. 2015, no. 105, Article ID e53235, 2015.

[49] Z. Singh, "Applications and toxicity of graphene family nanomaterials and their composites," *Nanotechnology, Science and Applications*, vol. 9, pp. 15–28, 2016.

[50] T. Zhou, X. Zhou, and D. Xing, "Controlled release of doxorubicin from graphene oxide based charge-reversal nanocarrier," *Biomaterials*, vol. 35, no. 13, pp. 4185–4194, 2014.

[51] Z. Xu, S. Zhu, M. Wang, Y. Li, P. Shi, and X. Huang, "Delivery of paclitaxel using PEGylated graphene oxide as a nanocarrier," *ACS Applied Materials & Interfaces*, vol. 7, no. 2, pp. 1355–1363, 2015.

[52] M. Hashemi, A. Yadegari, G. Yazdanpanah et al., "Normalization of doxorubicin release from graphene oxide: New approach for optimization of effective parameters on drug loading," *Biotechnology and Applied Biochemistry*, vol. 64, no. 3, pp. 433–442, 2017.

[53] T. Jiang, W. Sun, Q. Zhu et al., "Drug Delivery: Furin-Mediated Sequential Delivery of Anticancer Cytokine and Small-Molecule Drug Shuttled by Graphene (Adv. Mater. 6/2015)," *Advanced Materials*, vol. 27, no. 6, pp. 958-958, 2015.

[54] H. Zhang, Y. Ji, Q. Chen et al., "Enhancement of cytotoxicity of artemisinin toward cancer cells by transferrin-mediated carbon nanotubes nanoparticles," *Journal of Drug Targeting*, vol. 23, no. 6, pp. 552–567, 2015.

[55] N. Kuźnik and M. M. Tomczyk, "Multiwalled carbon nanotube hybrids as MRI contrast agents," *Beilstein Journal of Nanotechnology*, vol. 7, no. 1, pp. 1086–1103, 2016.

[56] S. Surti, "Radionuclide methods and instrumentation for breast cancer detection and diagnosis," *Seminars in Nuclear Medicine*, vol. 43, no. 4, pp. 271–280, 2013.

[57] M. Hernández-Rivera, N. G. Zaibaq, and L. J. Wilson, "Toward carbon nanotube-based imaging agents for the clinic," *Biomaterials*, vol. 101, pp. 229–240, 2016.

[58] J. Meng, X. Liang, X. Chen, and Y. Zhao, "$[Gd@C_{82}(OH)_{22}]_n$ nanoparticles as fullerene derivatives for cancer therapy," *Integrative Biology*, vol. 5, no. 1, pp. 43–47, 2013.

[59] A. Servant, I. Jacobs, C. Bussy et al., "Gadolinium-functionalised multi-walled carbon nanotubes as a T1 contrast agent for MRI cell labelling and tracking," *Carbon*, vol. 97, pp. 126–133, 2016.

[60] I. Marangon, C. Ménard-Moyon, J. Kolosnjaj-Tabi et al., "Covalent functionalization of multi-walled carbon nanotubes with a gadolinium chelate for efficient T1-weighted magnetic resonance imaging," *Advanced Functional Materials*, vol. 24, no. 45, pp. 7173–7186, 2014.

[61] R. Pavani and K. Vinay, "Carbon nanotubes and pharmaceutical applications," *International Research Journal of Pharmacy*, vol. 2, no. 7, pp. 15–21, 2011.

[62] K. Mallick and A. M. Strydom, "Biophilic carbon nanotubes," *Colloids and Surfaces B: Biointerfaces*, vol. 105, pp. 310–318, 2013.

[63] A. T. Georgieva, V. Pappu, V. Krishna et al., "Polyhydroxy fullerenes," *Journal of Nanoparticle Research*, vol. 15, no. 7, article no. 1690, 2013.

[64] R. Xie, Z. Wang, H. Yu et al., "Highly Water-soluble and Surface Charge-tunable Fluorescent Fullerene Nanoparticles: Facile Fabrication and Cellular Imaging," *Electrochimica Acta*, vol. 201, pp. 220–227, 2016.

[65] T. Grobner and F. C. Prischl, "Gadolinium and nephrogenic systemic fibrosis," *Kidney International*, vol. 72, no. 3, pp. 260–264, 2007.

[66] A. A. P. Kartamihardja, T. Nakajima, S. Kameo, H. Koyama, and Y. Tsushima, "Impact of Impaired Renal Function on Gadolinium Retention after Administration of Gadolinium-Based Contrast Agents in a Mouse Model," *Investigative Radiology*, vol. 51, no. 10, pp. 655–660, 2016.

[67] Y. Liu, C. Chen, P. Qian et al., "Gd-metallofullerenol nanomaterial as non-toxic breast cancer stem cell-specific inhibitor," *Nature Communications*, vol. 6, article no. 5988, 2015.

[68] H. Chen, X. Ma, Z. Li et al., "Functionalization of single-walled carbon nanotubes enables efficient intracellular delivery of siRNA targeting MDM2 to inhibit breast cancer cells growth," *Biomedicine & Pharmacotherapy*, vol. 66, no. 5, pp. 334–338, 2012.

[69] D. E. J. G. J. Dolmans, D. Fukumura, and R. K. Jain, "Photodynamic therapy for cancer," *Nature Reviews Cancer*, vol. 3, no. 5, pp. 380–387, 2003.

[70] H. Wang, P. Agarwal, S. Zhao, J. Yu, X. Lu, and X. He, "Combined cancer therapy with hyaluronan-decorated fullerene-silica multifunctional nanoparticles to target cancer stem-like cells," *Biomaterials*, vol. 97, pp. 62–73, 2016.

[71] F. Yan, H. Wu, H. Liu et al., "Molecular imaging-guided photothermal/photodynamic therapy against tumor by iRGD-modified indocyanine green nanoparticles," *Journal of Controlled Release*, vol. 224, pp. 217–228, 2016.

[72] Y. Xiao, X. Gao, O. Taratula et al., "Anti-HER2 IgY antibody-functionalized single-walled carbon nanotubes for detection and selective destruction of breast cancer cells," *BMC Cancer*, vol. 9, article no. 1471, p. 351, 2009.

[73] H. K. Moon, S. H. Lee, and H. C. Choi, "In vivo near-infrared mediated tumor destruction by photothermal effect of carbon nanotubes," *ACS Nano*, vol. 3, no. 11, pp. 3707–3713, 2009.

[74] R. O. Ogbodu, J. L. Limson, E. Prinsloo, and T. Nyokong, "Photophysical properties and photodynamic therapy effect of zinc phthalocyanine-spermine-single walled carbon nanotube conjugate on MCF-7 breast cancer cell line," *Synthetic Metals*, vol. 204, Article ID 14908, pp. 122–132, 2015.

[75] L. Lin, L. Xiong, Y. Wen et al., "Active targeting of nano-photosensitizer delivery systems for photodynamic therapy of cancer stem cells," *Journal of Biomedical Nanotechnology*, vol. 11, no. 4, pp. 531–554, 2015.

[76] A. Herreros-López, M. Carini, T. Da Ros et al., "Nanocrystalline cellulose-fullerene: Novel conjugates," *Carbohydrate Polymers*, vol. 164, pp. 92–101, 2017.

[77] B. Fan, H. Guo, J. Shi et al., "Facile one-pot preparation of silver/reduced graphene oxide nanocomposite for cancer photodynamic and photothermal therapy," *Journal of Nanoscience and Nanotechnology*, vol. 16, no. 7, pp. 7049–7054, 2016.

[78] B. N. Eldridge, B. W. Bernish, C. D. Fahrenholtz, and R. Singh, "Photothermal Therapy of Glioblastoma Multiforme Using Multiwalled Carbon Nanotubes Optimized for Diffusion in Extracellular Space," *ACS Biomaterials Science and Engineering*, vol. 2, no. 6, pp. 963–976, 2016.

[79] P. Chakravarty, R. Marches, N. S. Zimmerman et al., "Thermal ablation of tumor cells with antibody-functionalized single-walled carbon nanotubes," *Proceedings of the National Acadamy of Sciences of the United States of America*, vol. 105, no. 25, pp. 8697–8702, 2008.

[80] J. Shi, L. Wang, J. Gao et al., "A fullerene-based multi-functional nanoplatform for cancer theranostic applications," *Biomaterials*, vol. 35, no. 22, pp. 5771–5784, 2014.

[81] M. Nurunnabi, Z. Khatun, G. R. Reeck, D. Y. Lee, and Y.-K. Lee, "Photoluminescent graphene nanoparticles for cancer phototherapy and imaging," *ACS Applied Materials & Interfaces*, vol. 6, no. 15, pp. 12413–12421, 2014.

[82] M. Azimzadeh, M. Rahaie, N. Nasirizadeh, K. Ashtari, and H. Naderi-Manesh, "An electrochemical nanobiosensor for plasma miRNA-155, based on graphene oxide and gold nanorod, for early detection of breast cancer," *Biosensors and Bioelectronics*, vol. 77, pp. 99–106, 2016.

[83] Rajesh, Z. Gao, R. Vishnubhotla et al., "Genetically Engineered Antibody Functionalized Platinum Nanoparticles Modified CVD-Graphene Nanohybrid Transistor for the Detection of Breast Cancer Biomarker, HER3," *Advanced Materials Interfaces*, vol. 3, no. 17, Article ID 1600124, 2016.

[84] M. A. Ali, K. Mondal, Y. Jiao et al., "Microfluidic Immuno-Biochip for Detection of Breast Cancer Biomarkers Using Hierarchical Composite of Porous Graphene and Titanium Dioxide Nanofibers," *ACS Applied Materials & Interfaces*, vol. 8, no. 32, pp. 20570–20582, 2016.

[85] M. T. Hwang, P. B. Landon, J. Lee et al., "Highly specific SNP detection using 2D graphene electronics and DNA strand displacement," *Proceedings of the National Acadamy of Sciences of the United States of America*, vol. 113, no. 26, pp. 7088–7093, 2016.

[86] M. Fiorillo, A. F. Verre, M. Iliut et al., "Graphene oxide selectively targets cancer stem cells, across multiple tumor types: Implications for non-toxic cancer treatment, via differentiation-based nano-therapy," *Oncotarget*, vol. 6, no. 6, pp. 3553–3562, 2015.

Hindawi
Journal of Nanomaterials
Volume 2018, Article ID 1810846, 12 pages
https://doi.org/10.1155/2018/1810846

*Research Article*

# Icariin-Loaded $TiO_2$ Nanotubes for Regulation of the Bioactivity of Bone Marrow Cells

**Yanli Zhang,[1] Chundong Liu,[2] Liangjiao Chen,[3] Aijie Chen,[1] Xiaoli Feng,[1] and Longquan Shao[1]**

[1]*Nanfang Hospital, Southern Medical University, Guangzhou 510515, China*
[2]*Department of Stomatology, Zhujiang Hospital, Southern Medical University, Guangzhou, Guangdong, China*
[3]*Key Laboratory of Oral Medicine, Guangzhou Institute of Oral Disease, Stomatology Hospital of Guangzhou Medical University, Guangzhou 510140, China*

Correspondence should be addressed to Longquan Shao; shaolongquan@smu.edu.cn

Received 28 August 2017; Revised 11 January 2018; Accepted 23 January 2018; Published 28 February 2018

Academic Editor: Mauro Pollini



To explore the effects of icariin on the biocompatibility of dental implants, icariin- (ICA-) loaded $TiO_2$ nanotubes were fabricated on Ti substrates via anodic oxidation and physical absorption. The surface characteristics of the specimens were monitored by field emission scanning electron microscopy (FE-SEM), X-ray diffractometry (XRD), contact angle measurements (CA), and high-pressure liquid chromatography. Additionally, the activities of bone marrow cells, such as cytoskeletal, proliferative activities, mineralization, and osteogenesis-related gene expression on the substrates were investigated in detail. The characterization results demonstrated that ICA-loaded $TiO_2$ nanotubes were successfully fabricated and the hydrophilicity of these $TiO_2$ nanotubes was significantly higher than that of the pure Ti groups. The results also showed that ICA-loaded $TiO_2$ nanotubes might not have enhanced effects on cell proliferation and ALP expression. However, it seemed to significantly promote differentiation of bone marrow cells, demonstrated by enhancing the formation of mineralized nodule and the upregulation of the gene expression such as OC, BSP, OPN, and COL-1. The results indicated that ICA-loaded $TiO_2$ nanotubes can modulate bioactivity of bone marrow cells, which is promising for potential applications in the orthopedics field.

## 1. Introduction

Bone marrow cells, a type of multilineage potential cell, can proliferate and differentiate into a variety of mesodermal lineages, such as osteoblasts [1], chondrocytes [2], and adipocytes [3]. In vivo, damaged bone tissue will recruit bone marrow cells from the surrounding bone marrow or peripheral circulation to participate in the osseointegration of bone-implant surfaces [4–7]. Therefore, preferentially inducing bone marrow cells differentiation toward osteoblast cells and further accelerating osteoanagenesis are imperative. Previous studies have suggested that the rate and extent of osseointegration are mainly determined by the properties of the implant surface [8]. $TiO_2$ nanotube (NT) modification of the surfaces of titanium substrates has been attracting increasing attention. Several investigators have revealed that the nanostructure influences the adhesion, differentiation, and migration of bone marrow cells significantly [9–12] and that the fates of cells on NT arrays are size dependent [9, 13, 14], while the optimal diameter is still controversial. They found that cell adhesion and spreading are severely impaired on NTs with diameters larger than 50 nm [9, 15]. However, some previous studies confirmed that NTs with diameters of 70 nm can increase the bone-implant contact and osteogenesis-related gene expression [10]. Therefore, we employed NTs with diameters of 30 nm and 80 nm on the surfaces of Ti substrates for further study.

Previous studies have demonstrated that NT arrays could control the release of drugs, such as antibiotics and proteins, for hours [16]. Loading bioactive factors that can induce the adhesion and proliferation of bone marrow cells on titanium implants are the most common strategy to improve early osseointegration. Herba Epimedii is widely used as a complementary and alternative traditional Chinese medicine

for the treatment of osteoporosis in China. Icariin (ICA, $C_{33}H_{40}O_{15}$; molecular weight: 676.67) is the major flavonoid glycoside extracted from Epimedium and is considered the main active constituent. ICA may exert favorable osseointegration effects by enhancing the differentiation of MSCs into osteoblasts while inhibiting the adipogenesis of bone marrow cells [17] and can treat osteoporosis by increasing bone mineral content [18]. Recently, ICA has been widely applied for bone tissue engineering due to its safe, nontoxic, and osteoinductive properties as well as its low cost [19, 20]. The porous PLGA/TCP composite scaffold loaded with ICA was filled in mouse calvarial bone defects and induced significant new bone formation [21]. A recent study reported the generation of a novel bone repair scaffold consisting of a chitosan/nanosized hydroxyapatite system loaded with ICA that can control the release rate and extent of ICA and enhance bone repair. The in vitro bioactivity assay revealed that the loaded ICA was biologically active [22]. ICA increases bone marrow cells differentiation and bone mineralization most likely by upregulating the expression of NO synthesis, subsequently regulating Cbfa1/Runx2 [23, 24]. Meanwhile, ICA can inhibit bone resorption by reducing osteoclastic differentiation and induce osteoclasts apoptosis through an MAPKs/NF-$\kappa$B mechanism [25]. Owing to these advantages, ICA may have a potential application as an ideal osteogenesis agent in bone tissue engineering.

To the best of our knowledge, there have been few experiments studying the application of this Chinese drug on the osseointegration of titanium implants. Therefore, the purpose of this study was to evaluate the effect of ICA on bone marrow cells, which will provide evidence for further applications in the modification of dental implants.

## 2. Materials and Methods

*2.1. Materials.* Titanium disks (14 mm in diameter, 0.3 mm in thickness, and 99.9% purity) were supplied by the Northwest Institute for Nonferrous Metal Research (Xi'an, China). ICA (molecular formula, $C_{33}H_{40}O_{15}$; molecular weight, 676.67 Da) was purchased from the National Institute for the Control of Pharmaceuticals and Biological Products (Beijing, China).

*2.2. Fabrication of $TiO_2$ Nanotubes.* $TiO_2$ NT arrays were fabricated according to previously described procedures via an electrochemical anodization method [11]. Briefly, all the Ti disks were mechanically polished with 800, 1000, and 1200 grit silicon carbide paper. Each sample was then ultrasonically cleaned with acetone, ethanol, and deionized water for 15 min. The cleaned pure Ti disks served as the anodes and a platinum sheet served as the cathode. The electrolyte consisted of 0.5 wt% $NH_4F$ and 3 vol % deionized water in ethylene glycol electrolyte. The anodization voltage was 10 V or 30 V for 2 h. Subsequently, the specimens were rinsed with deionized water and air-dried immediately. Finally, the NTs were sintered at 450°C for 3 h to crystallize the amorphous NTs into anatase structures. The morphologies of the titanium specimens were characterized using a field emission scanning electron microscope (FE-SEM) (Nova Nano SEM430, Netherlands). An X-ray diffractometer (XRD) (LD1-Y-2000, China) was used to determine the surface phase compositions of the treated specimens. Contact angle (CA) measurements were performed using a contact angle goniometer (Data Physics, Germany) with 3 $\mu$L of water on the surfaces.

*2.3. Drug Loading.* ICA was loaded onto the $TiO_2$ NT arrays via a simplified physical adsorption method. Briefly, an ICA solution of 0.5 mg/mL was prepared in ethyl alcohol supplemented with 0.1% dimethyl sulfoxide (DMSO, Sigma, USA) and stored at 4°C. The final DMSO concentration used in the medium was less than 0.01%. The NT substrates were cleaned with deionized water before the ICA loading. Subsequently, the specimens were fully immersed in the respective ICA solutions at room temperature for 30 min and then treated under ultrasonication for 5 min. After that, the surfaces of the titanium substrates were gently rinsed with PBS to remove the excess ICA and then lyophilized for 2 h.

*2.4. In Vitro Release Assay.* The ICA-loaded NT substrates were immersed in 3 mL of phosphate-buffered saline (PBS) solution (pH 7.4) in a 24-well plate with gentle shaking at 100 rpm at 37°C. At predetermined time points of 1, 6, 12, 24, 48, and 72 h, 500 $\mu$L of PBS was extracted and replaced with fresh medium. A high-performance liquid chromatograph (HPLC) (Agilent Technologies 1260 Infinity, USA) was used to examine the amount of ICA released. The mobile phase was composed of a mixture of water/acetonitrile (65/35, v/v) and the flow rate was 1.0 mL per minute. A variable wavelength detector was used to detect the column effluent at 270 nm with a column temperature of 25°C.

*2.5. Cell Culture.* The animal protocol received approval from the Southern Medical University Animal Research Committee. The bone marrow cells were derived from two-week-old Sprague-Dawley rats. Briefly, SD rats were treated with deep anesthesia and cervical dislocation. Then, the bilateral femur and tibia were isolated aseptically, and the marrow cells were flushed out with Dulbecco's Minimum Essential Medium (DMEM, Gibco). After that, the cells were cultured in low-glucose DMEM supplemented with 10% fetal bovine serum (FBS, Gibco) at 37°C in a humidified atmosphere with 5% $CO_2$. When reaching 80% confluence, the cells were detached with 0.25% trypsin (Sigma) and reseeded in new culture flasks. Bone marrow cells at passages 2–4 were used in this study.

*2.6. Cytoskeleton Observation.* Bone marrow cells were seeded onto the surfaces of titanium substrates (Ti, $NT_{10}$, $NT_{10}/ICA_{0.5}$, $NT_{30}$, and $NT_{30}/ICA_{0.5}$) at an initial density of $1 \times 10^4$/well. After 24 h of culture, the cells were gently rinsed with PBS, fixed for 15 min in 4% paraformaldehyde, and then permeabilized in 3% Trion X-100 for 5 min. After that, the samples were stained with TRITC-Phalloidin (YEASEN, Shanghai, China) for 40 min to visualize the actin

Table 1: Primer sequences utilized for quantitative real-time PCR.

| Gene | Forward primer sequence (5′-3′) | Reverse primer sequence (5′-3′) |
|---|---|---|
| COL- I | GGAGAGAGCATGACCGATGG | AAGTTCCGGTGTGACTCGTG |
| OC | GGAGGGCAGTAAGGTGGTGAA | TCCTGGAAGCCAATGTGGTC |
| BSP | GAACGGGTTTCAGCAGACGA | GGGGCCTTCACTGGTGGTA |
| OPN | AGCATTCTCGAGGAAGCCAG | AGTGTTTGCTGTAATGCGCC |
| Runx2 | AGCGGACGAGGCAAGAGTTT | GGGTTCTGAGGCGGGACA |
| $\beta$-actin | TGAAGTACCCCATTGAACACGG | GGGTCATCTTTTCACGGTTGG |

cytoskeleton and then counterstained with 4′,6-diamidino-2-phenylindole (DAPI, Sigma, USA) to visualize the cell nuclei. Subsequently, the cytoskeleton and nuclei of the bone marrow cells were observed under an inverted fluorescence microscope (Olympus, Japan).

*2.7. Cell Adhesion, Proliferation, and Mineralization.* The initial attachment of the bone marrow cells was evaluated by quantifying the cells attached to the titanium surface. After culturing for 1, 2, and 4 h, the plates were gently rinsed with PBS to remove all nonadherent cells and then placed into new 24-well plates for assessment of cell numbers using the Cell Counting Kit-8 assay (CCK-8, Dojindo Molecular Technologies, Japan) in accordance with the manufacturer's instructions. For the proliferative assay, the cells were cultured on the plates for 1, 3, 5, and 7 d, and the cell numbers were measured using the CCK-8 assay.

Bone marrow cells were seeded on each sample at a density of $2 \times 10^4$/well. After culturing for 7 and 14 days, the cell supernatants were collected and frozen at −80°C. An alkaline phosphatase activity fluorometric assay kit (BioVision, Milpitas, CA, USA) was used to assess the ALP activity according to the manufacturer's instructions. The fluorescence intensity was measured at Ex/Em of 360/440 nm using a multimode reader (Spectra Max M5, US) and then the values of the ALP activities were calculated according to the standard curve.

Cell mineralization was assessed by Alizarin Red staining. Briefly, $2 \times 10^4$ cells per well were seeded onto each sample, and the mineralized solution was refreshed every two days. After culturing for 21 days, the specimens were washed three times with PBS, and then the cells were then fixed with 4% paraformaldehyde. After rinsing with deionized water, the specimens were dyed with 0.1% Alizarin Red solution (Cyagen, USA) for 30 min. Finally, the formation of mineralized nodules was observed under a stereomicroscope (SZXl6, Olympus, Japan). The quantification of mineralization was performed as described previously [26]. Briefly, 10% cetylpyridinium chloride was added to each well to dissolve the deposition, and the solution was then collected. The absorbance at 562 nm was measured with a microplate reader.

*2.8. Gene Expression Analysis.* The expression of osteogenesis-related genes was analyzed using the reverse transcription polymerase chain reaction (RT-PCR). At 7 and 14 d of culture, the MSCs were rinsed with PBS, and the total RNA was extracted using TRIzol (Gibco, USA). Then, the RNA was used in reverse transcription to generate cDNA using a Prime Script TM RT reagent kit (TaKaRa, Japan). PCR was performed using a real-time PCR kit (SYBR Premix Ex Taq II, TaKaRa) to detect osteopontin (OPN), osteocalcin (OC), bone sialoprotein (BSP), Runx2, and type I collagen (COL-I) mRNA on a Light Cycler 480 II (Roche, Germany). The primer sequences for the osteogenic genes are shown in Table 1. The housekeeping gene $\beta$-actin was used to normalize the relative expression quantities of target genes.

*2.9. Statistical Analysis.* All data are expressed as the mean ± standard deviation. Comparisons between groups were tested by one-way ANOVA, least significant difference (LSD) post hoc test (when the variance was regular), or Dunnett T3 test post hoc test (when the variance was irregular). The differences were considered statistically significant when $P < 0.05$.

## 3. Results

*3.1. The Characterization of the $TiO_2$ Nanotube Substrates.* After anodization at 10 V and 30 V and annealing at 450°C for 3 h, the morphologies of the $TiO_2$ NT arrays were observed by FE-SEM. Before modification, the titanium surface was smooth with visible parallel polishing scratches as shown in Figure 1(a). However, the $TiO_2$ NTs fabricated with ethylene glycol displayed smooth walls and uniform diameters of approximately 30 nm and 80 nm for the 10 V and 30 V anodizations, respectively (Figures 1(b) and 1(c)). The result showed that the diameters of the $TiO_2$ NTs were positively correlated with the anodic oxidation voltage.

The XRD diffraction patterns of the $TiO_2$ NT array specimens before and after heat treatment are shown in Figure 2. The results indicated that the $TiO_2$ NT arrays before heat treatment contain crystalline Ti substrate peaks, and no anatase phase was detected (Figure 2(a)), while most of the $TiO_2$ NTs were transferred into the anatase phase by sintering at 450°C for 3 h (Figure 2(b)).

The $TiO_2$ NT substrates displayed significantly lower contact angles compared with pure Ti, which illustrated that the nanostructure increased the hydrophilicity of the Ti specimens, especially for NTs with 80 nm diameters, while the loading of ICA had little effect on the surface properties of the titanium substrates (Figure 3).

*3.2. ICA Release Profile.* The amount of ICA loaded onto the NT arrays was determined by the NT diameters. The $NT_{30}/ICA_{0.5}$ group accounted for approximately 7-fold more

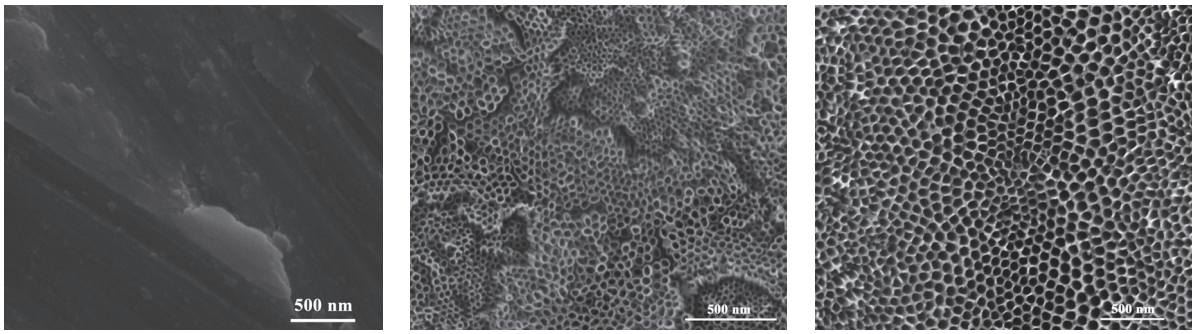


Figure 1: FE-SEM images of the surfaces of Ti specimens before and after anodization. (a) Pure Ti, (b) NT arrays after anodization at 10 V ($NT_{10}$), and (c) NT arrays after anodization at 30 V ($NT_{30}$). $TiO_2$ NTs with different diameters can be fabricated with ethylene glycol, and the resulting diameter is positively related to the voltage of anodic oxidation.

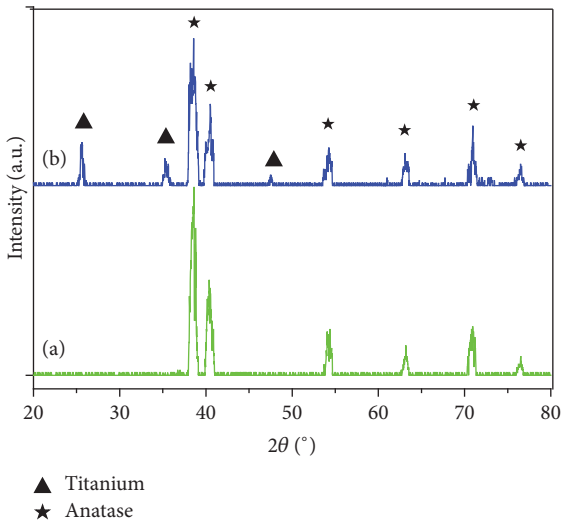


Figure 2: XRD patterns of the NT substrates before and after calcination. (a) NT substrate before sintering and (b) NT substrate after sintering. The results showed that most of the $TiO_2$ NTs can be transferred from the amorphous to anatase phase after sintering.

ICA than the $NT_{10}/ICA_{0.5}$ group. The total quantity of ICA released from the NT arrays was less than $10^{-5}$ M. Figure 4 shows that the $NT_{30}/ICA_{0.5}$ group expressed a faster release time than the $NT_{10}/ICA_{0.5}$ group. A large amount of the release occurred on the first day, and, after that, the release profiles were similar. The ICA released from the NT array groups decreased obviously at 3 d, and no ICA was detected by HPLC after that.

*3.3. The Cell Morphology.* To investigate cell behaviors on ICA-loaded NT array substrates, we observed the morphologies of bone marrow cells using an inverted fluorescence microscope (Figure 5). The cells adhered to the NT array surfaces spread out sufficiently with irregular or polygon shapes. Bone marrow cells cultured on small diameter NT arrays demonstrated well-spread morphologies with more lamellipodia, whereas the cells on large diameter NT arrays displayed noticeable filopodium. Cells seeded on the surfaces of ICA-loaded NT substrates expressed more filopodium than nonloaded NT groups. In contrast, the cells on pure Ti substrates were partly inadequate with fewer protrusions.

*3.4. Assay of Bone Marrow Cell Adhesion.* CCK-8 assays were used to examine the adhesion rates of the experimental groups and the control group of Ti specimens. Figure 6(a) shows the adhesion of bone marrow cells on different substrates after culturing for 1, 2, and 4 h. The number of cells increased with the incubation time. Bone marrow cells cultured on the pure Ti and small diameter NT samples displayed comparatively higher adhesion abilities than the NTs with large diameters at 2 and 4 h ($P < 0.01$). These results show the adverse influence of the NTs with 80 nm diameters on the cytocompatibility. The loading of the ICA failed to significantly promote the early adhesion of cells.

*3.5. Assay of Bone Marrow Cell Proliferation.* The proliferation of the bone marrow cells seeded on the pure Ti and NT-modified substrates was measured using the CCK8 assay. After culturing for 1 d, there were no statistically significant differences among all of the groups ($P > 0.05$). On day 3, there were no statistically significant differences between the pure Ti and small diameter groups, while the viability of the cells on the $NT_{30}$ substrates was lower than on the untreated samples. However, the $NT_{30}/ICA_{0.5}$ group increased the viability of the bone marrow cells compared with $NT_{30}$ without ICA loading. Overall, no experimental groups promoted the proliferation of cells compared with pure Ti at day 5. After culturing for 7 d, the rate of cell proliferation in the $NT_{30}/ICA_{0.5}$ group was significantly higher than those of the Ti group and the $NT_{30}$ group, which may be attributed to the sealing of NT constructure by cells and the long-term additive effect of ICA. In summary, the NT array structure and the ICA loading yielded no prominent advantage on cell proliferation except on individual groups (Figure 6(b)).

*3.6. Alkaline Phosphatase Activity of Bone Marrow Cells.* The ALP activities of the bone marrow cells cultured on the

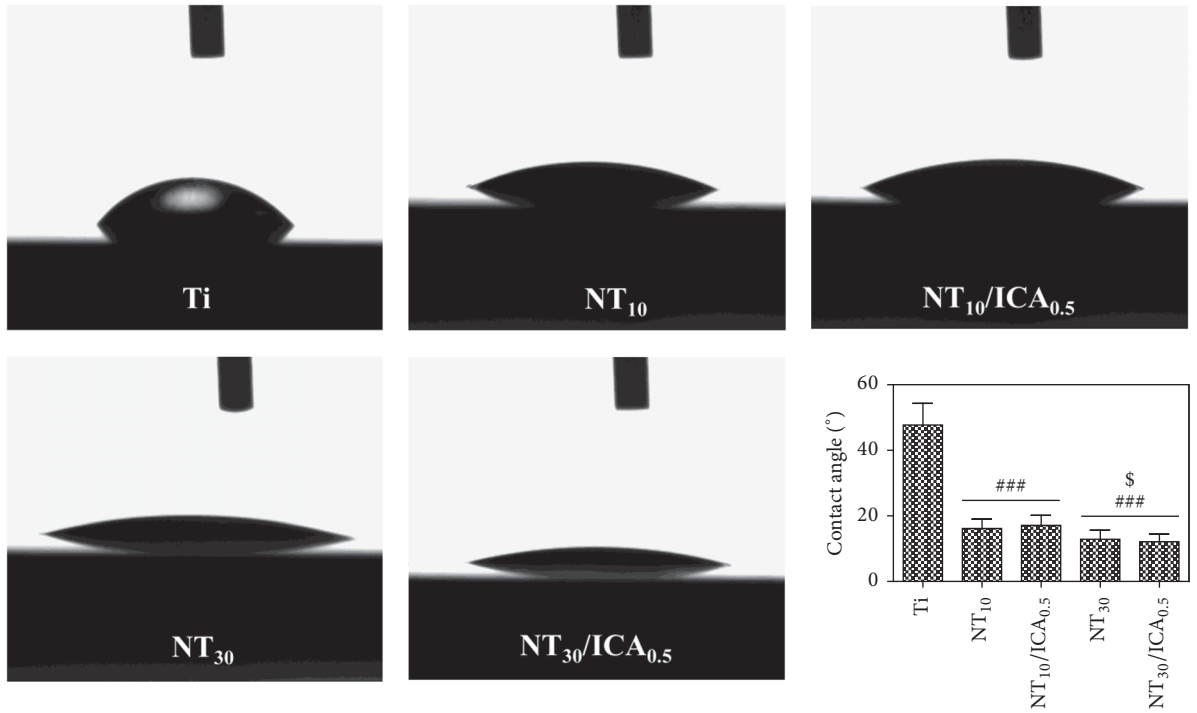


FIGURE 3: Images and the water contact angle results. The contact angles of the NT plates were lower than those of the Ti plates, and the contact angles decreased as the NT diameters increased, while ICA had no influence on the contact angle ($^{###}P < 0.001$ with Ti; $^{\$}P < 0.05$ with the NT groups with the 10-V treatment).

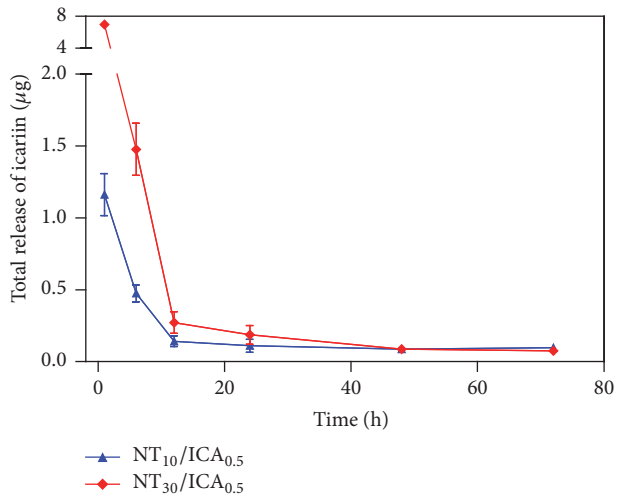


FIGURE 4: The total release of ICA in the different treatment groups. The release profile confirmed that the $TiO_2$ NTs with large diameters can be loaded with more ICA, and the release time lasted 3 d in each group.

different titanium substrates were detected after culturing for 7 and 14 d (Figure 7). The results showed that there were no statistically significant differences between the pure Ti group and the experimental groups, while the $NT_{30}/ICA_{0.5}$ group was significantly higher than the $NT_{30}$ group ($P < 0.01$) after culturing for 7 d. There were no significant differences in the ALP activities between the pure Ti group and the experiment groups after culturing for 14 d.

*3.7. Mineralized Nodule Formation.* The Alizarin Red staining results of different specimens after 21 days of culture are shown in Figure 8. The mineralized area on the NT-treated surfaces was significantly larger than that on the pure Ti surface because many blank areas could be observed on the control group, whereas cell calcification occurred homogenously on NT treated surfaces. The highest Alizarin Red staining of calcium deposition was observed on the $NT_{30}/ICA_{0.5}$ groups, followed by the NT-treated group, whereas no significant difference was observed among the latter three groups. The results indicated that the calcium deposition on $NT_{30}$ group was enhanced by addition of ICA.

*3.8. Osteogenesis-Related Gene Expression.* The gene expression profiles for OPN, OC, COL-1, BSP, and Runx 2 mRNA at 7 and 14 d are shown in Figure 9. After culturing for 7 d, the $NT_{10}$ and $NT_{30}$ groups displayed statistically higher COL-I levels than the pure Ti group ($P < 0.05$), while the loading of ICA failed to increase the expression of COL-I. The expression of OPN in the experimental groups was statistically higher than that of the pure Ti group, while no significant differences were detected among the experimental groups. $NT_{10}$, $NT_{30}$, and $NT_{30}/ICA_{0.5}$ expressed higher levels of OC than that of the Ti group. The experimental groups of $NT_{10}/ICA_{0.5}$, $NT_{30}$, and $NT_{30}/ICA_{0.5}$ upregulated the level of BSP, $NT_{30}$ was superior to $NT_{10}$, and $NT_{10}/ICA_{0.5}$

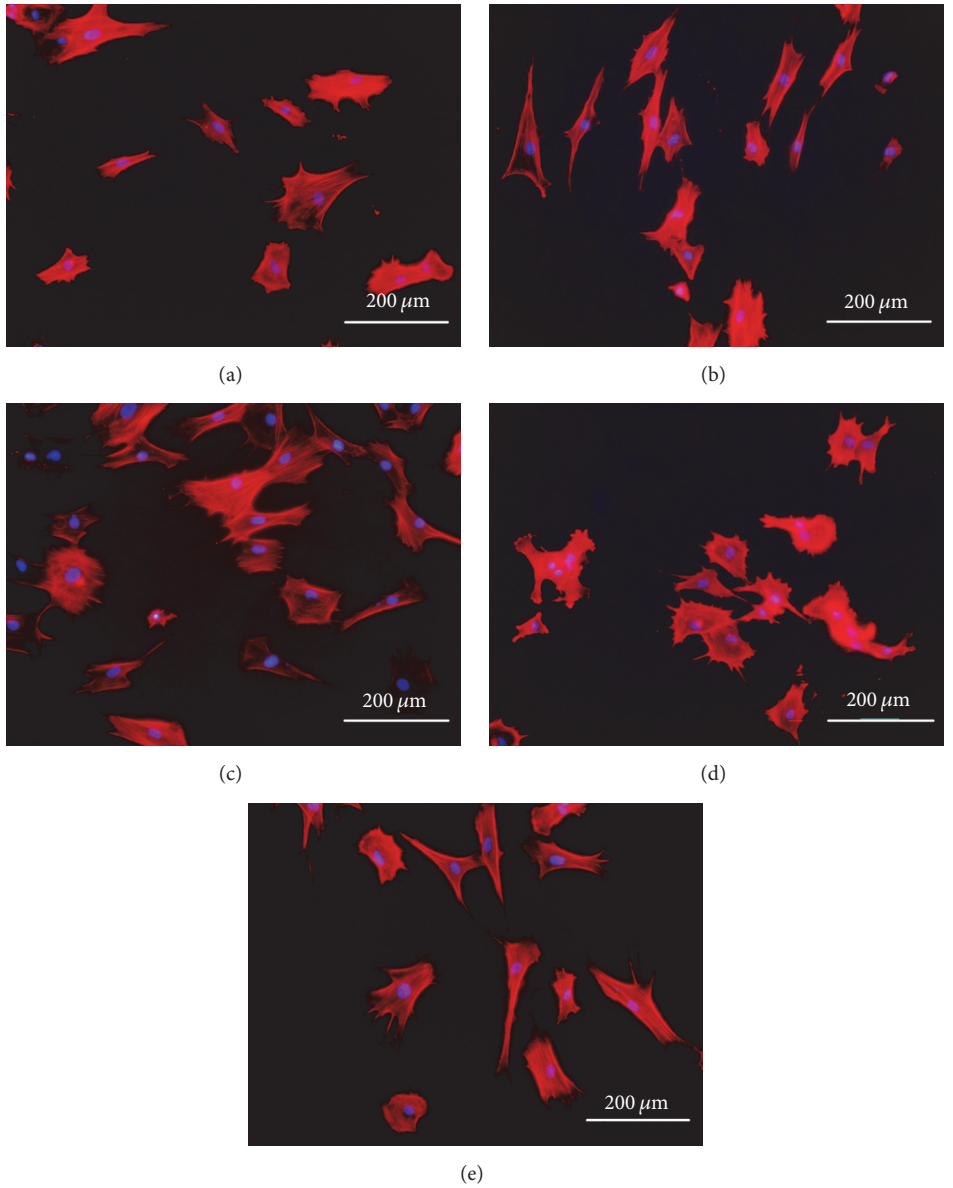


Figure 5: Fluorescence images of bone marrow cells after culturing for 24 h. (a) Ti, (b) $NT_{10}$, (c) $NT_{10}/ICA_{0.5}$, (d) $NT_{30}$, and (e) $NT_{30}/ICA_{0.5}$.

significantly increased the expression of BSP compared with $NT_{10}$. However, only the $NT_{10}/ICA_{0.5}$ group upregulated the expression of Runx2 mRNA compared with pure Ti. The above results indicated that NT characteristics enhanced mRNA expression of OPN, OC, BSP, and COL-I. While ICA had no significantly positive effects on the expression of bone-related genes. After culturing for 14 d, the NT substrates significantly upregulated the expressions of BSP and OC. More importantly, $NT_{10}/ICA_{0.5}$ further increased the expressions of both genes significantly compared with $NT_{10}$ groups, while there was no significant difference between $NT_{30}$ and $NT_{30}/ICA_{0.5}$ groups. In addition, there were no significant differences in the expressions of COL-I, OPN, and Runx2 among the groups, with the exception of the $NT_{30}$ group (Figure 9).

## 4. Discussion

In this study, we fabricated $TiO_2$ NTs with different diameters and loaded them with ICA. The structures were expected to simulate the natural bone structure and promote the integration of implants with the surrounding bone tissue.

$TiO_2$ NTs have attracted great interest due to their simple preparation process of anodic oxidation, low costs, and adjustable resistances. The diameters of the $TiO_2$ NTs were positively correlated with the anodic oxidation voltage. In this study, even and uniform $TiO_2$ NT arrays with diameters of approximately 30 nm and 80 nm were formed on the titanium plates. The results fully demonstrated the diversity and controllability of the $TiO_2$ NT structures; these properties are consistent with previous studies [15, 27, 28]. These studies

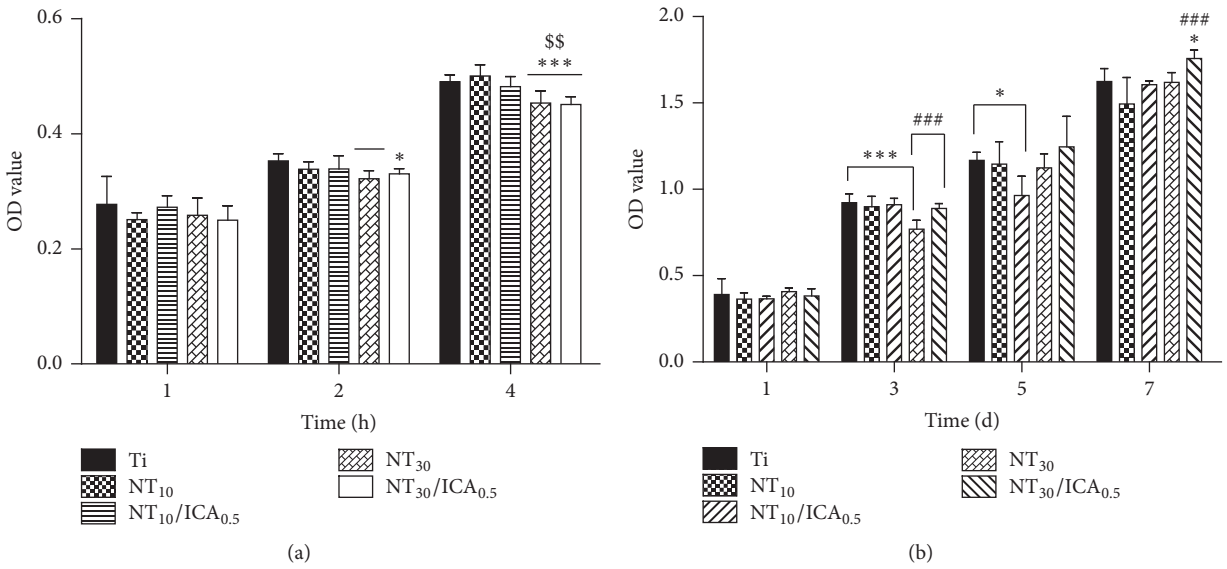


Figure 6: Adhesion and proliferation of bone marrow cells on the different surfaces. (a) The average adhesion of the cells on the surfaces of the NTs and the untreated Ti after culturing for 1, 2, and 4 h. (b) The proliferation of the cells on the specimens after culturing for 1, 3, 5, and 7 d ($^{*}P < 0.05$ with Ti; $^{***}P < 0.001$ with Ti; $^{\$\$}P < 0.01$ with small diameter NT array specimens; $^{\#\#\#}P < 0.001$ between the $NT_{30}$ and $NT_{30}/ICA_{0.5}$ groups).

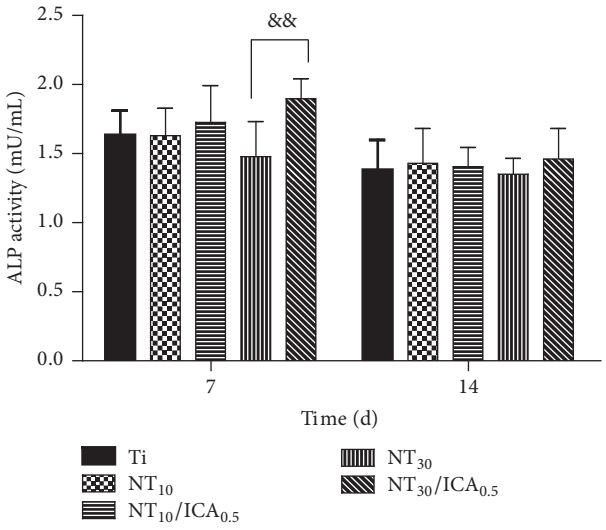


Figure 7: ALP activities of the MSCs on the different surfaces after culturing for 7 and 14 d ($^{\&\&}P < 0.01$ between the $NT_{30}$ and $NT_{30}/ICA_{0.5}$ groups). The $NT_{30}/ICA_{0.5}$ group exhibited upregulated ALP activity after culture for 7 d compared with the $NT_{30}$ group, whereas no significant difference was observed with the other groups, which showed that ICA was slightly beneficial for ALP activity.

found that the bioactivities of cells were decided by the $TiO_2$ NT diameter. Park suggested that a smaller diameter of 15 nm could promote the proliferation and differentiation of osteoblasts, while large diameters of more than 50 nm caused serious damage to the cells due to the diverse surface morphologies [13, 15]. However, large diameter titanium NTs (70 nm) had advantages compared with small diameter NTs in promoting the osteoanagenesis and increasing bone mass around an implant in vivo [10]. Because the optimal diameter of $TiO_2$ NTs has not reached a consensus, we fabricated $TiO_2$ NT specimens with two different diameters (30 nm and 80 nm) for subsequent research. $TiO_2$ NT plates were sintered at 450°C for 3 h. XRD showed that the amorphous $TiO_2$ changed into the anatase phase after sintering. It has been reported that anatase $TiO_2$ NTs have improved cell activity due to the similarity in the crystal lattice of the anatase structure and hydroxyapatite [29].

The physical and chemical properties of the titanium surfaces have an effect on the biological characteristics of the cells due to the direct contact with the surfaces of the implants. Rupp et al. [30] took advantage of a dynamic contact angle analysis system to monitor the hydrophilia of titanium specimens and found that the hydrophilia could be greatly affected by the roughness and morphology of the titanium surface. In this study, the water contact angle was used to measure the hydrophilia of various titanium specimens. The contact angles of the $TiO_2$ NT substrates were significantly lower than that of the pure Ti. Takebe [31] indicated that the hydrophilia of the $TiO_2$ NT structures may have increased greatly because the water easily infiltrated into the $TiO_2$ porous network, which caused the contact angle to decrease. In addition, the ICA loaded onto the NTs failed to influence the surface properties of titanium substrates.

Physical adsorption as a method to load the bioactive molecules and drugs onto the biomaterial scaffolds has been widely applied in previous studies [32–34]. This method has the advantages of ensuring the chemical structure and biological properties of the molecules, except for the inexpensive and efficacious characteristics. Here, the HPLC results showed that the ICA released from the NT structure in a

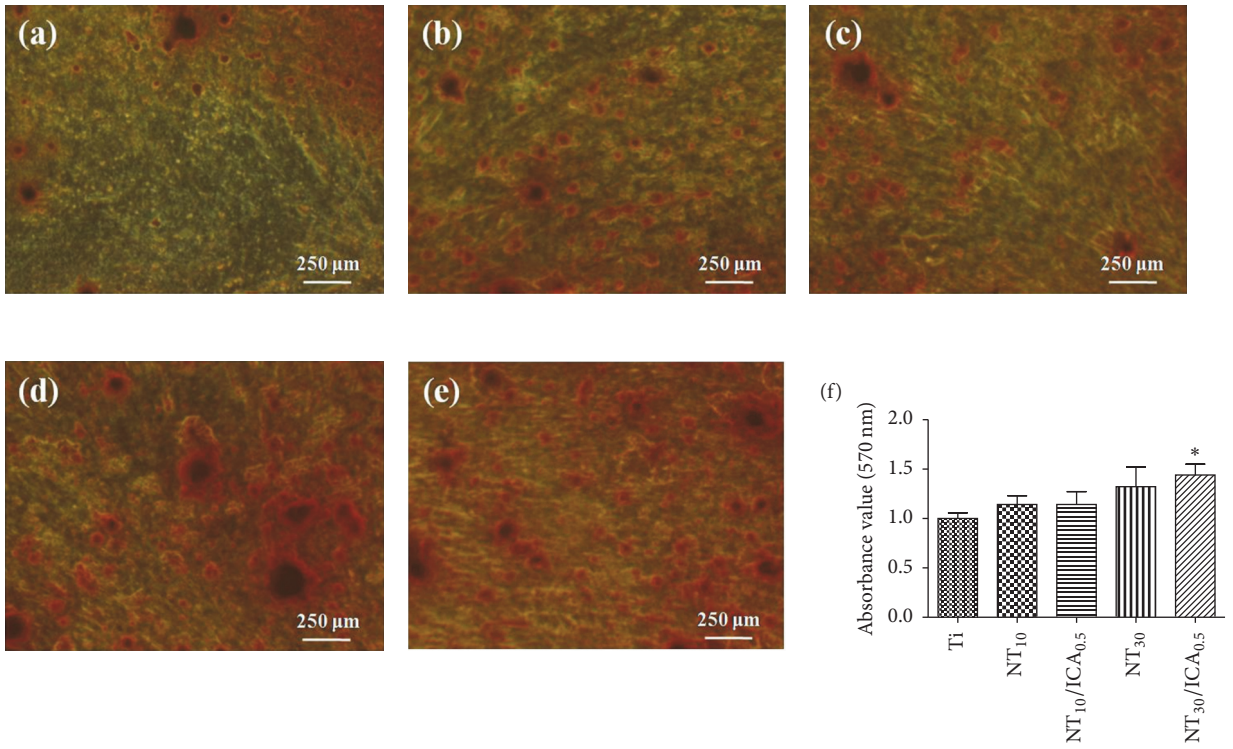


Figure 8: Alizarin Red staining and calcium deposition of bone marrow cell culture on various surfaces for 21 days. (a) Ti, (b) $NT_{10}$, (c) $NT_{10}/ICA_{0.5}$, (d) $NT_{30}$, and (e) $NT_{30}/ICA_{0.5}$. The formation of mineralized nodules was slightly enhanced in $NT_{30}/ICA_{0.5}$ group ($^*P < 0.05$ between the Ti and $NT_{30}/ICA_{0.5}$ groups).

sustained manner, which indirectly confirmed the successful loading of ICA onto the NT surface and retention of the activity of the medicine. NT substrates as drug nanoreservoirs may represent a potential drug delivery system and the absorbing capacity was primarily dependent on the nanotube size and concentration of a drug, [35]; thus more drug was loaded with increasing diameter of NTs.

The initial adhesion of cells on the titanium substrates played an important role in the regulation of potential cell functions including proliferation, migration, and differentiation. Overall, large diameter NT arrays had adverse effect on the adhesion and proliferation of bone marrow cells compared with Ti and small diameter NT groups. Previous studies have suggested that the effects of $TiO_2$ NTs with various diameters on the behaviors of cells were more important than the surface topographies of the titanium substrates, which is consistent with the results of this study [36]. The inhibition of cell proliferation by NTs with large diameters may be related to differentiation due to the reciprocal relationship between cell proliferation and differentiation [37]. The effects of ICA on the proliferation of cells were dose-dependent: concentrations higher than $10^{-4}$ M are toxic to cells, and no positive effect on cell proliferation was detected even in lower dose group, which was consistent with the present study [38]. In this study, the quantity of ICA released from the NTs was less than $10^{-5}$ M. In addition, the bone marrow cells seeded on the small diameter $TiO_2$ NTs extended many lamellipodia, while more filopodia were observed on the surfaces of the large diameter NT and ICA-loaded specimens. These results were also confirmed in previous studies [9]. Some scholars suggested that the filopodia may be generated to block the NT structures from the cells. The extracellular matrix secreted by osteoblasts was deposited on the surfaces of the NT walls with large diameter, which affects the cell adhesion [39].

In this study, the ALP activities of the MSCs adhered to the different substrates were assessed. This property is commonly used to indicate the early stages of osteoblast differentiation. After culturing for 7 d, the ICA-loaded $NT_{30}$ substrates displayed advantages over the NT and pure Ti substrates. The potential mechanism may be that the released ICA promoted the differentiation of the MSCs into osteoblasts. There were no significant differences among the groups at day 14. The phenomenon may be explained by the fact that the MSCs had entered into the late stage of differentiation and reduced the sensitivity to the topography of the titanium surface. On the other hand, the ICA was fully released from the NTs. The accumulated evidence proved that the NT structure could improve the ALP activity of the primary osteoblasts and cell lines [40], which was not in agreement with the results of this study and the concrete mechanism remains to be further studied. Mineralized nodule formation served as a marker of late stage differentiation, which is an essential sign for the osteogenic differentiation of bone marrow cells. Therefore, the above described results verified that ICA, particularly on the $NT_{30}$ surface, can significantly enhance the mineralization of bone marrow

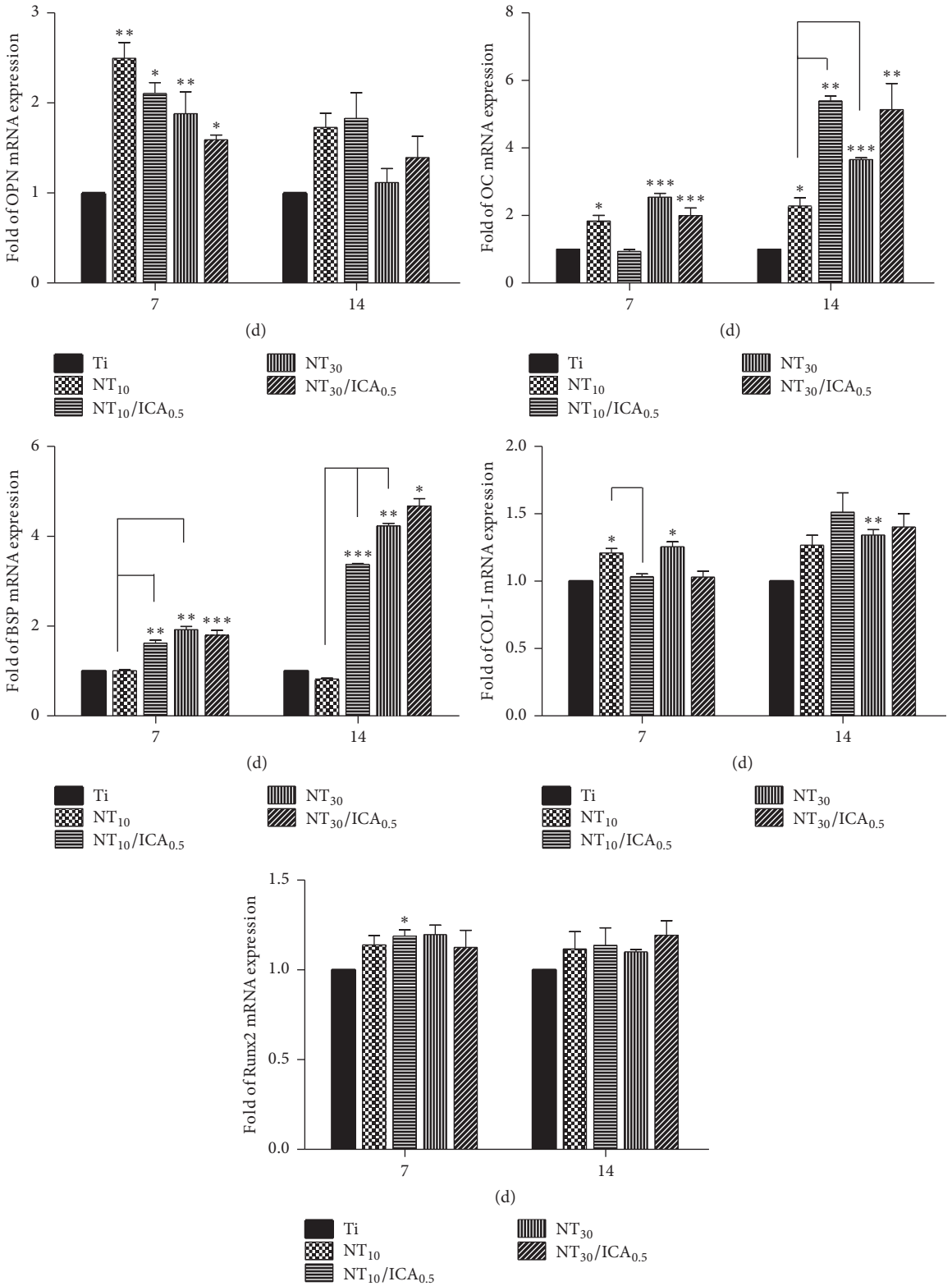


Figure 9: Expressions of bone-related genes in bone marrow cells on different substrates for 7 d and 14 d ($^{*}P < 0.05$, $^{**}P < 0.01$, and $^{***}P < 0.001$ with Ti). NT and ICA-loaded NT groups exhibited significantly increased gene expression compared with the pure NT arrays.

cells, which was consistent with previous reports that ICA can promote the mineralization of cells [41].

We then investigated the molecular basis of Ti samples by assessing the mRNA expression of osteoblast-related genes, including OPN, OC, BSP, COL-I, and Runx2, which are important indices of bone maturity. Previous studies confirmed that BSP, OC, and COL-I are related to the cell cycle and regulate generation of the extracellular matrix and thus play an indispensable role in osteogenesis [42–44]. A previous study found that ICA displayed osteogenic capability to activate the PKG signaling pathway, further regulating the transcription of downstream osteogenic genes, such as COL-I, OC, and BSP [45]. After incubation for 7 d, the osteogenesis-related genes, such as OPN, OC, BSP, and COL-I, were upregulated by NT groups compared with the Ti group. We attributed the upregulation of the genes to the special nanostructures. Oh et al. [9] proposed that $TiO_2$ NTs with large diameters (70–100 nm) could selectively induce the differentiation of stem cells. BSP and OC are the most closely related to bone marrow cell differentiation [43]. A previous study demonstrated the effect of PLGA/TCP/icariin scaffold on upregulating BSP mRNA expression in dose-dependent manner. The mRNA expression level of OC in the icariin treated groups was higher than that in the control group [21]. In the present study, the ability of ICA to upregulate the levels of BSP and OC mRNA expression indicated that ICA is conducive to improving the osteogenesis potential of the bone marrow cells.

Taken together, the results indicate that both ICA and $TiO_2$ nanotubes are beneficial for improving the expression of osteogenesis-related genes in vitro, resulting in favorable molecular responses. However, the osteogenesis capability of ICA was weaker than $TiO_2$ nanotubes.

## 5. Conclusion

In this study, NT array specimens were fabricated and it was beneficial for controlling the release of ICA. NT array substrates facilitate the initial spreading, mineralization, and expression of bone-related genes of bone marrow cells, indicating a potential application on Ti implant. In addition, ICA significantly promoted the osteogenic differentiation in the later stage, such as enhancing the formation of mineralized nodule and upregulating the gene expression of BSP and OC. While it had no positive effect on cell bioactivity, thus the potential application of ICA as a substitute bioactive molecule on Ti implants should be further modified.

## Conflicts of Interest

The authors declare that they have no conflicts of interest.

## Acknowledgments

This work was supported by the National Natural Science Foundation of China (31070857 and 50973045); the Project on the Integration of Industry, Education and Research of Guangdong Province, China (2012B091000147); Scientific research projects of Guangzhou Medical University (2015C43); and the Medical Research Foundation of Guangdong Province (A2015132).

## Supplementary Materials

Schematic illustration of the fabrication of icariin-loaded NT substrates and cellular responses. *(Supplementary Materials)*

## References

[1] J. Chen, Z.-D. Shi, X. Ji et al., "Enhanced osteogenesis of human mesenchymal stem cells by periodic heat shock in self-assembling peptide hydrogel," *Tissue Engineering Part: A*, vol. 19, no. 5-6, pp. 716–728, 2013.

[2] B. Zhang, S. Yang, Z. Sun et al., "Human mesenchymal stem cells induced by growth differentiation factor 5: An improved self-assembly tissue engineering method for cartilage repair," *Tissue Engineering - Part C: Methods*, vol. 17, no. 12, pp. 1189–1199, 2011.

[3] C. Lange, B. Brunswig-Spickenheier, L. Eissing, and L. Scheja, "Platelet lysate suppresses the expression of lipocalin-type prostaglandin D2 synthase that positively controls adipogenic differentiation of human mesenchymal stromal cells," *Experimental Cell Research*, vol. 318, no. 18, pp. 2284–2296, 2012.

[4] C. Vater, P. Kasten, and M. Stiehler, "Culture media for the differentiation of mesenchymal stromal cells," *Acta Biomaterialia*, vol. 7, no. 2, pp. 463–477, 2011.

[5] R. Tasso, F. Fais, D. Reverberi, F. Tortelli, and R. Cancedda, "The recruitment of two consecutive and different waves of host stem/progenitor cells during the development of tissue-engineered bone in a murine model," *Biomaterials*, vol. 31, no. 8, pp. 2121–2129, 2010.

[6] A. Nair, J. Shen, P. Lotfi, C.-Y. Ko, C. C. Zhang, and L. Tang, "Biomaterial implants mediate autologous stem cell recruitment in mice," *Acta Biomaterialia*, vol. 7, no. 11, pp. 3887–3895, 2011.

[7] A. I. Caplan, "Adult mesenchymal stem cells for tissue engineering versus regenerative medicine," *Journal of Cellular Physiology*, vol. 213, no. 2, pp. 341–347, 2007.

[8] L. Le Guéhennec, A. Soueidan, P. Layrolle, and Y. Amouriq, "Surface treatments of titanium dental implants for rapid osseointegration," *Dental Materials*, vol. 23, no. 7, pp. 844–854, 2007.

[9] S. Oh, K. S. Brammer, Y. S. J. Li et al., "Stem cell fate dictated solely by altered nanotube dimension," *Proceedings of the National Acadamy of Sciences of the United States of America*, vol. 106, no. 7, pp. 2130–2135, 2009.

[10] N. Wang, H. Li, W. Lü et al., "Effects of $TiO_2$ nanotubes with different diameters on gene expression and osseointegration of implants in minipigs," *Biomaterials*, vol. 32, no. 29, pp. 6900–6911, 2011.

[11] L. Zhao, L. Liu, Z. Wu, Y. Zhang, and P. K. Chu, "Effects of micropitted/nanotubular titania topographies on bone mesenchymal stem cell osteogenic differentiation," *Biomaterials*, vol. 33, no. 9, pp. 2629–2641, 2012.

[12] M. Tzaphlidou, "The role of collagen in bone structure: An image processing approach," *Micron*, vol. 36, no. 7-8, pp. 593–601, 2005.

[13] J. Park, S. Bauer, K. A. Schlegel, F. W. Neukam, K. D. Von Mark, and P. Schmuki, "$TiO_2$ nanotube surfaces: 15 nm—an

optimal length scale of surface topography for cell adhesion and differentiation," *Small*, vol. 5, no. 6, pp. 666–671, 2009.

[14] K. S. Brammer, S. Oh, C. J. Cobb, L. M. Bjursten, H. van der Heyde, and S. Jin, "Improved bone-forming functionality on diameter-controlled $TiO_2$ nanotube surface," *Acta Biomaterialia*, vol. 5, no. 8, pp. 3215–3223, 2009.

[15] J. Park, S. Bauer, K. von der Mark, and P. Schmuki, "Nanosize and vitality: $TiO_2$ nanotube diameter directs cell fate," *Nano Letters*, vol. 7, no. 6, pp. 1686–1691, 2007.

[16] K. C. Popat, M. Eltgroth, T. J. LaTempa, C. A. Grimes, and T. A. Desai, "Decreased Staphylococcus epidermis adhesion and increased osteoblast functionality on antibiotic-loaded titania nanotubes," *Biomaterials*, vol. 28, no. 32, pp. 4880–4888, 2007.

[17] H. Sheng, X.-F. Rui, C.-J. Sheng et al., "A Novel semisynthetic molecule Icaritin stimulates osteogenic differentiation and inhibits adipogenesis of mesenchymal stem cells," *International Journal of Medical Sciences*, vol. 10, no. 6, pp. 782–789, 2013.

[18] J.-F. Zhang, G. Li, C.-L. Meng et al., "Total flavonoids of Herba Epimedii improves osteogenesis and inhibits osteoclastogenesis of human mesenchymal stem cells," *Phytomedicine*, vol. 16, no. 6-7, pp. 521–529, 2009.

[19] M. Li, Q. Gu, M. Chen, C. Zhang, S. Chen, and J. Zhao, "Controlled delivery of icariin on small intestine submucosa for bone tissue engineering," *Materials Science and Engineering C: Materials for Biological Applications*, vol. 71, pp. 260–267, 2017.

[20] L. Yin, K. Wang, X. Lv et al., "The fabrication of an ICA-SF/PLCL nanofibrous membrane by coaxial electrospinning and its effect on bone regeneration in vitro and in vivo," *Scientific Reports*, vol. 7, no. 1, article no. 8616, 2017.

[21] Y. Lai, H. Cao, X. Wang et al., "Porous composite scaffold incorporating osteogenic phytomolecule icariin for promoting skeletal regeneration in challenging osteonecrotic bone in rabbits," *Biomaterials*, vol. 153, pp. 1–13, 2018.

[22] J. Fan, L. Bi, T. Wu et al., "A combined chitosan/nano-size hydroxyapatite system for the controlled release of icariin," *Journal of Materials Science: Materials in Medicine*, vol. 23, no. 2, pp. 399–407, 2012.

[23] T.-P. Hsieh, S.-Y. Sheu, J.-S. Sun, M.-H. Chen, and M.-H. Liu, "Icariin isolated from *Epimedium pubescens* regulates osteoblasts anabolism through BMP-2, SMAD4, and Cbfa1 expression," *Phytomedicine*, vol. 17, no. 6, pp. 414–423, 2010.

[24] J. Zhao, S. Ohba, M. Shinkai, U.-I. Chung, and T. Nagamune, "Icariin induces osteogenic differentiation in vitro in a BMP- and Runx2-dependent manner," *Biochemical and Biophysical Research Communications*, vol. 369, no. 2, pp. 444–448, 2008.

[25] K.-M. Chen, B. F. Ge, X. Y. Liu et al., "Icariin inhibits the osteoclast formation induced by RANKL and macrophage-colony stimulating factor in mouse bone marrow culture," *Die Pharmazie*, vol. 62, no. 5, pp. 388–391, 2007.

[26] A. Manescu, A. Giuliani, S. Mohammadi et al., "Osteogenic potential of dualblocks cultured with human periodontal ligament stem cells: In vitro and synchrotron microtomography study," *Journal of Periodontal Research*, vol. 51, no. 1, pp. 112–124, 2016.

[27] K. Huo, X. Zhang, H. Wang, L. Zhao, X. Liu, and P. K. Chu, "Osteogenic activity and antibacterial effects on titanium surfaces modified with Zn-incorporated nanotube arrays," *Biomaterials*, vol. 34, no. 13, pp. 3467–3478, 2013.

[28] L. Zhao, H. Wang, K. Huo et al., "The osteogenic activity of strontium loaded titania nanotube arrays on titanium substrates," *Biomaterials*, vol. 34, no. 1, pp. 19–29, 2013.

[29] X. Fan, B. Feng, Z. Liu et al., "Fabrication of TiO2 nanotubes on porous titanium scaffold and biocompatibility evaluation in vitro and in vivo," *Journal of Biomedical Materials Research Part A*, vol. 100, no. 12, pp. 3422–3427, 2012.

[30] F. Rupp, L. Scheideler, D. Rehbein, D. Axmann, and J. Geis-Gerstorfer, "Roughness induced dynamic changes of wettability of acid etched titanium implant modifications," *Biomaterials*, vol. 25, no. 7-8, pp. 1429–1438, 2004.

[31] J. Takebe, S. Itoh, J. Okada, and K. Ishibashi, "Anodic oxidation and hydrothermal treatment of titanium results in a surface that causes increased attachment and altered cytoskeletal morphology of rat bone marrow stromal cells in vitro," *Journal of Biomedical Materials Research Part B: Applied Biomaterials*, vol. 51, no. 3, pp. 398–407, 2000.

[32] X. Xie, F. Pei, H. Wang, Z. Tan, Z. Yang, and P. Kang, "Icariin: A promising osteoinductive compound for repairing bone defect and osteonecrosis," *Journal of Biomaterials Applications*, vol. 30, no. 3, pp. 290–299, 2015.

[33] L. Xia, Y. Li, Z. Zhou, Y. Dai, H. Liu, and H. Liu, "Icariin delivery porous PHBV scaffolds for promoting osteoblast expansion in vitro," *Materials Science and Engineering C: Materials for Biological Applications*, vol. 33, no. 6, pp. 3545–3552, 2013.

[34] C. R. Yang and J. Di Chen, "Preparation and biological evaluation of chitosan-collagen-icariin composite scaffolds for neuronal regeneration," *Neurological Sciences*, vol. 34, no. 6, pp. 941–947, 2013.

[35] D. H. Kwon, S. J. Lee, U. M. E. Wikesjö, P. H. Johansson, C. B. Johansson, and Y.-T. Sul, "Bone tissue response following local drug delivery of bisphosphonate through titanium oxide nanotube implants in a rabbit model," *Journal of Clinical Periodontology*, vol. 44, no. 9, pp. 941–949, 2017.

[36] A. Tian, X. F. Qin, A. Wu et al., "Nanoscale $TiO_2$ nanotubes govern the biological behavior of human glioma and osteosarcoma cells," *International Journal of Nanomedicine*, vol. 10, pp. 2423–2439, 2015.

[37] G. S. Stein, J. B. Lian, and T. A. Owen, "Relationship of cell growth to the regulation of tissue-specific gene expression during osteoblast differentiation," *The FASEB Journal*, vol. 4, no. 13, pp. 3111–3123, 1990.

[38] Y. Wu, L. Xia, Y. Zhou, Y. Xu, and X. Jiang, "Icariin induces osteogenic differentiation of bone mesenchymal stem cells in a MAPK-dependent manner," *Cell Proliferation*, vol. 48, no. 3, pp. 375–384, 2015.

[39] Y. Hu, K. Cai, Z. Luo et al., "$TiO_2$ nanotubes as drug nanoreservoirs for the regulation of mobility and differentiation of mesenchymal stem cells," *Acta Biomaterialia*, vol. 8, no. 1, pp. 439–448, 2012.

[40] K. C. Popat, L. Leoni, C. A. Grimes, and T. A. Desai, "Influence of engineered titania nanotubular surfaces on bone cells," *Biomaterials*, vol. 28, no. 21, pp. 3188–3197, 2007.

[41] T. Wu, T. Shu, L. Kang et al., "Icaritin, a novel plant-derived osteoinductive agent, enhances the osteogenic differentiation of human bone marrow- and human adipose tissue-derived mesenchymal stem cells," *International Journal of Molecular Medicine*, vol. 39, no. 4, pp. 984–992, 2017.

[42] L. Prodanov, J. te Riet, E. Lamers et al., "The interaction between nanoscale surface features and mechanical loading and its effect on osteoblast-like cells behavior," *Biomaterials*, vol. 31, no. 30, pp. 7758–7765, 2010.

[43] P. Han, P. W. Ji, and L. Zhao, "Improved osteoblast proliferation, differentiation and mineralization on nanophase Ti6Al4V," *Chinese Medical Journal*, vol. 124, no. 2, pp. 273–279, 2011.

[44] K. Maekawa, Y. Yoshida, A. Mine, B. Van Meerbeek, K. Suzuki, and T. Kuboki, "Effect of polyphosphoric acid pre-treatment of titanium on attachment, proliferation, and differentiation of osteoblast-like cells (MC3T3-E1)," *Clinical Oral Implants Research*, vol. 19, no. 3, pp. 320–325, 2008.

[45] Y. K. Zhai, X. Y. Guo, B. F. Ge et al., "Icariin stimulates the osteogenic differentiation of rat bone marrow stromal cells via activating the PI3K–AKT–eNOS–NO–cGMP–PKG," *Bone*, vol. 66, pp. 189–198, 2014.